Study of the effect of environmental toxicants on the intracellular Ca^{2+} signaling of human defense system

ヒトの身体防御システムで働く環境毒による Ca^{2+} シグナリング機構の研究

2017 年 2 月

Wen-Li HSU

許　文俐

Study of the effect of environmental toxicants on the intracellular Ca^{2+} signaling of human defense system

ヒトの身体防御システムで働く環境毒による Ca^{2+} シグナリング機構の研究

2017 年 2 月

早稲田大学　大学院先進理工学研究科

Wen-Li HSU

許　文俐

Table of Contents

List of illustrations

Japanese abstract

身体に与える化学的および物理的因子による傷害や細菌による感染などは、代表的な環境毒の作用といえる。それらは老化はもとより、数千にも上る病気の原因となっていることが知られている。こうした環境毒から我々の体を防ぐために、ヒトには防御システムが備わっている。それらは例えば皮膚とか免疫細胞などであり、そのような細胞は環境毒に我々の細胞が曝されると、まず細胞内の Ca^{2+}濃度が急速に上昇し、それに引き続いて活性酸素種（ROS）が産生される。これまで多くの論文で確認されてきたことであるが、Ca^{2+}シグナリングの他に ROS の細胞内の発生は、意外にも細胞の生と死のバランスを決めるところで決定的な役割を果たしている。というのも、これらは細胞を防御するためのシステムのキー分子であるシャペロンタンパク質(熱ショックタンパク質: HSP）を誘導することが知られているからである。細胞内における transient receptor potential (TRP)チャネルを経由する Ca^{2+}シグナリングと ROS の産生研究は、全く別々の分野で発展してきた。本博士論文では、このように別々に研究が進展してきた課題を、ヒトの防御システムとして同時に考慮することによって、細胞の生存戦略を理解し得ると考え、以下の第 1 章から第 5 章にまとめた。

第 1 章では序論として、身体防御システムにおける Ca2+シグナリングの重要性について述べる。細胞内 Ca^{2+}の上昇は、生理学的には電位依存性 Ca2+チャネルから、また生化学的には細胞内小胞体（ER）からの遊離によって生じるが、環境毒によって起こる Ca^{2+}の流入は、TRP チャネルを経由することが主である。またこの Ca^{2+}の濃度変化は一過性であるため、ミトコンドリアのユニポーターを刺激し、細胞内に ROS を産生させ、Ca^{2+}と ROS の双方の一過性の上昇が HSP の産生を誘導する。皮膚への刺激が、第２章で述べる化学的刺激（ヒ素）であれ、第３章で述べる物理的刺激（紫外線）であれ、または第 4 章で述べる生物的刺激（細菌、ケモカイン）のいずれであれ、TRP チャネルの開放が引き金となっていることを述べる。

第２章では化学的環境毒の代表的な例として、ヒ素が皮膚に与える影響を、Ca^{2+}シグナリングを解析することよって得られた結果から述べる。ヒ素は皮膚のがん化のみならず、他の種々のがんの原因となる要素であると認識されている。そのヒ素ががん化をもたらす最初の段階は Ca^{2+}シグナリングによって左右されていることをケラチノサイトの初期細胞を用いて見出した。また、同じ効果をがん化した細胞でも観察した。そして、その結果、我々はヒ素が ER 上にあるイノシトール3リン酸(IP3)受容体タンパクをリン酸化することによって、細胞内 Ca^{2+}導入を阻害することがわかった。IP3 受容体は 1～3 までの 3 種類あるが、このうち IP3R1 のみがリン酸化することを確認した。これとは別にヒ素はがん化した細胞には何の影響ももたらさないこともわかった。この結果から皮膚細胞におけるがん化の初期過程は、ヒ素によって活性化された IP3R1 のリ

ン酸化による Ca^{2+}シグナリングの低下であることがわかった。

第３章では物理的環境毒の代表的な例として、B 領域の紫外線（UVB）による細胞毒効果を、同じく皮膚細胞内の Ca^{2+}シグナリングを解析することによって得られた結果を用いて述べる。UVB を細胞に照射すると直ちに ROS が産生され、しばらくして DNA の損傷が起こることが確認された。その詳細なステップは以下の通りである。まず、UVB に皮膚細胞に照射されると細胞内 Ca^{2+} が上昇し、引き続いて細胞内の ROS レベルが上昇し、その後徐々に DNA の損傷が進行した。ところが、TRPC タイプチャネル（TRPC チャネル）の阻害剤（Derinat：DNA Na 塩、および SKF96365）を用いると、ROS の産生や DNA の損傷が阻害された。また、マウス皮膚に紫外線を与えてできる皮膚の潰瘍も Derinat で防止できることも確認した。この事実から、TRPC チャネルの活性化が UVB によって損傷を受ける際の最初の現象であるということがわかった。おそらくこれは老化のプロセスでの第一段階なのでもあろう。

第 4 章では細菌毒素の細胞に対する作用にも Ca^{2+}シグナリングが重要であることについて述べる。マクロファージは免疫系で最初に応答する細胞である。ここではその代表的なものとして、グラム陰性桿菌の一種であるツツガムシに刺されたときに何が起こるのかを調べた。グラム陰性桿菌とはグラム染色で赤色に染まる細菌のことである。マクロファージは食作用を有する大型細胞で、免疫系の最先端で働く細胞である。これまでマクロファージがグラム陰性桿菌によって感染されると何が起こるのかは知られていなかった。最初に起こる現象がこれもまた Ca^{2+}の上昇であることがわかった。このときの Ca^{2+}の流入は store operated Ca^{2+} entry（SOCE：ER の中の Ca がなくなったときにこれを検知して Ca^{2+}を中に流入させる特殊な TRP チャネル）であることを見出した。SOCE を経由するということは SOCE の特別な阻害剤として知られる 2-APB の使用によってわかる。ところが、意外なことにこの 2-APB で処理をすると、細胞内の HSP70 が増加し、細胞内シグナル伝達系の一つである ERK シグナリング経路を活性化し、細胞から遊離される腫瘍壊死因子である TNF-α の産生を抑制することで細胞の生存率が上昇することがわかった。したがって、SOC チャネル（SOC’s）の阻害剤である 2-APB の作用の解明は十分ではないが、細胞生存のためには単に HSP が増加するだけでは十分ではないということがわかった。

第 5 章では、本博士論文において得られた結果を総合的に考察する。細胞内 Ca^{2+}の一過性の上昇は連続的な上昇と異なり、最終的には HSP70 をはじめとする生存に必須な HSP を誘導する。そして、HSP は細胞内では老化したタンパク質を処理し、細胞外に流出したときは免疫系の効率を上昇させることになり、細胞の生存確率を上げる。また、この仕組みは老化したタンパク質を処理することにより、細胞老化の速度を低下させることにも繋がることが期待される。本博士論文の研究結果は、あらゆる環境に存在する毒性因子、例えばヒ素、紫外線、細菌などに対する人体の防御機構は、いずれもが TRP チャネルを活性化

し、細胞内 Ca^{2+}の増加をもたらし、これらが細胞の防御システムとして HSP の発現を増加していることを示している。ところで、TRP チャネルも HSP の発現もいずれも熱によって行われることが、個別に行われた研究ですでに証明されているので、時系列を考えると、TRP チャネルの活性化が HSP の発現の引き金を引くと考えている。すなわち、病気や老化といった様々な障害を克服するためには TRP-HSP ラインの活性化が重要であると考えられた。

English abstract

Chemical and physical stimulation that induces cellular damage, as well as microorganism infections, are common environmental toxicants and are known to cause thousands of diseases. In order to protect living cells from environmental toxicants, human defense systems, such as skin or immune cells, can immediately mount responses to exposure to environmental toxicants by triggering Ca^{2+} signaling and reactive oxygen species (ROS) production intracellularly.

The first part of this study concentrates on the effects of environmental toxicant arsenic (As) on Ca^{2+} signaling in skin, because As is a well-known human carcinogen that enhances tumor formation associated with various malignant diseases. During the initial processes in the development of arsenic-induced toxic effects, Ca^{2+} signaling was found to be critical at the earliest stages of arsenic treatment (incubation, exposure) of primary keratinocytes (KC). These Ca^{2+} signaling results were compared with the signaling results of arsenic treatment of malignant cells.

In the next step, physical environmental toxicant ultraviolet B (UVB) was examined. It was found that the most cytotoxic and mutagenic electromagnetic wave, UVB, induced intracellular Ca^{2+} elevation, ROS production, and DNA damage in human skin cells (KC, fibroblasts) and this toxic effect was inhibited by transient receptor potential canonical (TRPC) channel inhibitors Derinat and SKF96365.

Finally, the effect of microorganisms on Ca^{2+} signaling in the adaptive immune system was studied using macrophages. The experimental results emphasized that intracellular Ca^{2+} was initially increased in *O. tsutsugamushi*-infected macrophages via store operated Ca^{2+} entry (SOCE), which originates from TRP channels. SOCE inhibitor, aminoethoxydiphenyl borate (2-APB), but not SKF96365, restrained *O. tsutsugamushi*-induced cytokine storm, especially TNF-α and 2-APB, which promoted the level of HSP70.

Abbreviations

Abbreviation	*Full name*
ROS	Reactive oxygen species
UVB	Ultraviolet B
DDR	DNA damage response
SIR	Senescence-associated inflammatory response
O. tsutsugamushi	*Orientia tsutsugamushi*
KC	Keratinocytes
AS	Arsenic
TRP	Transient receptor potential
STIM1	Stromal interaction molecule 1
ER	Endoplasmic reticulum
SOCE	Store-operated calcium entry
TLR	Toll-like receptor;
PLC	Phospholipase-C
PIP2	Phosphatidylinositol (4,5)-bisphosphate
IP3	Inositol 1,4,5-trisphosphate
IP3R	Inositol 1,4,5-trisphosphate receptor
As-BD	Arsenic bowen's disease
RyRs	Ryanodine receptors
CREB	cAMP response element binding protein
NFAT	Nuclear factor of activated T-cells
8-oxodG	8-oxo-2'-deoxyguanosine
TG	Thapsigargin
NAC	N-acetylcysteine
2-APB	Aminoethoxydiphenyl borate
HDF	Human dermal fibroblast
HSPs	Heat shock proteins
CaMK	Calmodulin kinase
Cys	Cysteine
GPCRs	G protein-coupled receptors
P2YR	Purinergic 2Y receptor
DAG	Diacylglycerol
OAG	1-oleoyl-2-acetyl-sn-glycerol
COX-2	Cyclooxygenase-2
2-ME	β-mercaptoethanol
DCFH-DA	2',7'-dichlorofluorescein-diacetate

SDS-PAGE	Sulfate-polyacrylamide gel electrophoresis
LPS	Lipopolysaccharides
BAPTA	1,2-Bis(2-aminophenoxy)ethane-N,N,N',N'-tetraacetic acid tetrakis
TNF	Tumor necrosis factor
MAPK	Mitogen-activated protein kinase
GSH	Glutathione
SOD	Superoxide dismutase
HSF	Heat-shock transcription factor
PBS	Phosphate-buffered saline
MTT	5-dimethyl-2-thiazolyl)-2,5-diphenyl-2H-tetrazolium bromide
FBS	Fetal bovine serum
DMEM	Dulbecco's modified Eagle's medium
PMA	Phorbol 12-myristate 13-acetate
DAPI	4, 6-diamidino-2-phenylindole
BSS	Balanced salt solution

Chapter I Introduction

1.1 Environmental toxicants making ROS

Environmental toxicology covers the subjects of environmental chemistry, physics, microbiology, and genetics [1]. The most important categories among environmental toxicants are chemistry, physics and microbiology, which are responsible for thousands of diseases because of ROS production and accumulation[2]. The most famous example is Blackfoot disease due to heavy metal contamination with arsenic[3]. According to the various associated studies carried out so far, drinking water contaminated with arsenic can induce not only Blackfoot disease but also skin cancer [3,4]. Previously, many possible mechanisms for arsenic induced skin diseases have been proposed for *in vitro* and *in vivo* studies, pointing out that arsenic may be a carcinogen that promotes oncogene upregulation and decreases tumor suppressor gene downregulation and/ or mutation [5]. Effects induced by arsenic result in genomic instability, which is caused by intracellular ROS production [6]. Based on the lack of ROS generation in experimental cells to initially treat the oxidation stress from outside, ROS is also a crucial signal to decide the fate of the cell: survival or death[7]. However, despite a wealth of evidence for arsenic induced malignant diseases, the molecular mechanisms during the initial stages of arsenic exposure are still unclear.

ROS production was also demonstrated during UVB induced skin damage and aging [8]. Environment physiological damage by UVB is also a known trigger for ROS to induce DDR and SIR, affecting skin homeostasis. Obstruction of ROS production is known to interrupt UVB induced skin damage and aging [9,10], thus, many types of drugs or cosmetics have been developed against UVB-induced ROS production. These products were expected to be efficient in prevention of skin aging and aging associated diseases [10,11]. Interestingly, ROS production is also the key factor for environmental pathogen infection, contributing to severe afflictions such as adult respiratory distress syndrome, acute renal failure, acute hepatic failure, and multiple organ dysfunction syndrome [12-14]. For instance, a gram-negative bacteria, *O. tsutsugamushi*, induced scrub typhus is endemic across many regions of Asia and the Western Pacific, where more than one million cases occur each year. The majority of patients infected with *O. tsutsugamushi* have a high fatality rate due to cytokine storm from a severe inflammatory response [15]. Additionally, gram negative bacteria, *O. tsutsugamushi*, is known to stimulate ROS production via activating TLRs, which are the major receptors for responding to inflammation as a result of pathogen infection[16,17]. The role of ROS production via UVB exposure or by *O. tsutsugamushi* infection needs to be independently established. To investigate the direct effects of oxidative stress on cellular function, H_2O_2 was applied directly to cell culture solution. H_2O_2 is well known to produce the strongest ROS, a hydroxyl radical [18]. An application of H_2O_2

induced a reduction of the Ca^{2+} response when KC was activated by ATP via the G protein coupling receptor, P2YR. This reduction was found to be recovered by a reducing reagent, such as 2-ME and hydrogen gas (submitted paper). Initially ROS was thought to be quenched by using a reducing agent, but the true molecular explanation was that a disulfide bond was reduced to two cysteine residues.

1.2 Human defense system in response to environmental toxicants

As was discussed previously, ROS is initially produced in the cell as a response to outside environmental toxicants. Interestingly, in the human defense system, the skin or the immune system is more sensitive to environmental toxicants[19,20]. For instance, KC, the first barrier of skin, displays severe pathological effects in As-BD, such as basal cell carcinoma and squamous cell carcinoma [21]. Histologically, As-BD displays epidermal acanthosis, dysplasia, hyperkeratosis, and dyskeratosis [22,23]. The associated mechanisms of arsenic-induced skin cancer are highly relevant to ROS production[24]. Thus, skin cells, especially KC, could generate ROS due to response to environmental toxicants, but it is still unknown how KC initially responds to environmental stress.

Based on UVB induced skin damage, elevation of intracellular Ca^{2+} is the first response to UVB-induced intracellular ROS generation in KC[25]. A similar result is also shown in the immune system [26]. The immune system defends the body from infectious pathogens in two major ways: innate and adaptive immunity. The innate immune system is the first line of host defense against invading organisms, with the adaptive immune system acting as the second line of defense [27]. The primary defense mechanisms of macrophages against pathogen infection are phagocytosis and cytokine production; pathogens and antigens can induce an inflammatory response [28]. An increase of intracellular Ca^{2+} is crucial for the activation of macrophages and for them to release cytokines and perform phagocytosis[29]. Once Ca^{2+} signaling increases intracellularly, it induces mitochondrial Ca^{2+} uptake and a large amount of intracellular ROS production [30]. For protection in human defense system, intracellular ROS production is efficient to quench pathogen infection via phagocytosis [31]. Consequently, it seems Ca^{2+} signaling could be involved in the human defense system response to environmental toxicants in the initial stage. Yet, the relationship between Ca^{2+} signaling and intracellular ROS production is unclear during the initial stage to response environmental toxicants.

1.3 Role of intracellular Ca^{2+} signaling in the cell of human defense system

Based on the previous study, ROS production is an important molecule that influences the cell's survival and death balance [7]; in contrast, the increasing Ca^{2+} level facilitates the elevation of intracellular ROS concentration because of mitochondrial

dysfunction [30]. When considering the role of Ca^{2+} signaling in cell, the first task is to classify the underlying mechanism of Ca^{2+} signaling in regulating cell physiology. To maintain the intracellular Ca^{2+} homeostasis (~100 nM), STIM1 monitors the Ca^{2+} pump of ER, and links with Orai1 to trigger Ca^{2+} influx when the intracellular space is insufficient to maintain intracellular Ca^{2+} homeostasis [32]. The cells belonging to human defense system possesses two major mechanisms to govern intracellular Ca^{2+} homeostasis [33].

1.3.1 TRP channels in Ca^{2+} signaling

The TRP protein superfamily is divided into seven sub families: TRPCs, TRPVs, TRPMs, TRPN, TRPA, TRPPs and TRPML. Each type of TRP channel has different mechanism that can be activated [34]. For instance, the majority of TRPCs are activated by elevated intracellular Ca^{2+} concentration. STIM1-Orai1 interaction is associated with TRPCs to regulate SOCE; however, the function of TRPCs is independent on STIM1-Orai1 interaction. In skin, the PLC pathway is able to activate TRPCs, where IP3 can activate TRPC1, TRPC4 and TRPC5, and DAG to activate TRPC6 and TRPC7 via cleaving PIP2[35,36]. TRPCs are applied to implement the function of macrophages in defending against pathogen infections; TRPC3 is involved in migration and efferocytosis, and TRPC1 activate calcineurin and BAD pathways to induce apoptosis of macrophages [37]. Some TRP channels are also classified as temperature and pressure sensors, such as TRPV1 andV3, TRPM8 and TRPA1 in the skin [35]. The TRPV1 group, known as pain receptors, regulates longevity and metabolism by neuropeptide signaling [38].

1.3.2 IP3 receptors in Ca^{2+} signaling

Except for TRP channels, intracellular Ca^{2+} can be released from ER via IP3Rs or RyRs. Eventually, the cells in the human defense system use IP3Rs to regulate Ca^{2+} release from ER to cytoplasm, consequently activating downstream molecules, such as CaMK Ⅱ, CREB, NFAT or NF-κB [32]. The three types of IP3Rs have been identified as IP3R1, IP3R2 and IP3R3, but the function of each IP3R is still unclear [39]. Interestingly, the structure of RyRs is similar to that of IP3Rs, particularly since it is one of the largest channel complexes at around 560 kDa. There are also three types of RyRs, but they have the most important function in excitable cells [40].

1.4 A role of the intracellular Ca^{2+} for cell survival and death balance

As mentioned previously, ROS and Ca^{2+} signaling are involved in determining cell survival or death under outside stress stimulation. But it is still not well known how ROS and Ca^{2+} signaling can decide the life or death of cells. An elegant system exists

in the cell to defend against any immediate stress. To rescue the cell from outside stress, expression of HSPs is the first defense reaction against cell damage signals [8]. Downstream of HSPs there are many survival molecules, such as Bcl-2, HIF-1α and NF-κB [41]. Those molecules are dedicated to quenching various outside cell death-inducing signals, such as apoptotic molecules like Bax, Bad and Bid from the mitochondria[42], or accumulated dysfunction proteins in cytoplasm via activation of the UPR pathway [43]. Outside stress, no matter whether it comes from the effects of chemistry, physics or microbiology, can simultaneously induce survival and death signaling molecules in response to attack from environmental toxicants. [7,8]. However, once HSP-induced survival signals can't control the regular death or stress signal molecules, the cell tends to respond to death signals because of the interruption of the balance between survival and death signals. So far, there is no absolute, detailed answer to explain the mechanism of how the cell determines survival or death. Many studies have focused on the effect of exposures to environmental toxicants on cell survival and balance, but actually the cell may decide its future life in the initial stage, immediately after it responds to environmental toxicants. However, there is no related study to explain what constitutes the exact immediate response of the cell to those environmental toxicants. To react with the environmental toxicants immediately, it is necessary to use second messenger system. Thus, second messenger Ca^{2+} is the most advantageous pathway to activate many downstream molecules at the same time. Furthermore outside Ca^{2+} concentration of the cell is higher 10^4 fold than intracellular concentration which also supports the advantage of Ca^{2+} as a second messenger, because changes in Ca^{2+} concentration of less than 0.1% has no effect on membrane potential. This means the role of Ca^{2+} signaling could be involved in the initial cellular response to environmental toxicants.

1.5 The specific aim of this study

To identify the role of Ca^{2+} in the response to environmental toxicants and intracellular Ca^{2+} signaling by the human defense system, this thesis studies how the cell responds to environmental toxicants in the initial stage of exposure, and examines the parameters determining cell destiny: survival or death. Additionally, the relationship between Ca^{2+} and ROS is explored in this study. Even though ROS production and Ca^{2+} signaling are closely related, both of them are generated in response to outside stress by environmental toxicants. The underlying mechanism regulating cell survival or death is still unknown. To investigate these unsolved problems, this thesis investigates how skin immediately responds to stimulation by arsenic and UVB. Additionally, how the immune system responds to pathogen infection was studied. Human macrophages were utilized in this study to detect the

relationship between HSP expression and Ca^{2+} signaling. The results from this thesis help to clarify the underlying mechanism between Ca^{2+}, ROS and HSPs in determining cell survival and death when exposed to environmental toxicants.

Chapter Ⅱ Effect of toxic arsenic on Ca^{2+} signaling in human KC

The original work was reported in Cell Calcium (2012), and the publisher, Elsevier, has allowed me to use this paper a s part of my own PhD thesis.

Arsenic is known as an environmental toxicant and human carcinogen that promotes tumor generation associated with various types of malignant diseases [23]. Arsenic skin cancer is equivalent to an arsenic-associated malignant cancer that is caused by low-dose and long-term exposure to arsenic contamination of drinking water [5]. The most common arsenical skin cancer is Bowen's disease (AS-BD), which is an in situ carcinoma with abnormal KC proliferation and peripheral immune cell dysfunction [5]. Also, increasing number of studies suggest that among malignant cancers, intracellular Ca^{2+} signaling is regulated the way that normal cell death is prevented and the malignant characteristics of the cells are maintained [44,45]. To investigate the role of Ca^{2+} elevation on environmental toxicants for intracellular Ca^{2+} signaling of the human defense system, the first part of this thesis describes the toxic effect of arsenic on intracellular signaling in human KC.

2.1 Arsenic attenuates Ca^{2+} release from ER and reduces Ca^{2+} entry from SOC channel by promoting phospho-Akt function

2.1.1 Effect of arsenic on ATP-induced Ca^{2+} elevation in primary KC

IP3Rs-mediated Ca^{2+} release from ER, which is known as "Ca^{2+} stores", is central to several normal physiological processes [46]. Over-stimulation by agonists, such as some cytokines or ATP, generates a large number of second messenger IP3s through activating GPCRs and PLC, which results in Ca^{2+} release from the ER and, normally, cell death via Ca^{2+} overload in the mitochondria [33,47,48]. Cell death due to enormous Ca^{2+} elevation has been proposed to be inhibited in cancer cells because Ca^{2+} levels are regulated via alterations in Ca^{2+} pump activity or increases in IP3R1 phosphorylation levels through activation of the serine/threonine protein kinase Akt signaling pathway [44,45]. Thus, regulation of intracellular Ca^{2+} levels may be an important condition in the survival of arsenic-induced cancer cells. In order to examine how KC responds to arsenic-induced damage through regulation of Ca^{2+} signaling from the ER, KC was pretreated with either 1 μM or 5 μM sodium arsenite ($AsNaO_2$) for 1 h, and the Ca^{2+} elevation after ATP stimulation was observed. Treatment with arsenic for 1 h decreased Ca^{2+} levels dose-dependently from peak mean values of 565 nM Ca^{2+} (0 μM arsenic) to 450 nM Ca^{2+} (5 μM arsenic) in human primary KC (Fig. 1A). Moreover, arsenic not only reduced the Ca^{2+} response, but also changed the time course of Ca^{2+} release (Fig. 1A). With ATP stimulation, Ca^{2+} elevation appeared immediately, then decayed exponentially in controls ($t_{1/2}$ = 216.4 s; Fig. 1A). Incubation of KC with 1 μM or 5 μM

arsenic reduced the decay time to $t_{1/2}$ = 165.9 s and $t_{1/2}$ = 137 s, respectively (Fig. 1A). However, normalized traces of controls, 1 μM, and 5μM arsenic-exposed groups revealed no significant difference in the time course of ATP-induced Ca^{2+} response as shown in Fig. 1B

.

2.1.2 Arsenic altered SOCE in primary KC

According to the above results, arsenic decreased Ca^{2+} release from the ER, which may inhibit cell death by reducing the Ca^{2+} overload in the mitochondria [33,44]. As a next step, further experiments were done to seek how arsenic affects the mechanism of Ca^{2+} release from the ER. Ca^{2+} signaling through ATP from purinergic GPCRs may also be involved in regulating Ca^{2+} levels in ER. In the following experiments, the effect of arsenic on ER-dependent SOCE was examined. In order to absolutely deplete the Ca^{2+} stored in the ER, ATP was applied twice in Ca^{2+} free BSS solution. Unexpectedly, the second application of ATP induced a higher peak in the Ca^{2+} elevation in arsenic treated KC (5 μM arsenic) compared to control cells (Fig. 1C). Moreover, arsenic also reduced the SOCE in a dose-dependent manner (Fig. 1C). There are two possible explanations for the mechanism of arsenic effects on ATP-induced Ca^{2+} signaling: (1) arsenic directly affects Ca^{2+} binding, which would reduce Ca^{2+}release from the ER and SOCE, or (2) arsenic influences Ca^{2+} release from the ER by regulating IP3Rs in ATP-induced Ca^{2+} signaling. The peak of Ca^{2+} release was higher in arsenic-treated KC than in control cells (Fig. 1C), indicating that arsenic may modify the function of IP3Rs. This result may be due to insufficient Ca^{2+} release from the ER by the first ATP application, contributing to a reduction in the Ca^{2+} influx via SOC channels. If arsenic affected the amount of Ca^{2+} stored in the ER directly, however, the Ca^{2+} response to stimulation by TG would be different from that in the controls. The Ca^{2+} response of KC to a rapid alternation in extracellular Ca^{2+} (from 0 mM to 2 mM) exhibited the same pattern following the application of TG and ATP, independent of the arsenic treatment (Fig. 1D). Because TG and ATP deplete ER with different mechanisms [49], it is reasonable to conclude that arsenic mainly reduced IP3Rs-dependent Ca^{2+} release in KC but not in TG inductions.

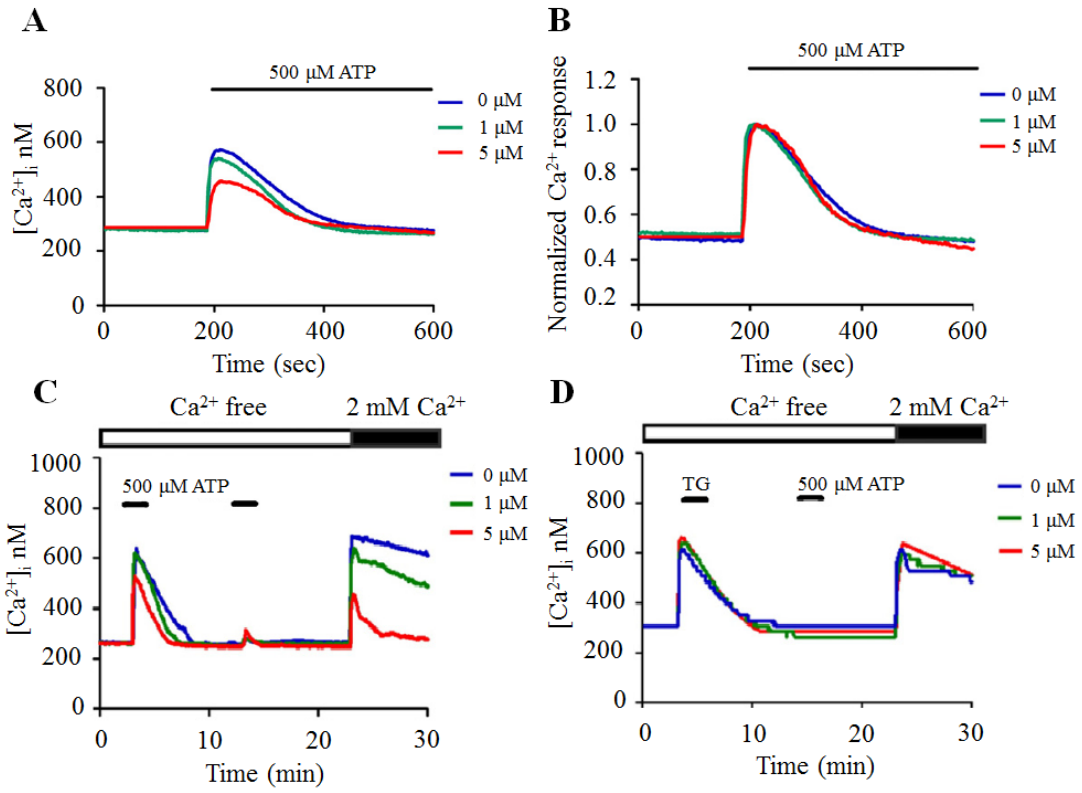

Figure 1. Arsenic reduced store-operated Ca^{2+} influx via the ATP-induced Ca^{2+} signal in human primary KC. (A) Ca^{2+} imaging analysis of the ATP-induced Ca^{2+} response after pre-treatment with control (0 μM, blue line), 1 μM (green line), and 5 μM (red line) arsenic. The Ca^{2+} signals represent the mean intracellular Ca^{2+} concentration change of 20 cells with five replicates for each group (N = 5). (B) Representative traces of normalized Ca^{2+} signals. The signals were normalized to the value from the maximum ATP-induced Ca^{2+} response (N = 5). (C) Repeated ATP stimulations at 10 min intervals in Ca^{2+} free BSS solution following 1 h of arsenic treatment. Twenty-three minutes after applying the ATP, the extracellular Ca^{2+} concentration abruptly increased from 0 to 2 mM to open the SOC channels (N = 5). (B) Instead of ATP, 20 nM Tg was applied to deplete the ER Ca^{2+} stores by inhibiting intracellular SERCA-type Ca^{2+} pumps. The lack of an increase in Ca^{2+} in response to the second 500 μM ATP application showed that TG had depleted the ER Ca^{2+} stores (N = 5). The step-wise response was due to a difference in the time constant used for averaging the signal. The Ca^{2+} signals represent the mean value of 20 cells.

2.2 Arsenic reduced Ca^{2+} release and SOCE dose-dependently by increasing phosphorylation of IP3R1 by increasing phospho-Akt formation

The above results indicate that arsenic did not affect the amount of Ca^{2+} stored in the ER, but influenced Ca^{2+} release from the ER by controlling IP3Rs. Therefore the next step was to examine how arsenic influences IP3Rs and SOC channels. KC was treated with caged IP3 contained in DMSO solution for 2 h. A UV beam was used to uncage the IP3 without activating it. If IP3Rs are phosphorylated in the upstream signaling pathway in advance, the uncaged IP3 molecules cannot completely activate the IP3Rs because of electrostatic Coulomb interactions. This is because the phosphate group in phosphorylated protein and IP3 molecule are negatively charged. Therefore, the Ca^{2+} response must be inversely dependent on the degree of IP3R1 phosphorylation [5]. In the control experiment, the peak fluorescence Ca^{2+} response was found to be more than 2.3-fold that of the baseline fluorescence (Fig. 2A, 2B). The peak values of Ca^{2+} responses in the 1 μM and 5 μM arsenic-exposed groups were 2-fold and 1.2-fold higher, respectively, compared to the baseline (Fig. 2A, 2B). The black area under the Ca^{2+} response curve displayed increased Ca^{2+} influx induced by a rapid increase (from 0 mM to 2 mM) in extracellular Ca^{2+} concentration, which was used to gain entry into the cell via SOC channels. Arsenic also dose-dependently reduced the SOCE. It was reported that sodium arsenite activates Akt signaling pathways in human lung epithelial cells [50] and IP3Rs are inhibited independently by IP3R1 phosphorylation [44]. Thus, in this study, arsenic could reduce ATP-induced Ca^{2+} release by activating Akt, resulting in IP3R1 phosphorylation. To test this possibility, KC was pretreated for 30 min with the Akt inhibitor wortmannin, which was known to inhibit Akt phosphorylation, before incubation with arsenic. The results of the subsequent focal uncaging experiment indicated that wortmannin pre-treated cells showed an increased Ca^{2+} signal in KC treated with either 1μM arsenic or 5 μM arsenic (Fig. 2A, 2B) relative to that without wortmannin pre-treatment (Fig. 2A, 2B).

Wortmannin also rescued the ATP-induced Ca^{2+} increase in arsenic treated cells (Fig. 2C). Incubation of cells with 1 μM or 5 μM arsenic after pretreatment with wortmannin increased ATP induced Ca^{2+} levels from 450 nM to 500 nM and from 520 nM to 540 nM, respectively (Fig. 2C). Taken together with the above findings, this result indicates that wortmannin contravened the effects of arsenic on Ca^{2+} signaling induced not only by stimulation with uncaged IP3, but also by application of ATP. Furthermore in order to demonstrate that arsenic leads to the phosphorylation of IP3R1, a specific phospho-IP3R1 antibody was used to explore IP3R1 phosphorylated IP3R. Western blot analysis showed that arsenic promoted IP3R phosphorylation (Fig. 2D). Also Western blot analysis indicated that Akt activation was required for arsenic-induced IP3R1 phosphorylation (Fig. 2E). Thus, phosphorylation of both Akt and IP3R1 was

promoted by arsenic treatment and the level of phosphorylation was reduced by wortmannin (Fig. 2D, 2E), which inverted the arsenic-induced decrease in Ca^{2+} signaling and SOCE. Thus, arsenic may induce malignant tumor of KC through activation of the Akt signaling pathway, thereby decreasing Ca^{2+} release from the ER by increasing IP3R1 phosphorylation levels.

2.3 Arsenic did not affect Ca^{2+} signaling in HSC-1 (malignant) cells

The results of the experiments indicate that arsenic reduced ATP stimulated and uncaged IP3-induced Ca^{2+} elevation by increasing IP3R1 phosphorylation levels through activation of the Akt signaling pathway. Many previous studies have used malignant cell lines to examine the effects of arsenic on the regulation of Ca^{2+} signaling. The following experiment attempted to clarify whether arsenic influenced ATP-induced Ca^{2+} by imaging the processes in HSC-1 cells under the same conditions as were previously used in this study to evaluate the effects of arsenic in primary KC. In order to detect the effects of arsenic on ATP- induced Ca^{2+} elevation in HSC-1 cells, the cells were treated with arsenic for 1 hour. Compared with human primary KC, however, neither arsenic-treated nor HSC-1 cells not treated with arsenic exhibited any apparent difference in ATP induced Ca^{2+} signaling or in SOCE (Fig. 3A). Focal uncaging established that arsenic had no effect on Ca^{2+}levels; the peak Ca^{2+} response in all groups was more than 2-fold higher than the baseline induced by uncaged IP3 stimulation (Fig. 3B). The total amount of Ca^{2+}released, estimated from the curve of Ca^{2+} responses in the gray and black areas of Fig. 3B, demonstrated that arsenic treatment had no significant effect (Fig. 3C). Correspondingly, arsenic did not influence IP3R1 or Akt phosphorylation, as shown by Western blot analysis (Fig. 3D). The results indicated that Ca^{2+} mobilization in the malignant cell line was not affected by arsenic treatment. This suggests that the effects of arsenic on Ca^{2+}mobilization are limited to the initial stage of the development of cancer in skin cells.

The results of this part of the experiment demonstrated that primary KC was largely affected by arsenic, but cancer cells, HSC-1, were not. In the case of KC, application of arsenic induced the phosphorylation of IP3R1 of the ER. Furthermore, it was also established that arsenic also suppressed SOCE. These findings suggest that arsenic-induced malignancy is related to IP3Rs-mediated regulation of Ca^{2+} signaling in primary KCs. This IP3R related mechanism depends on Akt-mediated phosphorylation. The results show that arsenic targets IP3R1 phosphorylation and decreases Ca^{2+} release from the ER in KC, but not in carcinoma (HSC-1 cells) (Fig. 4). These findings suggest that mechanism of arsenic reduces Ca^{2+} release to suppress the innate immune system and in this way maintains survival signals in primary KC. The findings also suggest that arsenic is associated with the initial stages of skin cancer by

inducing the malignant transformation of skin cells.

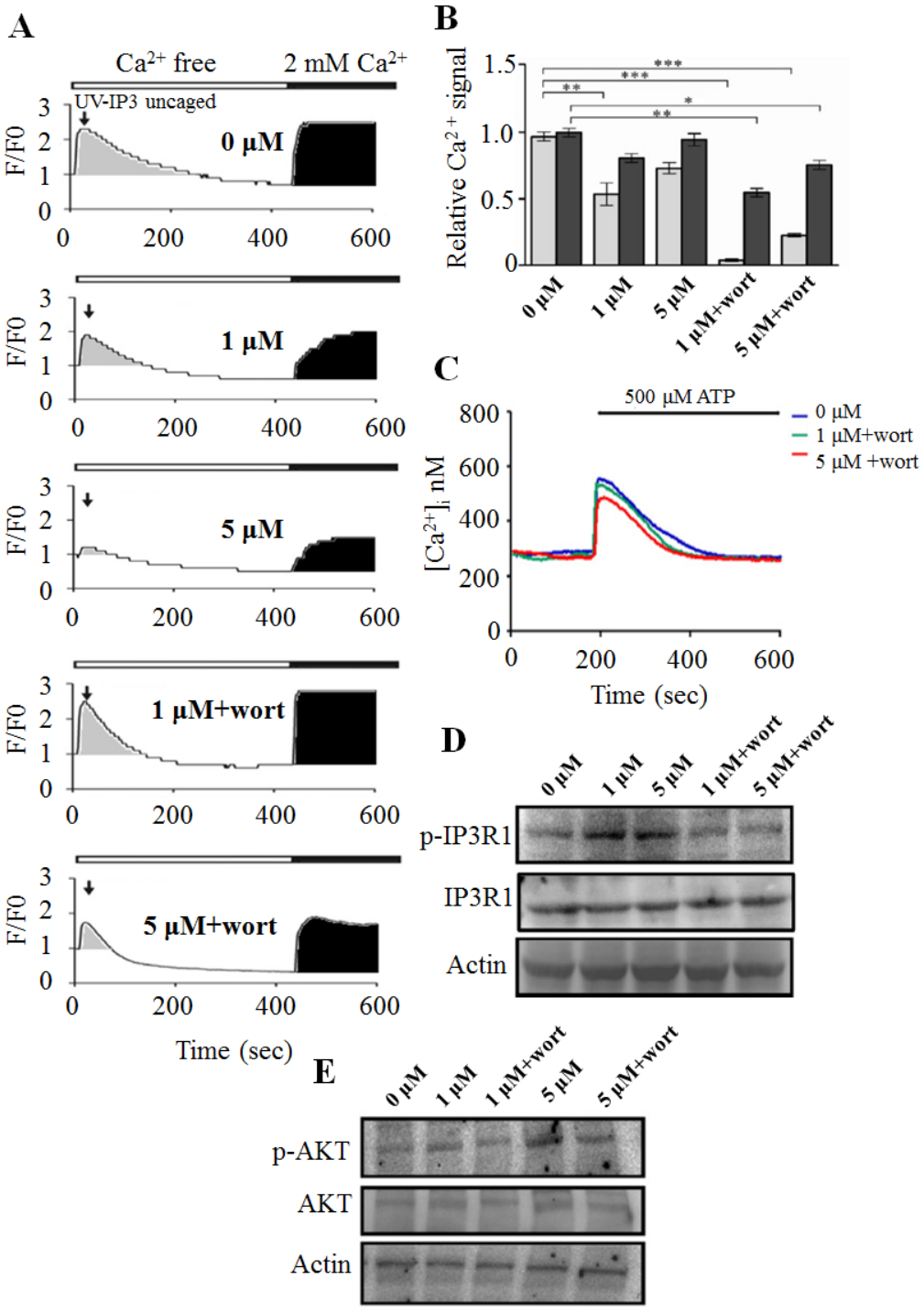

Figure 2. Arsenic reduced Ca^{2+} release and SOC-channel Ca^{2+} influx dose-dependently by increasing phosphorylation of IP3R1 by enhancing phospho-Akt formation. (A) Effect of arsenic on IP3-induced Ca^{2+} response. The concentration of arsenic utilized is indicated. F/F0 shows Fluo-4 fluorescence (F) relative to baseline fluorescence (F0). Uncaging of caged-IP3 by UV irradiation released IP3 molecules in the cell, which induced Ca^{2+} elevation that was dependent on the arsenic concentration in Ca^{2+} free BSS buffer. Ca^{2+} entry via SOC channels was dependent on ER Ca^{2+} stores, as illustrated by the change in Ca^{2+} dynamics when extracellular Ca^{2+} was increased from 0 to 2 mM in the black-colored area. The gray-colored area illustrates the amount of Ca^{2+} released by uncaged IP3 (N = 5). Cells were pretreated with wortmannin (wort, 1 μM) for 30 min and then incubated with different arsenic concentrations for 1 h. The Ca^{2+} signal was induced by uncaging caged-IP3 molecules, then 2 mM $CaCl_2$ was added extracellularly to open SOC channels (N = 5). (B) Ca^{2+} signals were estimated by calculating the gray- and black-colored areas under the Ca^{2+} curve (*P < 0.05; **P < 0.01; ***P < 0.005). (C) Wortmannin rescued arsenic-induced reduction of Ca^{2+} mobilization by extracellular ATP stimulation. Ca^{2+} imaging shows that pretreatment with wortmannin and arsenic rescued ATP-induced (500 μM) Ca^{2+} signals of 20 cells (N = 5). (D) Western blot analysis of the expression of phospho-IP3R1 and IP3R1 following incubation of the cells with arsenic alone or with wortmannin. Arsenic treatment increased the density of the p-PI3R1band, while expression of the IP3R1 (about 260 kD) and actin (42 kD) were independent of arsenic treatment. (E) Western blot analysis of the expression of phospho-Akt (p-AKT), Akt (about 60 kD), and actin. Phospho-Akt, but not Akt or actin, was increased with 1 μM or 5 μM arsenic treatment, an effect that was blocked by pre-treatment with wortmannin. The concentration of arsenic used is indicated.

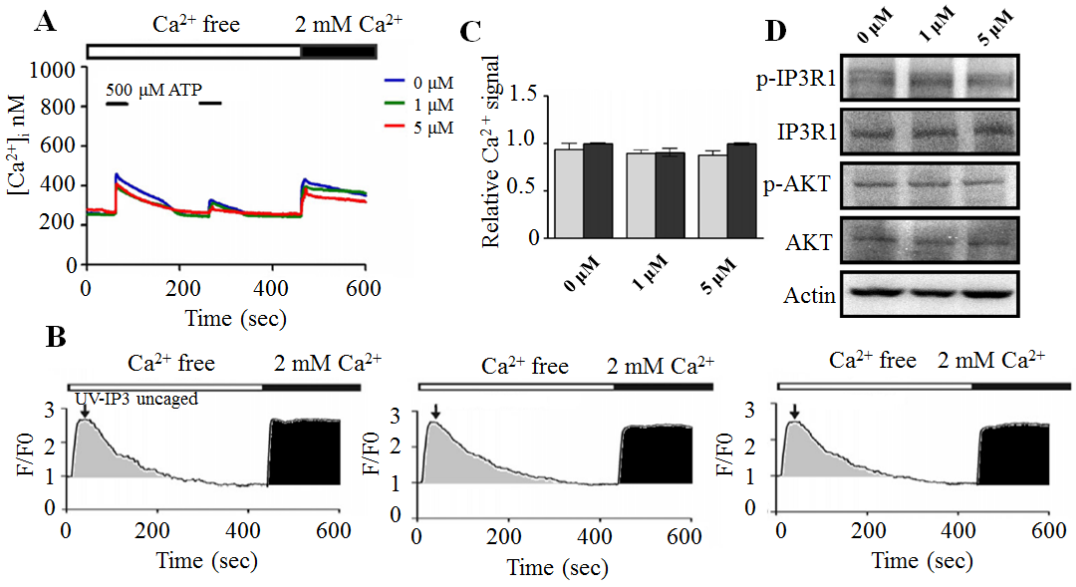

Figure 3. No effect of arsenic on IP3 receptor and store-operated Ca^{2+} influx in HSC-1 cells. (A) The effect of arsenic on the Ca^{2+} signal and SOC channel-mediated Ca^{2+} influx with ATP application in HSC-1 cells (N = 4). (B) The effect of arsenic on uncaged IP3-induced Ca^{2+} release and Ca^{2+} influx from SOC channels. Gray- and black-colored areas are relative to Ca^{2+} signal with stimulation of uncaged IP3 and Ca^{2+} (N = 3). (C) Ca^{2+} signals were estimated by quantifying the gray- and black-colored areas under the Ca^{2+} signal curve. (D) Western blot analysis of phospho-IP3R1 (p-IP31), IP3R1, phospho-Akt (p-AKT), and Akt expression. The concentration of arsenic used is indicated.

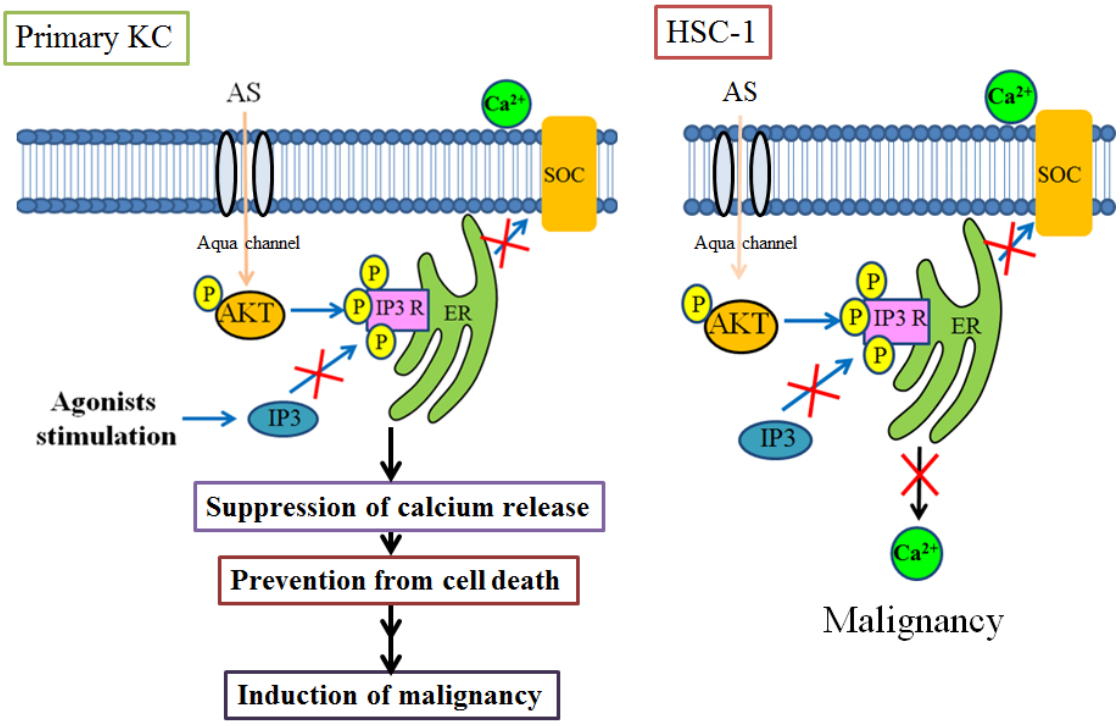

Figure 4. The effect of arsenic on calcium signaling in primary KC and HSC-1. Arsenic phosphorylates IP3R via activating the AKT pathway, suppressing Ca^{2+} release and preventing cell death. Malignancy is then induced by the activation of oncogenes and inhibition of tumor suppressor genes in primary KC. In contrast, malignant KC has an activated AKT pathway; thus, the IP3R is still non-phosphorylated and there is no influence by arsenic stimulation.

2.4 Materials and Methods

2.4.1 Cell culture

Human primary KC were isolated from the foreskins of 7- to 12–year-old boys obtained via routine circumcision. The skin specimens were washed with phosphate-buffered saline, cut into small pieces, and cultured in medium containing 0.25% trypsin (Gibco BRL) overnight at 4°C. The epidermal sheet was lifted from the dermis using fine forceps. The epidermal cells were then pelleted by centrifugation (500g, 10 minutes) and separated into individual cells through repeated aspiration. The KC were incubated in serum-free KC growth medium, supplemented with human recombinant epidermal growth factor and bovine pituitary extract (5 μg/mL each), insulin (5 μM/mL), and hydrocortisone (5 μg/mL; Gibco BRL) at 37°C in humidified 5% CO_2, and supplemented with KC growth medium for five generations. Human squamous carcinoma cells, HSC-1 (a kind gift from Dr. Chih-Hung Lee, Taiwan), were

cultured at 37°C in low-glucose Dulbecco's Modified Eagle Medium (Gibco BRL), supplemented with 10% FBS and antibiotics (100 IU/mL penicillin and 100 μg/mL streptomycin) in a 5% CO_2 atmosphere.

2.4.2 Calcium imaging

To detect the intracellular calcium responses to stimulation, such as by ATP or by TG, a calcium imaging system was equipped with a perfusion system. Before the experiments, the cells were stained with 1 μM Fluo-4-AM at 37°C for 20 minutes and then washed with BSS buffer (5.4 mM KCl, 5.5 mM D-glucose, 1 mM $MgSO_4$, 130 mM NaCl, 20 mM Hepes pH 7.4, and 2 mM $CaCl_2$). Intracellular calcium concentrations were estimated based on the ratio of fluorescence intensities emitted upon excitation with consecutive 3-second pulses of 488-nm light at a resolution of 1376 × 1038 pixels using an Olympus Cell^R IX81 fluorescence microscope (Olympus, Essex, UK) equipped with an MT 20 illumination system (Olympus) and UPLanApo 10× objective lens. Intracellular calcium concentration was estimated based on calibration curves as follows. A calcium calibration curve was created using a Calcium Calibration Buffer kit (Molecular Probes). Intracellular calcium ($[Ca^{2+}]_i$) was calculated from Fluo-4 excited at 488 nm and imaged using an Olympus Cell^R IX81 fluorescence microscope and UPLanApo 10× objective lens at 20°C. Fluo-4 signals were calibrated by measuring the fluorescence intensity from microcuvettes containing 10 mM K2EGTA (pH 7.20) buffered to various $[Ca^{2+}]$ levels. Calcium concentration was calculated using the following formula: $[Ca^{2+}]_i$= KD *(F−Fmin/Fmax−F). Plotting the fluorescence intensity versus $[Ca^{2+}]$ yielded a calibration curve with the formula of: $[Ca^{2+}]_i$= KD *(F−Fmin/Fmax−F),where KD= 345 nM, F= Fluo-4 intensity, Fmax= 640, and Fmin= 21.7 for Fluo-4.

2.4.3 Focal uncaging

Caged compounds were uncaged by photolysis using UV light (300-400 nm). For photolytic uncaging, an Olympus FV1000 MPE multiphoton laser scanning microscope equipped with an argon laser was utilized to produce a collimated light beam as the principal uncaging line at λ= 408 nm. To detect the effect of arsenic on IP3Rs in calcium pathways, 105 primary KC were plated on 2.4-mm coverslips in a 4-cm dish. For the arsenic treatment, the cells were pretreated with 1 μM caged IP3 for 2 hours and stained with the calcium dye Fluo-4 to analyze changes in intracellular calcium levels. The calcium-induced fluorescence was observed using an Olympus FV1000 laser-scanning microscope. Caged IP3 was uncaged by illumination with UV light (λ= 408 nm) and the released IP3 molecule was able to bind to an IP3R.

2.4.4 Western blot analysis

Western blot analyses were performed using whole-cell lysates. Briefly, cells were lysed by incubating for 30 minutes on ice in whole cell lysis buffer (1% glycerol, 1% Triton X-100, 1mM phenylmethanesulfonylfluoride, 10 μg/mL leupeptin, sodium 1 mM orthovanadate, 1 mM EGTA, 10 mM NaF, 1 mM sodium pyrophosphate, 100 μg β-glycerophosphate, 20 mM Tris-HCl, 137 mM sodium chloride, 5 mM EDTA, pH 7.9). Cell debris was removed by centrifugation at 10,000g for 10 minutes at 4°C. The protein concentration of cell lysates was determined using the Bradford method (Bio-Rad). Proteins (100 μg) in cell lysates were resolved using sodium dodecyl sulfate-polyacrylamide gel electrophoresis in a 7% gel and then transferred to a Hybond-P polyvinylidene fluoride membrane (Amersham Biosciences). The membrane was first incubated with primary antibodies against phospho-IP3R1 (Cell Signaling Technology), IP3R1 (Cell Signaling Technology), phospho-Akt (Epitomics, Burlingame), Akt (Epitomics), and actin (Sigma-Aldrich), and then with horseradish peroxidase-conjugated secondary antibodies. Immunoreactive proteins were visualized using enhanced chemiluminescence reagents (Amersham Biosciences).

Chapter III Exploring the role of TRP channels in UVB induced skin damage and aging

The original work was reported in Molecules (2015), and the publisher, MDPI, has allowed me to use this paper as part of my own PhD thesis.

The physical toxicant, UVB radiation with the wave length 280–320 nm, is the most cytotoxic and mutagenically stressful electro-magnetic wave, and leads to skin damage and aging [51]. Because the energy of UVB is sufficient to generate ROS in living tissue, UVB causes DNA impairment and tumorigenesis in skin associated with intracellular ROS and Ca^{2+} elevation [8]. These findings have all been independently established in different fields. This part of the research examines the role of Ca^{2+} signaling in response to UVB induced skin damage and aging.

3.1 Involvement of TRPCs in UVB induced Ca^{2+} elevation in skin cells

The role of Ca^{2+} signaling in the initial stages of response to UVB skin damage and aging was examined. Firstly, this study measured the intracellular Ca^{2+} concentration via fluo-4 staining. Initially the skin cells, KC and HDF, were exposed to UVB irradiation after pretreatment with Ca^{2+} influx inhibitors EDTA and Derinat for 30 min. After 30 min of UVB irradiation, the intracellular Ca^{2+} concentration was observed using an Olympus confocal fluorescence microscope and observed with an average fluorescence intensity of more than 150 cells. Fig. 5A, 5B show that EDTA and Derinat almost completely blocked the UVB-induced intracellular Ca^{2+} elevation in KC, while it showed a smaller but statistically significant reduction in the Ca^{2+} elevation for UVB treated HDF. These results suggested that blocking of Ca^{2+} influx inhibited the UVB induced Ca^{2+} elevation in both KC and HDF cells.

3.1.1 Mechanism of UVB induced Ca^{2+} elevation in skin cells

To further investigate the mechanism by which Ca^{2+} channels were involved in UVB induced Ca^{2+} elevation in skin, TG was utilized to raise cytosolic Ca^{2+} by depleting Ca^{2+} stores. As shown in Figure 5C, 5D, UVB did not alter the TG activated Ca^{2+} elevation in skin cells. Further experiments were designed to determine whether the TRP superfamily of cation channels were involved in UVB activated Ca^{2+} entry. Since DAG activates the majority of TRP channels [8,34], and UV light irradiation increases DAG [52], this study then attempted to decide whether the presence of cations precedes the activation of the TRP channels. As shown in Fig. 5E, 5F, TRPCs inhibitors, Derinat, 2-APB and SKF96365 [10,36,53], significantly decreased the Ca^{2+} elevation induced by a DAG analogue, membrane permeable OAG, in KC and HDF after 30 min of UVB exposure. Also, the OAG mediated Ca^{2+} peak was blocked by Derinat from 970 nM to 800 nM in KC (Fig. 5G) and from 1300 nM to 1100 nM in HDF (Fig. 5H), respectively.

Based on Venkatachalam's results published in 2007, TRPCs TRPV1 and TRPA1 are activated by DAG [34]. However, Figure 5E–H indicate that TRPV1 and TRPA1 are not involved in UVB induced Ca^{2+} elevation because no Ca^{2+} was increased with 2-APB treatment.

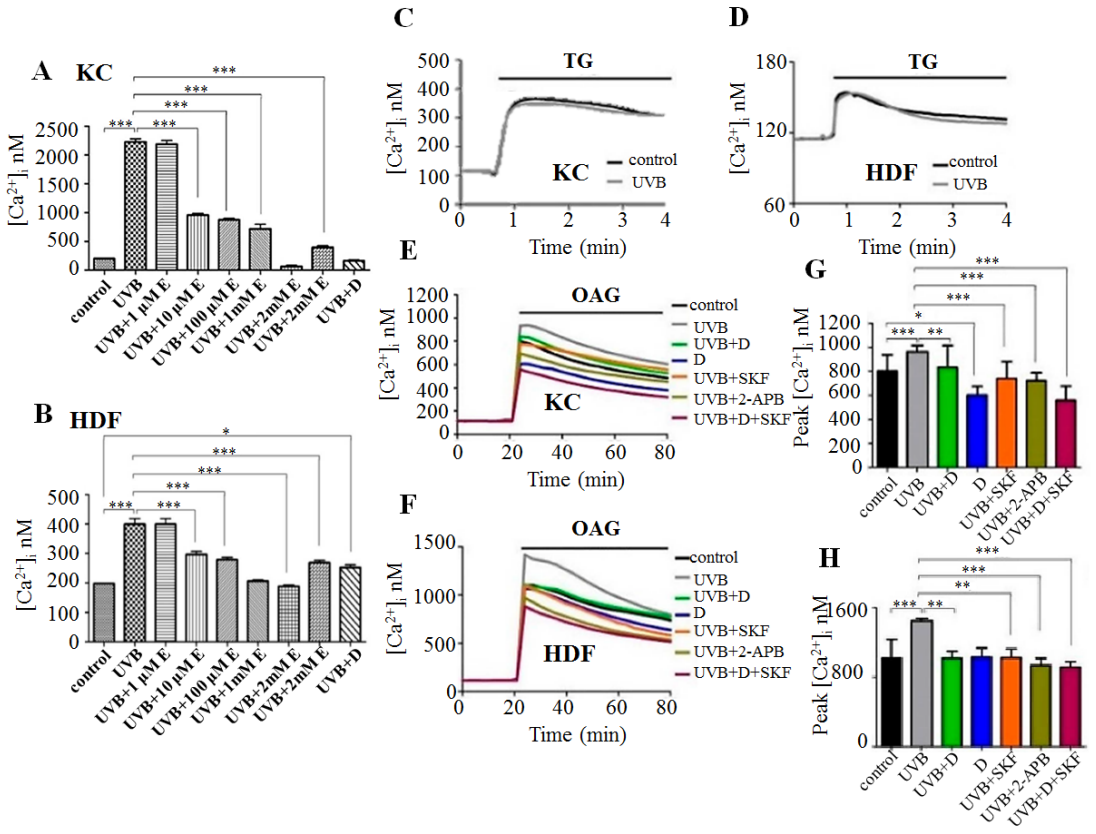

Figure 5. The effect of UVB irradiation on the intracellular Ca^{2+} signaling in skin cells. (A,B) After 30 min of UVB exposure, the mean value of intracellular Ca^{2+} was evaluated for control, UVB-exposed, UVB-exposed with different concentrations of EDTA, and UVB-exposure with Derinat and Derinat in KC and HDF cultured in BSS for 30 min pretreatment (*, $p < 0.05$; ***, $p < 0.001$). (C,D) Ca^{2+} imaging analysis was performed for the TG-induced Ca^{2+} response after the application of 20 nM TG (small black bars) in KC and 100 nM TG in HDF (n = 3). After 30 min of pretreatment with Derinat (D), SKF96365 (SKF, 20 μM in KC and 50 μM in HDF), 2-APB (2-APB, 50 μM in KC and 100 μM in HDF) and SKF+D, OAG at 100 μM and 200 μM was applied to (E) KC and (F) HDF, respectively, to stimulate the Ca^{2+} responses of TRPCs after 30 min of UVB exposure (n = 3). (G,H), quantification of the peak of the intracellular Ca^{2+} responses shown in (E) and (F) (*, $p < 0.05$; **, $p < 0.01$; ***, $p < 0.001$).

Whereas general TRP channel inhibitors efficiently blocked OAG activated TRP channels, experiments further confirmed whether TRPCs were activated by UVB or not. ATP was applied as a stimulator of TRPCs response, because ATP activates the PLC pathway via GPCR, which leads to the opening of TRPCs [36]. Therefore the effect of ATP on Ca^{2+} response induced by UVB was examined using skin cells. Irradiation with UVB slightly promoted the level of ATP activated Ca^{2+} response while the level of Ca^{2+} response was reduced slightly via treating with Derinat, SKF96365 and 2-APB (Fig. 6A-D). Thus, further attempts were carried out to demonstrate whether UVB activated TRPCs by DAG in the PLC pathway. As shown in the Fig. 6G–H, TRP channel inhibitors restrained UVB induced increase of Ca^{2+} influx by PLC stimulation in skin cells. Based on these results, it is reasonable to decide that TRPM5 and TRPM7 are also involved in PLC induced Ca^{2+} influx. Nevertheless, the population of TRPM5 in skin is in such a minute quantity [35] that TRPM can't be activated by DAG. Taken together, these results suggest that TRPCs are involved in UVB induced Ca^{2+} elevation, but it is important to determine which TRPCs are involved in UVB activated Ca^{2+} elevation by the use of each TRPC siRNA.

3.2 Effect of TRPCs inhibitor, Derinat, on UVB induced skin damage

3.2.1 Derinat reduced oxidative stress accumulation following UVB irradiation of skin cells

The first response to UVB irradiation is intracellular ROS generation in skin cells and then an elevation of intracellular Ca^{2+} [25]. Based on these results, Derinat decreased UVB induced Ca^{2+} increase. These results suggest that TRPCs inhibitor, Derinat, can protect skin cells from UVB induced damage by decreasing the level of Ca^{2+} dependent intracellular ROS production by mitochondria. This hypothesis was examined by performing the following experiments: 24 hours after UVB exposure, the level of intracellular Ca^{2+} was found to be slightly increased in KC and HDF (Fig. 7A, 7B). Pretreatment with TRPCs inhibitors Derinat or NAC, which is known as an intracellular ROS scavenger, inhibit UVB induced DNA damage in skin cells [54], and additionally suppress the UVB induced increased intracellular ROS levels in KC as well as HDF (Fig. 7C, 7D). The intracellular ROS production levels in KC and HDF were quantified and it was found that Derinat attenuated the UVB induced levels of ROS production by 2.25- to 1.67-fold and from 2.52- to 1.53-fold in KC and HDF, respectively (Fig. 7E, 7F). Similar results were also found in the NAC pretreated experiments (Fig. 7E, 7F). Taken together, it is reasonable to consider that the TRPC inhibitor, Derinat, suppressed UVB induced intracellular ROS production by reducing the intracellular Ca^{2+} elevation in skin cells.

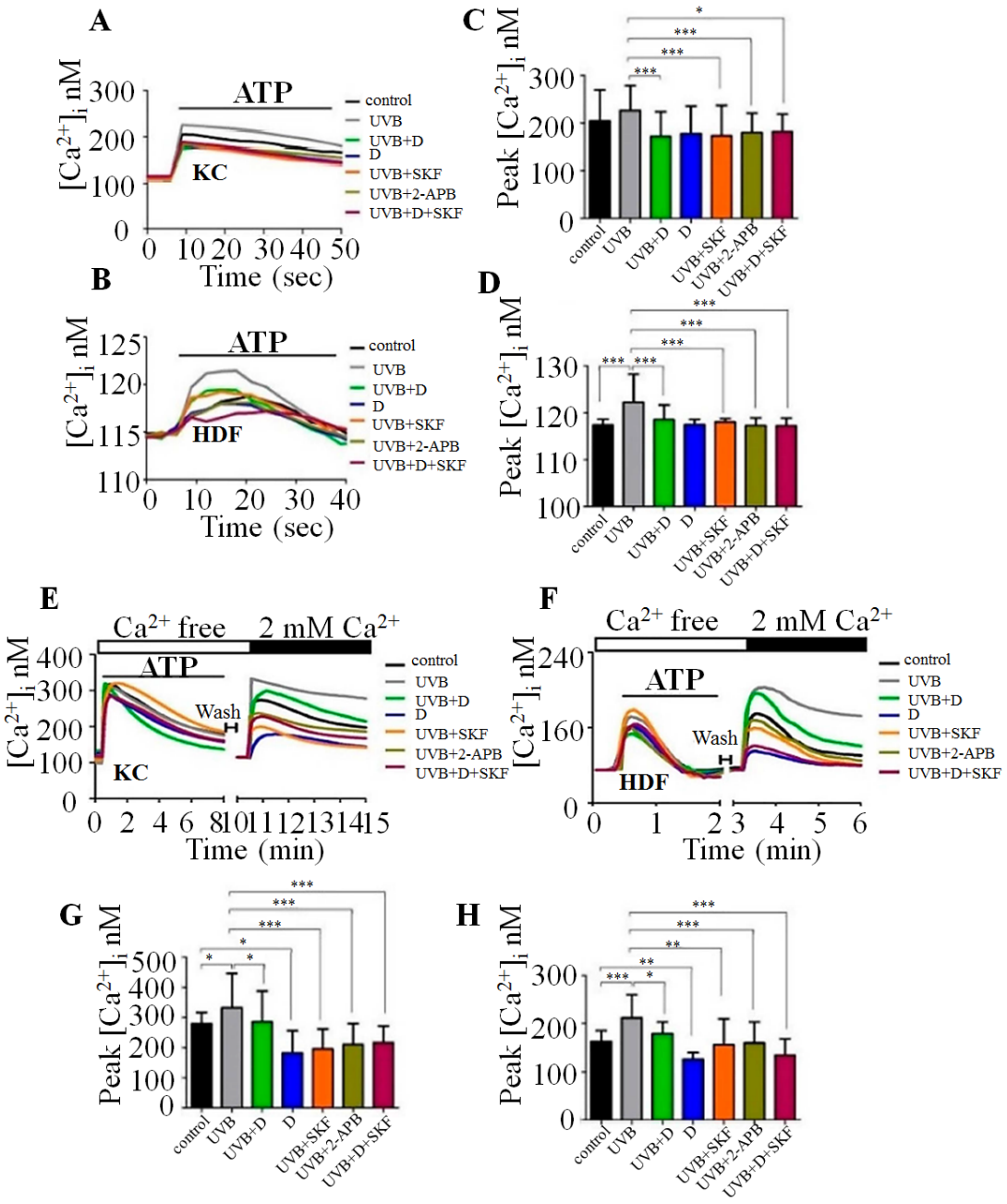

Figure 6. TRPCs inhibitors decreased UVB activated Ca^{2+} signaling in skin cells. Ca_{2+} imaging analysis of the adenosine triphosphate (ATP)-induced Ca^{2+} response. The application of 100 µM ATP (small black bars) in (A) KC and 200 µM ATP, and in (B) HDF (n = 3). (C,D), quantification of the peak of the intracellular Ca^{2+} responses shown in (A,B) (*, $p < 0.05$; ***, $p < 0.001$). $CaCl_2$ was extracellularly applied (large black bar) to increase Ca^{2+} from 0 to 2 mM and open the TRPCs after the application of ATP (small black bars) in (E) KC and in (F) HDF in Ca^{2+} free BSS solution (open bar) (n = 3). (G,H) quantification of the peak of the intracellular Ca^{2+} responses shown in (E,F) after applying $CaCl_2$ (*, $p < 0.05$; **, $p < 0.01$; ***, $p < 0.001$).

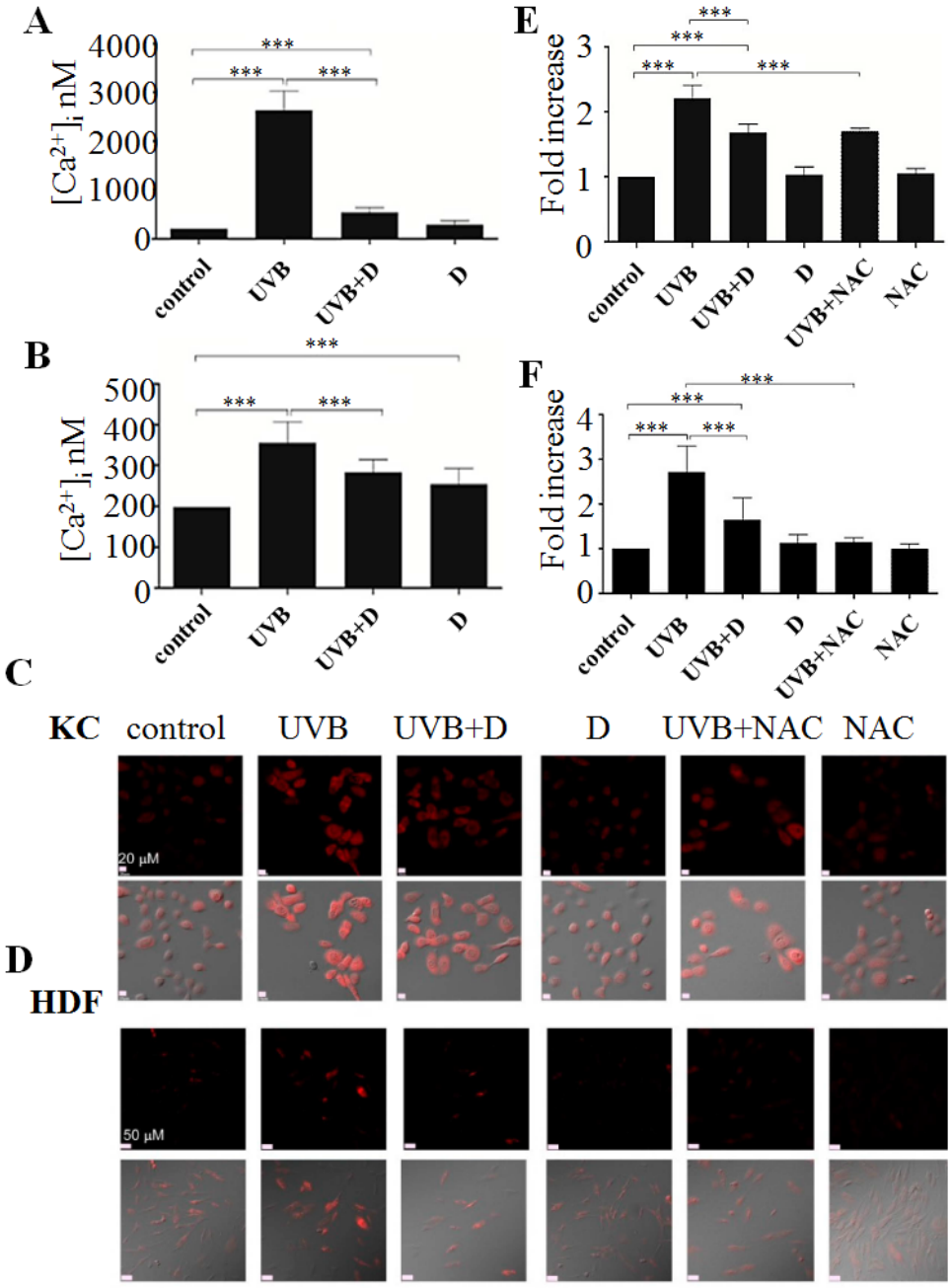

Figure 7. The effect of Derinat on UVB-induced intracellular Ca^{2+} concentration and ROS production in skin cells. (A) KC and (B) HDF were pretreated with or without the Derinat for 24 h and exposed to UVB. The intracellular Ca^{2+} concentration was then measured after 24 h of incubation in normal medium (***, $p < 0.001$). (C) KC and (D) HDF were pretreated with Derinat and 0.5 mM NAC for 24 h and then irradiated with UVB. The ROS generation was measured after 24 h of UVB irradiation by using 5 μM DHE staining. The intracellular ROS production level with an average fluorescence intensity of more than 150 cells from (C) and (D) is quantified in (E) KC and (F) HDF (***, $p < 0.001$).

3.2.2 Derinat protected skin Cells against UVB-induced DNA damage

UVB-induced intracellular ROS production has already been reported to contribute to nuclear and mitochondrial DNA damage, both of which are observed by 8-oxodG accumulations in skin cells [55]. As was described above, Derinat may protect skin cells from UVB-induced DNA damage by decreasing the level of intracellular ROS production. Therefore the effects of Derinat on UVB-induced DNA damage was investigated as follows. Skin cells were pretreated with Derinat or NAC for 24 h, and the ratio of DNA damage and then 8-oxodG was measured 24 h after UVB exposure. Pretreatment with both Derinat and NAC was found to reduce the ratio of DNA damage from 51% to 12% and from 51% to 23%, respectively (Fig. 8A, 8B). Similar results were also observed in HDF, but Derinat and NAC pretreatment reduced the ratio of DNA damage to 2% and 3%, respectively (Fig. 8C, 8D). These results support the above findings in skin cells: Derinat protects skin cells against UVB-induced injury by suppressing intracellular Ca^{2+} elevation, intracellular ROS production and DNA damage, all of which helps skin cells to avoid skin impairment and reduces the aging potential.

3.2.3 Interruption of TRPCs by Derinat protected BALB/c-nu mice from UVB-induced skin damage

Next, experiments were performed to determine whether blockade of TRPCs protected animal skin from UVB-induced damage by observing the desquamation, epidermal thickness, ROS production and DNA damage in BALB/c-nu mice. Derinat is a water-soluble reagent; therefore, Derinat does not easily enter into skin. I cooperated with SOMAPEX BIOTECH. Co. (Kaohsiung, Taiwan) to develop a special hydrogel of Derinat (D hydrogel). Derinat hydrogel was found to help skin tissue absorption of this drug by modification of the skin surface, perhaps by changing charge distribution on the pores of the skin surface [56,57]. The Derinat-containing hydrogel was formed into a 3-cm diameter circular chip. Three different concentrations of Derinat in hydrogels were prepared for the *in vivo* experiments as follows: 0 (control), 3.5 μg/cm2 (15 μg/mL) and 14 μg/cm^2 (60 μg/ml). During the experiment, the BALB/c-nu mice were mechanically immobilized. The skin of each mouse was covered with different concentrations of Derinat hydrogel for 3 h. After 3 h of treatment by Derinat hydrogel, the BALB/c-nu mice were irradiated with 360 mJ/cm^2 UVB light [9]. Seven days after treatment, this radiation exposure resulted in severe desquamation and erythema of the dorsal skin in BALB/c-nu mice, and, as demonstrated in Fig. 9A and 9B, the Derinat treatment resulted in recovery of the reduction of the epidermal thickness and intracellular ROS production induced by UVB. Since the intracellular Ca^{2+} concentration can upregulate COX-2, which is known to be controlled by UVB

induced inflammation [58,59], COX-2 expression was also expected to increase in response to UVB irradiation of the mouse epidermis [59]. Therefore, experiments were performed to determine whether Derinat can affect COX-2 expression in skin cells. As shown in Fig. 9A, 9C, Derinat treatment reduced the expression of COX-2 as was expected. Moreover, Derinat was found to protect skin cells from UVB-induced DNA damage in BALB/c-nu mice (Fig. 9A).

To further elucidate the protective effect of Derinat on skin cells for UVB- induced DNA damage, a small piece of dorsal skin was removed and then the genomic DNA was extracted from and the percentage of DNA damage was measured using an HT 8-oxodG ELISA kit II (Trevigen Inc., Gaithersburg, MD, USA). The quantitative analysis of 8-oxodG is depicted in Fig. 9D, which demonstrates that Derinat suppressed the UVB-induced DNA damage in a dose dependent manner in mouse skin. Taken together, the *in vivo* experimental results revealed that Derinat effectively decreased the UVB-induced destructive effects on skin, such as desquamation, epidermal proliferation, intracellular ROS production, DNA damage and the expression of COX-2 in BALB/c-nu mouse skin. Interestingly, the response of HDF to UVB irradiation was not as large as that of KC based on the results presented here. The inhibition of UVB-induced intracellular Ca^{2+} elevation contributed significantly to the decreased level of intracellular ROS production by mitochondria, which diminished DNA damage in skin cells. The results of the *in vivo* experiments further supported that TRPCs blocking effect by Derinat attenuated UVB-induced intracellular ROS production, COX-2 expression and DNA damage in the skin of BALB/c-nu mice exposed to UVB for seven days. Thus, TRPCs could be the initiator of UVB-induced skin damage and even aging (Fig. 10).

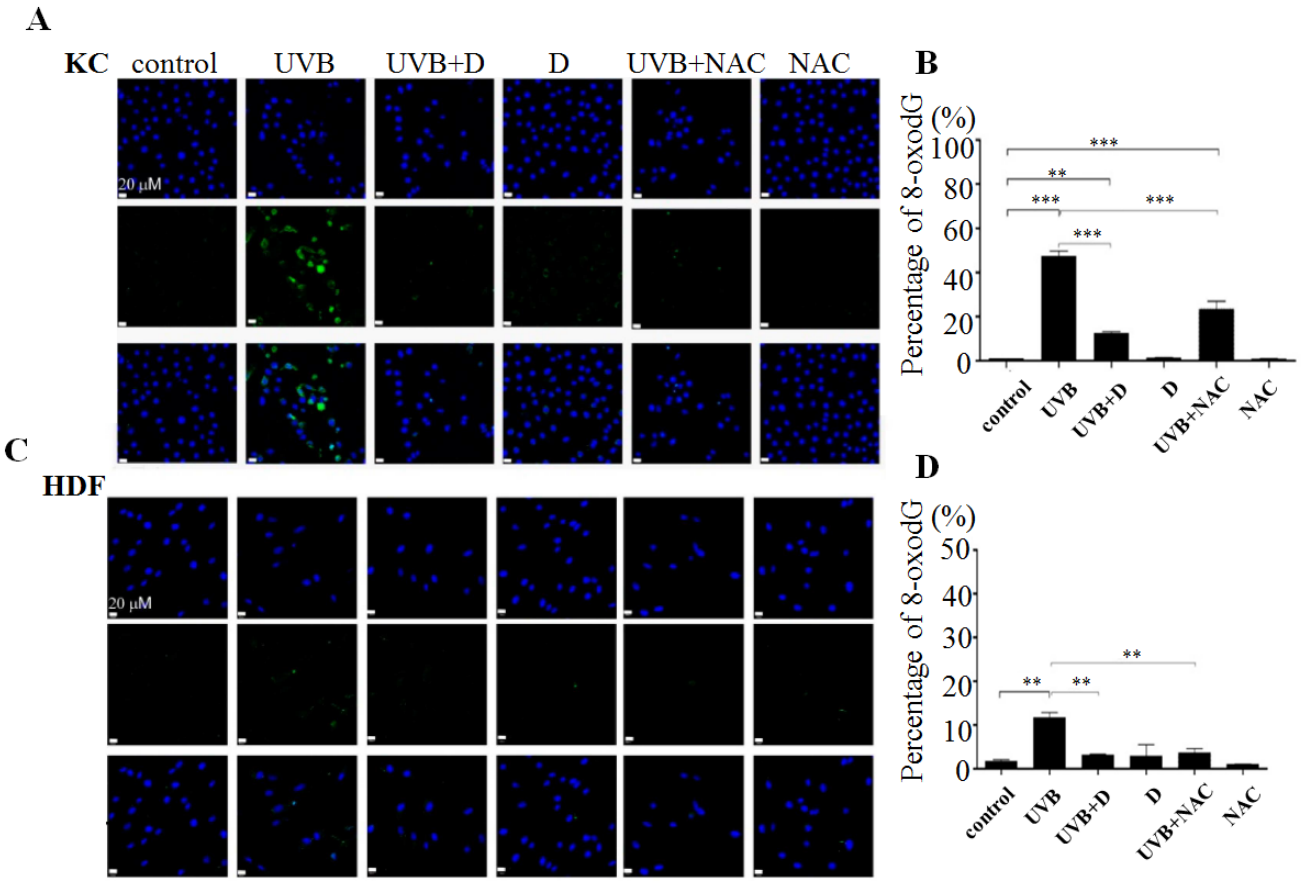

Figure 8. The effect of Derinat on the UVB-induced DNA damage in skin cells. 8-oxodG was detected to determine the DNA damage resulting from UVB exposure in cells pretreated with Derinat and NAC: (A) KC and (C) HDF. The relative values of DNA damage from 8-oxodG are quantified in (B,D) (**, $p < 0.01$; ***, $p < 0.001$). The data shown represent the average of three independent experiments.

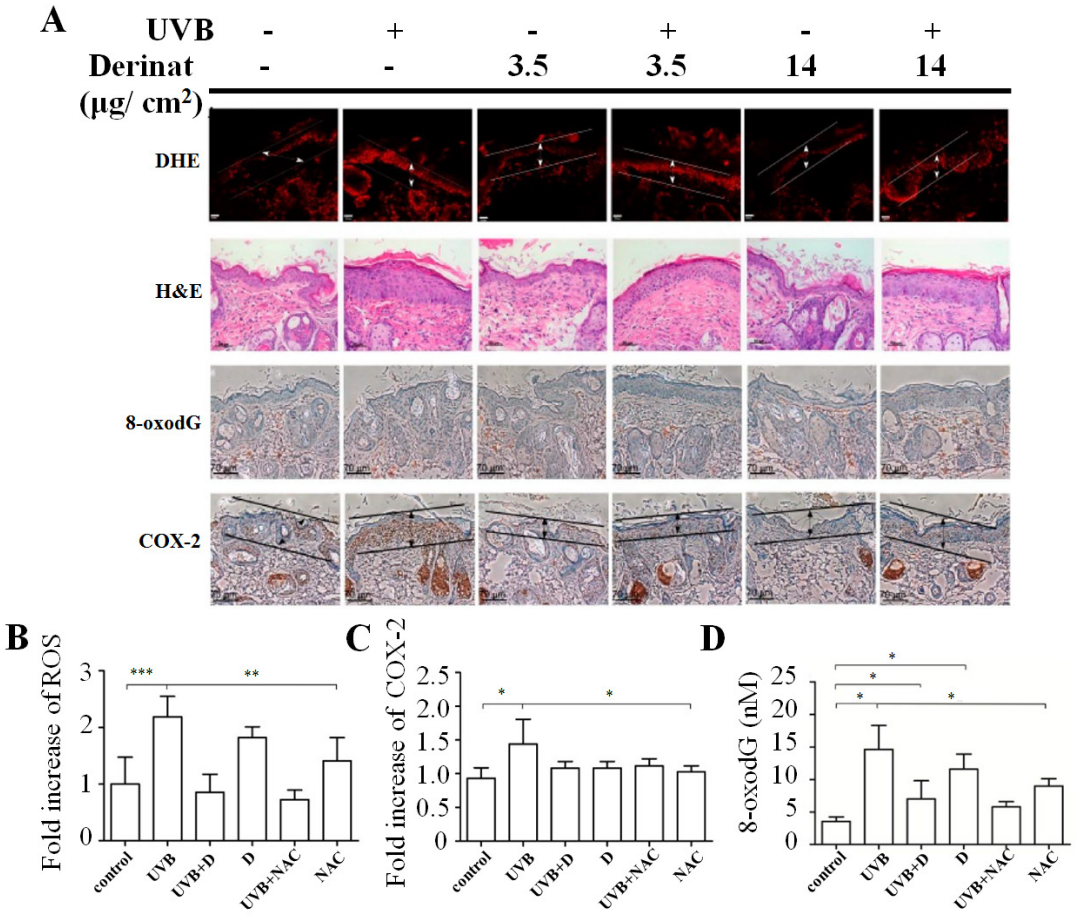

Figure 9. The effect of Derinat on UVB-induced skin damage in BALB/c-nu mice. BALB/c-nu mice were covered with Derinat hydrogel or pure hydrogel for 3 h and then irradiated with 360 mJ/cm^2 UVB. After seven days, the experimental animals presented UVB-induced damage in the dorsal areas of skin as determined by histological analysis. (A) Derinat protected BALB/c-nu mice skin from UVB-induced epidermal proliferation, DNA damage and cyclooxygenase COX-2 expression. The skins of normal and UVB irradiated mice covered with Derinat hydrogel or hydrogel were stained with DHE and H & E (hematoxylin and eosin), and the oxidative DNA damage as denoted by the presence of 8-oxodG was analyzed via an immunohistochemical assay with a specific anti-8-oxodG mouse monoclonal antibody. The expression of COX-2 in the epidermis was detected with an anti-COX-2 rabbit monoclonal antibody; (B,C), the quantification of intracellular ROS production and COX-2 level from (A) shown by regions indicated with arrows includes both epidermis and dermis without sebaceous glands (*, $p < 0.05$; **, $p < 0.01$; ***, $p < 0.001$). (D) Derinat downregulated the UVB-induced level of DNA damage indicated by 8-oxodG in BALB/c-nu mouse skin based on ELISA assays respectively (*, $p < 0.05$; **, $p < 0.01$).

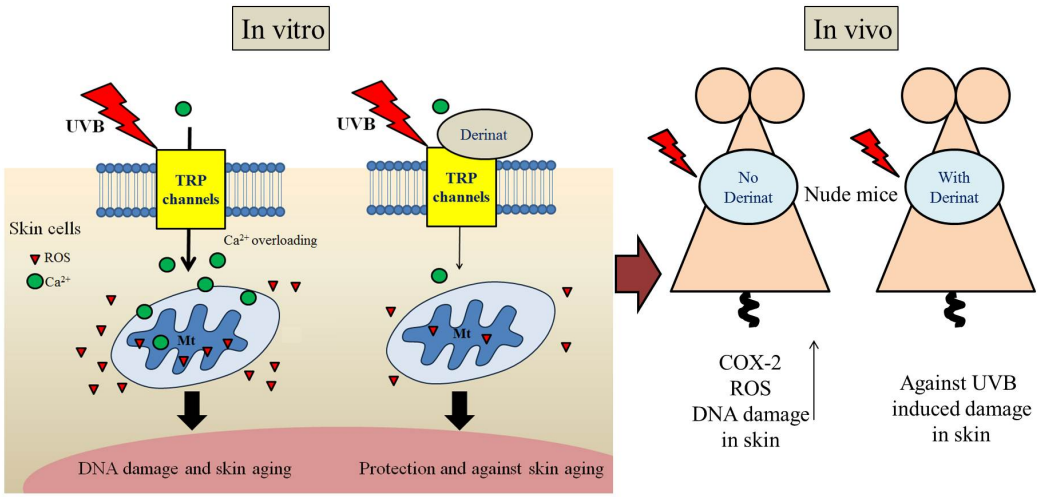

Figure 10. TRPCs inhibitor, Derinat attenuates UVB-induced skin damage. Derinat protects skin cells from UVB-induced damage by suppressing TRPCs-activated Ca^{2+} entry. The inhibition of intracellular Ca^{2+} elevation also contributed significantly to the decreased level of intracellular ROS production by mitochondria, which mitigated DNA damage *in vitro*. The results of the *in vivo* experiments further supported that Derinat attenuated intracellular ROS production, COX-2 expression and DNA damage in the skin of BALB/c-nu mice exposed to UVB for seven days.

3.3 Chemical reduction of oxidized protein by hydrogen gas solved water

As described above, Ca^{2+} elevation is crucial to produce large amounts of intracellular ROS. According to some theories, aging results from the accumulation of damaged and/or abnormal proteins in the cytosol, chemical damage in macromolecules, and mitochondrial DNA changes[60]. This hypothesis originated from the proposal that oxygen was poisonous[61], followed by the notion that ROS was a cause of aging, and it eventually evolved into the oxidative stress theory in 1972[62]. Among the large number of aging models proposed so far, the oxidative stress hypothesis seemed to be the most likely, because ROS are usually produced in aerobic cells. Several types of ROS, such as superoxide radicals ($\dot{O}_2^-$), hydrogen peroxide (H_2O_2), and hydroxyl radicals ($\dot{H}O$) may damage many types of cellular components. Data about damage caused by ROS comes from a plethora of cellular and biologic data from various model systems and organisms[63]. Despite the enormous amount of data, however, the molecular

mechanisms of aging are not clearly elucidated yet.

3.3.1 Disulfide bonds formation in intracellular proteins by ROS

The hydroperoxide, H_2O_2, is generally used as an instrumental ROS species despite some limitations, such as the complex effects of H_2O_2 on catalase. Further, H_2O_2 can enter into the cell across cell membranes by aquaporin channels[64] and act as superoxide anions. Major ROS released from the mitochondria are converted to H_2O_2 by superoxide dismutase[65]. The increased level of H_2O_2 is thought to mimic the aging process[66]. In addition, H_2O_2 selectively allowed for the oxidization of cysteine sulfhydryl groups to make cysteine sulfonic acid or disulfide bonds[67], inducing protein dysfunction in the cytosol with the formation of disulfide bonds[68]. Therefore, H_2O_2 impairs various physiologic processes via the oxidation of thiols, especially those in proteins. Over the last 20 years, Ca^{2+} signaling has been classified as essential for normal physiologic processes[69-71]. The effect of protein oxidation (or effects of aging) on Ca^{2+} signaling has accordingly become an important research topic. Based on several published results, most aged cells showed decreased Ca^{2+} responses due to the decreased Ca^{2+} release from endoplasmic reticulum[72-74]. These findings suggest that IP_3Rs arbitrated Ca^{2+} release from ER must also be lower [72]. Accordingly, the aging-related reduction of Ca^{2+} signaling may be initiated by H_2O_2 induced disulfide bond formation.

3.3.2 Reduced Ca^{2+} signaling in KC

To identify the types of signaling molecules affected by aging in skin cells, different concentrations of H_2O_2 were used to mimic the aging process oxidized by ROS. Approximately 10^5 KC cells were plated onto 24-mm coverslips in 3.5-cm^2 dishes, incubated for 2 days, were pre-stained with 20 μM DCFH-DA, then treated with 5 μM, 50 μM, or 500 μM H_2O_2. Imaging of the DCFH-DA staining showed ROS generation in the cells, as shown by an increase in fluorescence intensity, and dose-dependent effects of H_2O_2 exposure were monitored with time-lapse recordings (Fig. 11A). The cell morphology was not significantly different between treatments as visualized by differential interference contrast imaging (Fig. 11A). Similar results were also observed with 5 μM MitoSOX (Molecular Probes) staining (Fig. 11B). Quantification was done by flow cytometry (Fig. 11C), which showed that approximately 40% of the cells produced ROS following 500 μM H_2O_2 exposure, 20% after 50 μM H_2O_2 exposure, and 5% by 5 μM H_2O_2 exposure (Fig. 11C). A Ca^{2+}concentration and fluorescence intensity calibration curve was determined as shown in Fig. 12A. H_2O_2 decreased ATP (stimulant)-induced Ca^{2+} elevation and SOCE in a dose-dependent manner in KC cells (Fig. 12B). H_2O_2 also changed ATP-induced Ca^{2+} release via the

purinergic GPCRs and SOCE as well. To identify the intracellular Ca^{2+} changes in detail, the ATP-induced Ca^{2+} signal was observed by measuring the black area under the curve (Fig. 12C). Relative to the control response, the Ca^{2+} signal was reduced to 72 ± 13% by the 5 μM H_2O_2 group and to 54 ± 10% in the 50 μM H_2O_2 group, while the peak in each group was estimated to be 433 ± 43 nM for vehicle, and 383 ± 75 nM for 5 μM H_2O_2 treatment and 245 ± 21 nM for 50 μM H_2O_2 treatment (Fig. 12D, E). Interestingly, ATP stimulation did not induce Ca^{2+} elevation in treated KC when it was treated by 500 μM H_2O_2 (Fig. 12C). Here the value of baseline corresponded to 185 ± 23 nM of Ca^{2+}.

As was previously reported, increased phosphorylation of IP_3Rs suppresses both ATP induced Ca^{2+} release and SOC channel-mediated Ca^{2+} entry[75]. Therefore, further experiments examined whether H_2O_2 enhanced IP_3Rs phosphorylation levels using uncaged IP3. Intracellular application of uncaged IP3 resulted in Ca^{2+} elevation in Ca^{2+} free BSS buffer without involvement of PKC activation; in this case the Ca^{2+} elevation was reduced by treatment with H_2O_2, indicating that H_2O_2 condensed IP_3Rs function (Fig. 12F). The total Ca^{2+} response is represented by a bar chart, which was quantified by the measurement of the black areas under the Ca^{2+} response curves (Fig. 12G). Compared with vehicle application, H_2O_2 dose-dependently reduced the uncaged IP3-induced Ca^{2+}elevation, and the Ca^{2+} response was almost completely blocked by 500 μM H_2O_2 (Fig. 12G). The rate of Ca^{2+} concentration decay was found to be similar between the ATP- and uncaged IP3-induced Ca^{2+} responses (Fig. 12C, 12F). These findings indicate that H_2O_2 changed IP3Rs function, resulting in the suppression of Ca^{2+} elevation due to oxidative stress, therefore an increased IP3Rs phosphorylation model can be excluded as a mechanism underlying the ROS-dependent reduction in the Ca^{2+} response in KC.

3.3.3 ATP-induced Ca^{2+} signaling was inhibited by disulfide bond formation in KC IP3Rs

Because the suppression of the uncaged IP3-induced Ca^{2+} signal was clearly not due to IP3Rs phosphorylation, a novel mechanism to explain the results was hypothesized. It is worth noting that oxidative stress can induce disulfide bond formation, thus impairing molecular chaperoning, translation, glycolysis, cytoskeletal structure, cell growth, and signal transduction[68]. H_2O_2 can oxidize cysteine sulfhydryl groups to cysteine sulfenic acid or disulfide bonds[67], raising the possibility that H_2O_2 decreased the Ca^{2+} signal by eliciting IP3Rs disulfide bond formation. This possibility was examined using the reduction agent 2-ME. ATP-induced Ca^{2+} elevation was completely inhibited by 500 μM H_2O_2 (Fig. 13A, 13B), but the Ca^{2+} response partially recovered, increasing from 0% to 43 ± 3.5% when 10 mM 2-ME and H_2O_2 were applied together

(500 μM H_2O_2+ 2-ME; Fig. 13A,13B). 2-ME increased the Ca^{2+} peak from 198 nM (500 μM H_2O_2) to 248 (500 μM H_2O_2+ 2-ME; Fig. 13C). To further examine the effect of 2-ME on IP_3Rs, caged IP3 was utilized to detect whether only IP3Rs functionality was reduced by H_2O_2-induced disulfide bond formation. As expected, the Ca^{2+} released in response to uncaged IP_3 stimulation was largely recovered, increasing from 3 ± 3% to 62 ± 5% (500 μM H_2O_2+ 2-ME) relative to the vehicle, when 2-ME was applied with H_2O_2 (Fig. 13D, 13E). When 2-ME was applied alone 30 min before uncaging, the Ca^{2+} response partially decreased. When 2-ME and H_2O_2 were applied together, however, the H_2O_2-induced decrease was protected to some extent (Fig. 13D). Thus, it is reasonable to determine 500 μM H_2O_2-induced reduction of the Ca^{2+} signal was dependent on disulfide bond formation in IP3Rs. These results suggest that disulfide bond formation in IP3Rs induces a conformational change and obstructs IP_3 binding to IP3Rs under oxidative stress. Because the aging process is associated with both oxidative stress and Ca^{2+} deficiency[72], it is reasonable to suggest that ROS-induced protein disulfide bond formation is a mechanism involved in the skin aging process.

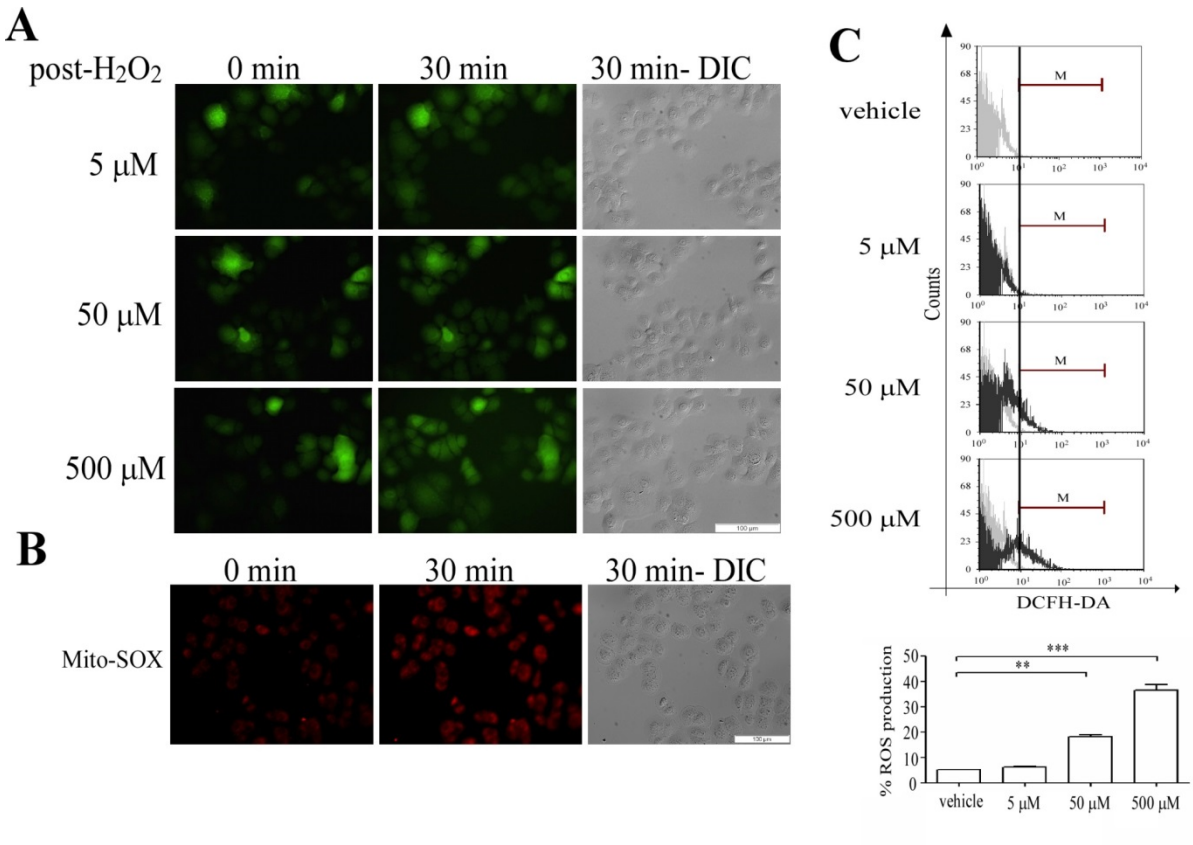

Figure 11. H_2O_2-induced oxidative stress in KC. ROS generation was stimulated by 5 µM, 50 µM, and 500 µM H_2O_2 for 30 min at 37°C in humidified 5% CO_2 and visualized using DCFH-DA or MitoSOX pre-staining. ROS are indicated by the fluorescent signals of (A) DCFH-DA or (B) MitoSOX, and cell morphology is shown using differential interference contrast (DIC) microscopy. Scale bars in A and B = 100 µm. (C) Quantification of ROS production was analyzed using flow cytometry after incubation with H_2O_2. Each group (black line) was compared with the vehicle (gray line) and ROS production was quantified (lower panel) by adding all black areas and subtracting all gray areas within the period marked by the red line "M", using FCS Express 4 Image Cytometry Software (De Novo Software) (**, P <0.01; ***, P <0.005).

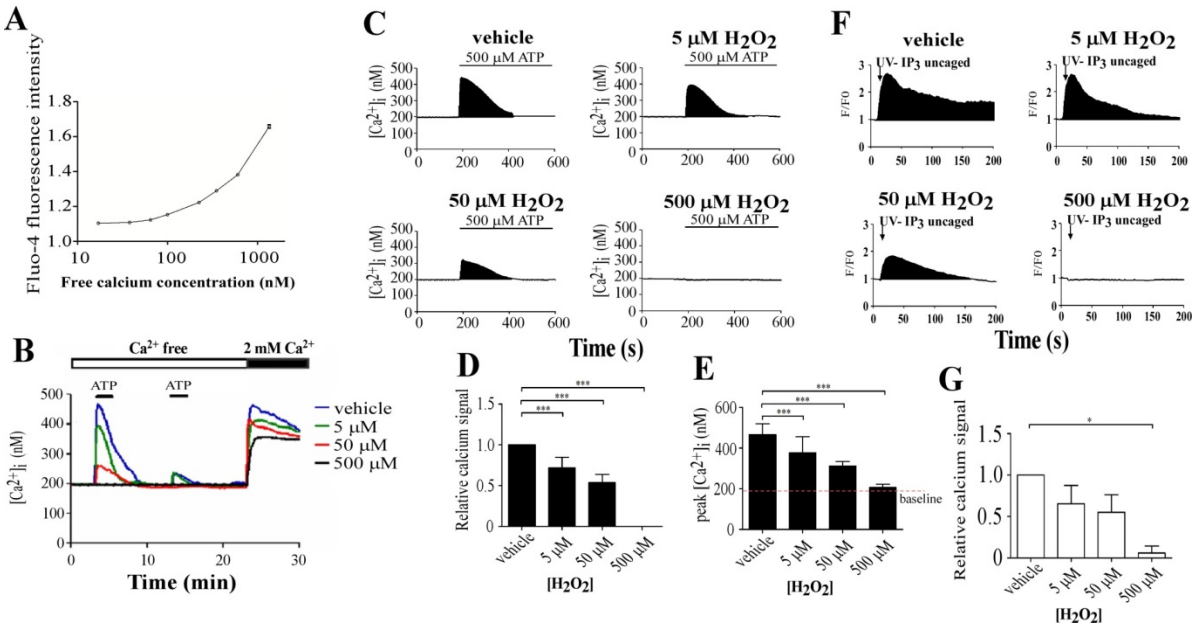

Figure 12. Effect of H_2O_2 on ATP-induced Ca^{2+} signaling in KC. (A) Ca^{2+} calibration curve. Horizontal axis indicates the free concentration of Ca^{2+} ($[Ca^{2+}]_i$) in standard buffer solution. Vertical axis indicates the ratio of Fluo-4 fluorescence intensity relative to that of baseline fluorescence. (B) Effect of H_2O_2 on ATP-induced Ca^{2+} signal. Ca^{2+} imaging analysis of the ATP-induced Ca^{2+} response after 30-min pretreatment with vehicle (blue), 5 μM (green), 50 μM (red), and 500 μM (black) H_2O_2. Ca^{2+} signals represent the mean value of 20 cells. Twenty-three minutes after two applications of ATP (small black bars) at 10-min intervals in Ca^{2+}-free BSS solution (open bar), $CaCl_2$ was applied extracellularly (large black bar) to increase Ca^{2+} from 0 to 2 mM to open the store-operated Ca^{2+} channels (N=5). (C) The Ca^{2+} signal from the first simulation with ATP in (B) is shown. (D) Relative Ca^{2+} signals were measured by calculating the black areas under the curves of the intracellular Ca^{2+} responses with or without H_2O_2 treatment in (C) (***, $P < 0.005$ in D and E). (E) Quantification of the peak ATP-induced Ca^{2+} elevation for all groups in (C). (F) Effect of H_2O_2 on the IP_3-induced Ca^{2+} response. The concentration of H_2O_2 used is indicated. F/F0 expresses the Fluo-4 fluorescence (F) relative to baseline fluorescence (F0), which corresponds to changes in the intracellular Ca^{2+} concentration. Uncaging of caged-IP_3 using UV irradiation released IP_3 molecules in the cell. The black area under the curve indicates the amount of Ca^{2+} released by uncaged IP_3 (N=5). (G) The amount of Ca^{2+} was calculated by quantifying the black areas under the Ca^{2+} curve (*, $P < 0.05$).

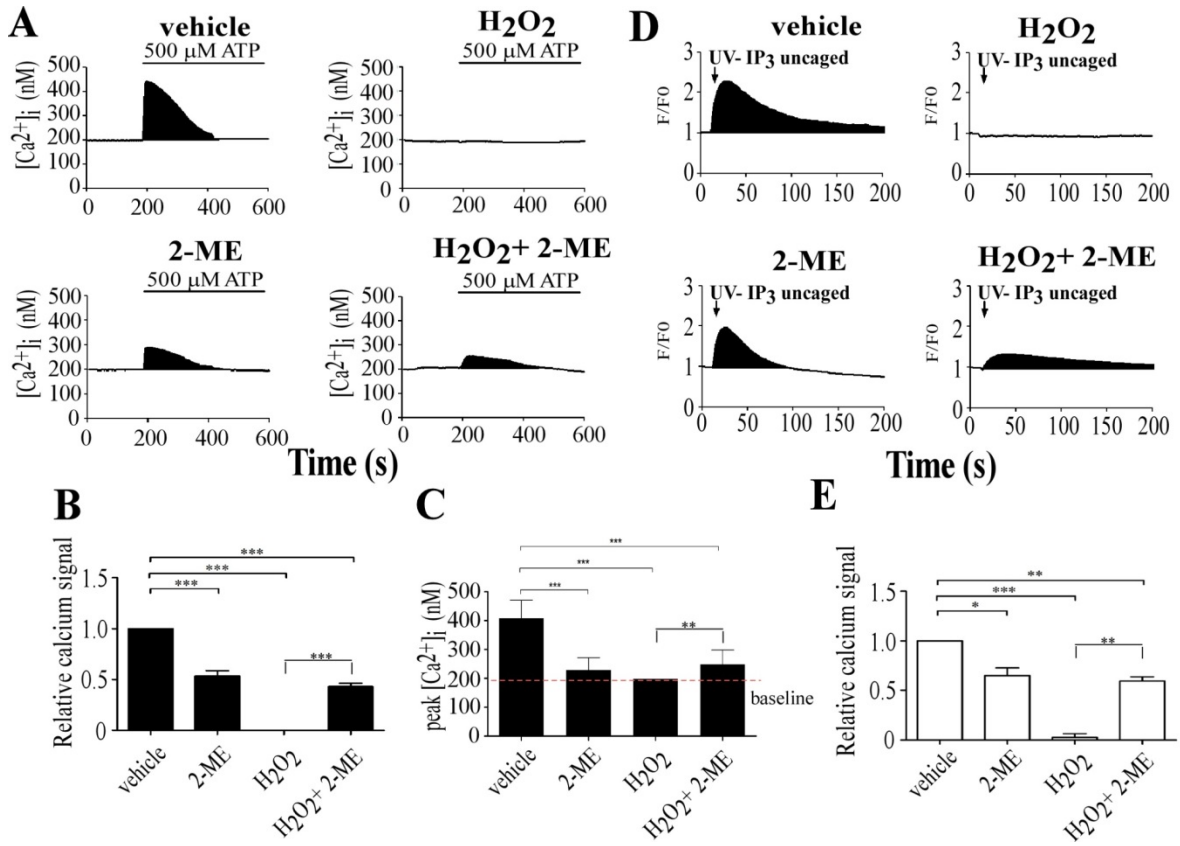

Figure 13. H_2O_2 impairment of ATP- and IP3-induced Ca^{2+} response in KC was restored by 2-ME. (A) Ca^{2+} signal in each group (pretreatment with vehicle, 2-ME, 500 μM H_2O_2, and 500 μM H_2O_2 + 2-ME) was induced by addition of ATP (black bars). (B, C) Quantification of the black areas representing ATP-induced Ca^{2+} signals (B) and the peak of the intracellular Ca^{2+} responses (C) shown in (A) (N=3). (D) Ca^{2+} signal in each group (pretreatment with vehicle, 2- ME, 500 μM H_2O_2, 500 μM H_2O_2 + 2-ME) was stimulated by UV-induced uncaging of caged-IP3. (E) Quantification of the black areas in (D) represent the amount of Ca^{2+} released by the uncaged IP3 (*, P< 0.05; **, P <0.01; ***, P <0.005).

3.3.4 Hydrogen gas containing media block disulfide bonds formation in proteins

Recently, H_2-containing medium was reported to protect against ROS-induced damage by buffering the effects of oxidative stress or superoxide formation[76]. Thus, the effect of H_2 was investigated to determine if it protects against H_2O_2 oxidized IP3Rs function and reduction of the resulting Ca^{2+} signal. Preparation and how to use H_2-containing BSS is described in the Materials and Methods section. The H_2-containing BSS was stored in an open glass bottle, and the hydrogen concentration in the media was measured every hour for 12 h using a hydrogen electrode. The half-life of H_2 concentration decrease was approximately 6 h in BSS (Fig. 14A). Because the lower limitation of effective H_2 concentration is 0.08 ppm[76], all the experiments were designed to finish within a few hours. To examine the effect of H_2-BSS on H_2O_2-recreased IP_3Rs function, the following four groups were evaluated: vehicle, 500 μM H_2O_2, 500 μM H_2O_2 with 2-ME, and 500 μM H_2O_2 with H_2 in BSS buffer. Ca^{2+} release in KC was induced with the addition of 500 μM ATP. Both the 500 μM H_2O_2 with 2-ME and the 500 μM H_2O_2 with H_2 groups produced similar results, in that the Ca^{2+} was 65 ± 14% (500 μM H_2O_2+ 2-ME) or 79 ± 12% (500 μM H_2O_2+ H_2) relative to that of the vehicle group (Fig. 14B, 14C, 14D) and peaked at 385 ±expected. IP3Rs function was partially protected by treatment with H_2. In the focal IP3 uncaging experiment, the IP_3 mediated Ca^{2+} signal in 2-ME treated cells was 71 ± 7% (500 μM H_2O_2+ 2-ME) that of vehicle and the Ca^{2+} signal of H_2-treated cells was 80 ± 3% (500 μM H_2O_2+ H_2; Fig. 14E, 14F). These results suggest that H_2-containing BSS protected the ATP-induced Ca^{2+} signal in skin by reducing the disulfide bonds in IP3Rs formed due to H_2O_2 exposure.

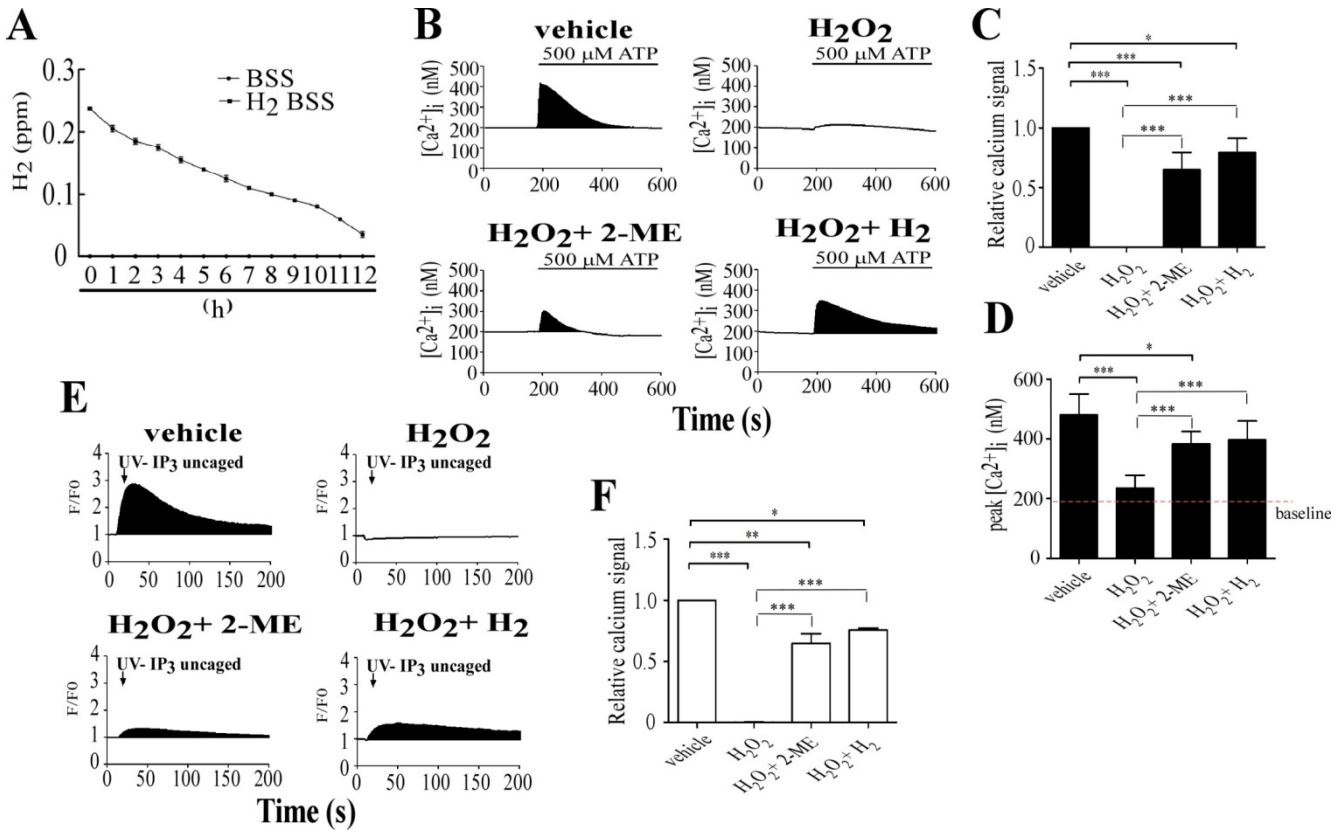

Figure 14. Effect of H_2 on H_2O_2-induced reduction of Ca^{2+} signaling in KC. (A) Time-dependent reduction of H_2 content in BSS buffer. (B) Mean Ca^{2+} response to ATP application in each group: vehicle, 500 μM H_2O_2, 500 μM H_2O_2+ 2-ME, and 500 μM H_2O_2+ H_2. (C) The Ca^{2+} response was quantified by measuring the black areas under the Ca^{2+} curve. (D) The peak of ATP-induced intracellular Ca^{2+} signal (N=5). (E) Protective effect of H_2-BSS on H_2O_2-induced reduction of the uncaged IP_3-stimulated Ca^{2+} response. Ca^{2+} signals are shown as black areas after uncaged IP3 stimulation. (F) Quantification of Ca^{2+} signals by measuring the black areas under the Ca^{2+} response curve (N=5) (*, P< 0.05; **, P <0.01; ***, P <0.005).

3.3.5 Recovery of Ca^{2+} mobilization by reducing disulfide bonds formation but not by quenching ROS

Since 2-ME-BSS and H_2-BSS had different effects on 500 μM H_2O_2-induced damage of Ca^{2+} release with IP_3Rs in KC, additional experiments were performed to define the difference between the effects of H_2 and 2-ME. Briefly, cells were pretreated with 2-ME or H_2 gas for 30 min and compared (Fig. 15A). Protection of the Ca^{2+} signal following pretreatment with H_2-BSS (500 μM H_2O_2+ pre-H_2) was 185 ± 19% of that following pretreatment with the vehicle (Fig. 15B and 15C), while no Ca^{2+} signal was observed following pretreatment with 2-ME (500 μM H_2O_2+ pre-2-ME) (Fig. 15B). The enormous difference between the effects of pre-treatment with H_2-BSS and 2-ME may be due to the different mechanisms by which they reduce disulfide bond formation in IP3Rs. 2-ME is a strong reducing agent that reduces all proteins in the cell, leading to considerable conformational change and thereby dysfunction. Pretreatment with 2-ME could reduce all proteins to the extent that no Ca^{2+} signal can be induced by ATP stimulation. Furthermore, to further examine whether H_2-BSS protected against H_2O_2 damage by reducing disulfide bond formation, non-reducing SDS-PAGE and Western blot analysis were performed. Further investigation concentrated on the formation of disulfide bonds of IP3Rs with three subtypes: IP3R1, IP3R2 and IP3R3. As shown in Fig. 15D, IP3R1 with disulfide bonds, observably detected by IP_3R1 antibodies, migrated in a broad band. However, IP3R2 and IP3R3 did not present clear disulfide bonds formation based on the similar molecular weight of broad bands (Fig. 15D). The formation of disulfide bonds affects the conformation and electrophoretic mobility of redox-sensitive proteins[77-79]. Proteins forming intra-molecular disulfide bonds exhibit distinct types of migration in non-reducing (without 2-ME) SDS-PAGE and reducing SDS-PAGE (with 2-ME). As expected, KC exposed to H_2O_2 had IP3R1 containing disulfide bonds, as evidenced by the lower broad band when electrophoresed under non-reducing conditions, but KC treated with a reducing agent (2-ME, H_2 or pre- H_2) had a higher band and lightly stained bands similar to the vehicle-treated KC (Fig. 15D). Western blot analysis also confirmed no effect on the level of IP3R1 phosphorylation (Fig. 15E). This finding suggests that the reducing agents potentially altered the conformation of the IP3R1 by breaking disulfide bonds, yet neither reducing agent completely reduced of IP3R2 and IP3R3 disulfide bonds in the cell. This result explains why the IP3Rs-mediated Ca^{2+} signal was not completely protected with application of 2-ME or H_2. These reducing agents may not be able to reach the inside of the protein structure; this was supported by prolonging treatment by an additional 30 minute treatment by H_2-BSS as shown in Figs. 15B and 15C.

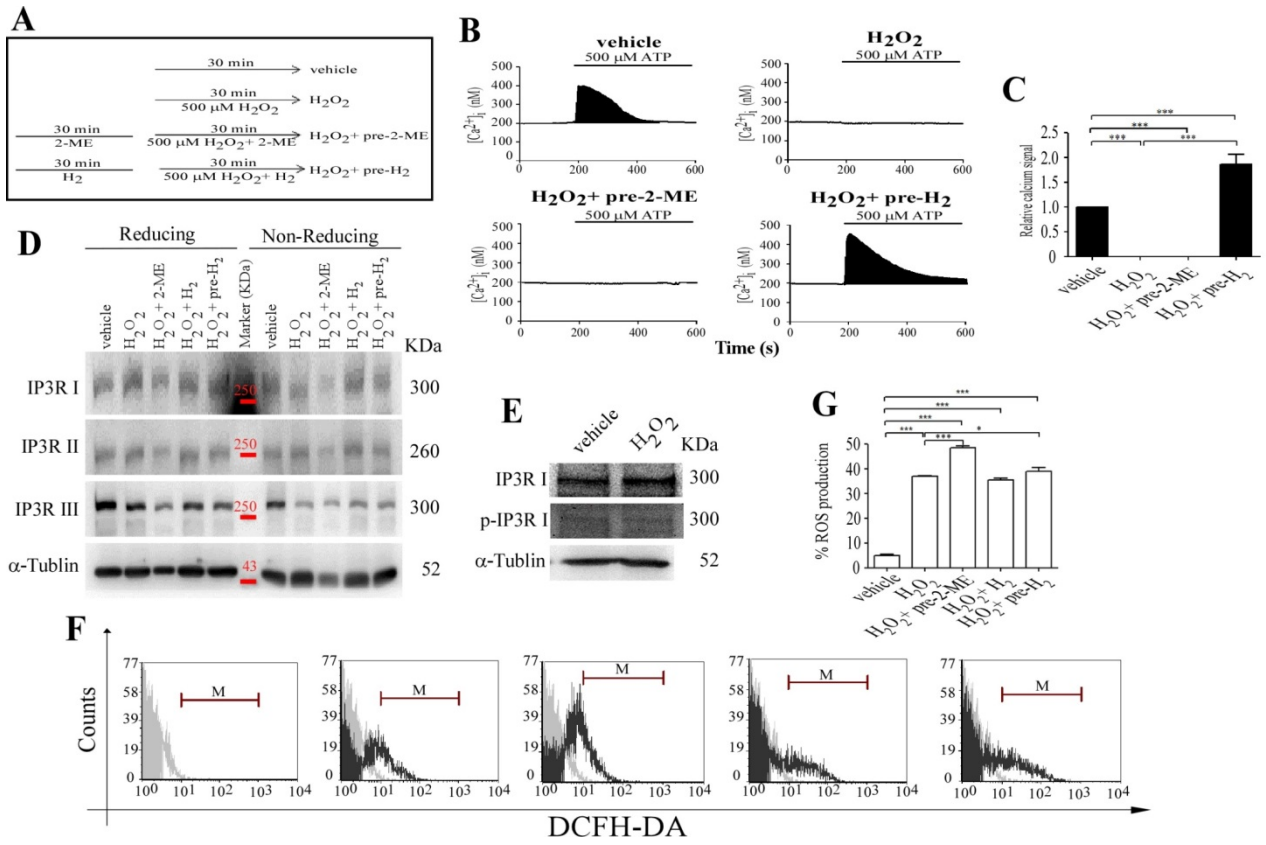

Figure 15. No effect of H_2 on H_2O_2-induced ROS production in KC. (A) Effect of pretreatment with 2-ME-BSS or H_2-BSS on the H_2O_2-induced reduction of ATP-induced Ca^{2+} signal in KC. Experimental design for treatment in each group: vehicle, 500 μM H_2O_2, 500 μM H_2O_2+ pre-2-ME, and 500 μM H_2O_2+ pre-H_2. Ca^{2+} signal was induced by ATP stimulation in each group (B) and calculated by the black-colored areas under the Ca^{2+} curve (N=3) (***, P <0.005) (C). (D) Expression of IP3Rs under non-reduced and reduced conditions is shown using SDS-PAGE and Western blot. Protein extracts from each group were resolved in non-reducing (without 2-ME) SDS-PAGE (7% gel), transferred onto Hybond-P polyvinylidene fluoride membranes, and incubated with antibodies against IP3R1, IP3R2 and IP3R3 and α-Tublin. As a control, the lysates were reduced using 100 mM 2-ME (reduced; right lanes). Proteins that form disulfide bonds exhibit faster migration and thus appear as lower molecular weight bands. (E) Western blot analysis of the expression of IP3R1 and phosphorylated IP3R1 (p- IP_3R1) after incubation of the cells with or without 500 μM H_2O_2. Treatment with 500 μM H_2O_2 had no effect on the density of the bands for phosphorylated-IP3R1 (p-IP3R1), and IP3R1 orα-Tublin. (F) Flow cytometry was estimated to quantify the (G) ratio of ROS generation in each group (*, P< 0.05; ***, P <0.005).

As previously established, superoxide dismutase converts superoxide anion radicals into H_2O_2, which is detoxified into H_2O by either glutathione peroxidase or catalase[80]. The examination of ROS production using flow cytometry revealed that neither H_2-BSS nor 2-ME reduced ROS production induced by 500 μM H_2O_2 in KC (Fig. 15F, 15G). The finding that H_2O_2 was not detoxified into H_2O with H_2 is similar to the results of a previous study, which showed that H_2 selectively reduces hydroxyl radicals, such as $^{\cdot}OH$ and $ONOO^-$, and only slightly reduces $NO^{\cdot}$[81].

The findings of the present study reveal the potential association of the skin aging process with Ca^{2+} signal dysfunction via the formation of H_2O_2 induced disulfide bonds in IP_3Rs that lead to selective damage of the IP3R. Co-treatment with 2-ME and 500 μM H_2O_2 decreased disulfide bond formation, evidenced by the protection of ATP-induced Ca^{2+} release in KC with 2-ME. This provides clear evidence that aging and aging-associated diseases are associated with Ca^{2+} signaling defects. Furthermore, similar to 2-ME, H_2 gas in BSS decreased IP_3R1 disulfide bond formation due to ROS exposure but not IP3R2 and IP3R3. The major function of H_2 in BSS in skin was the protection of ATP induced Ca^{2+} signaling, but not by direct quenching of ROS. When it is treated by H_2O_2, contribution of hydroxyl radicals will be small, because BSS media has no Cu and Fe to make hydroxyl radicals. Previous reports indicate that the presence of reducing agents decreased number of disulfide bonds, resulting in a loss of cross-link-induced stability produced by the chemical microenvironment[82]. It is reasonable to assume that the skin aging process is associated with ROS accumulation in the skin, which leads to IP_3Rs dysfunction by inducing conformational changes due to disulfide bond formation.

3.4 Materials and Methods

3.4.1 Cell culture

KC and HDF were isolated from foreskins obtained via routine circumcision (with approval from the Institutional Review Board / Ethics Committee, number KMUH-IRB-960119). Briefly, the foreskin samples were washed using PBS (Gibco Invitrogen, Carlsbad, CA) and disinfected with 70% alcohol. The harvested foreskins were minced into small pieces. To isolate the HDF, small pieces of the dermis were immersed in type I collagenase (3 mg/mL) (Sigma Chemicals Co.; St. Louis, MO) and type IV collagenase (3 mg/mL) (Sigma Chemicals Co.; St. Louis, MO) at 37°C for 2 hours. The samples were then incubated in 0.25% trypsin-EDTA solution (Gibco Invitrogen, Carlsbad, CA) at 37°C for 30 minutes. The isolated HDF were grown in DMEM (Gibco Invitrogen, Carlsbad, CA) supplemented with 10% FBS at 37°C in a humidified incubator containing a 5% CO_2-in-air atmosphere. To isolate KC, the small

pieces of foreskin sample were treated with 1 U/mL dispase II (neutral protease) (Gibco Invitrogen, Carlsbad, CA) at 4°C overnight. The epidermis was then separated from the foreskin sample and incubated in 0.25% trypsin-EDTA solution at 37°C for 15 minutes. The isolated KC were cultured in Keratinocyte-SFM medium (Gibco Invitrogen, Carlsbad, CA) at 37°C in a humidified incubator containing a 5% CO2-in-air atmosphere. The medium was changed every 3 days.

3.4.2 Cell viability assay

Skin cells, 2×10^5 KC or 1×10^5 HDF, were spread on 35-mm diameter dishes. Application of Derinat (Technomedservia Pharmaceutical Company, Russia) occurred after cells were allowed to spread on dishes for 2 h, then were incubated for 24 h at 37°C in humidified 5% CO_2. Skin cells were irradiated with 50 mJ/cm^2 for KC and 100 mJ/cm^2 for HDF by UVB (UV source, 5 x 8-watt , 312nm; BLX-312, Vilber Lourmat, France) then placed in normal medium for 24 h incubation. The ratios of the viabilities of skin cells were determined using MTT (Sigma Aldrich) at 570 nm in an ELISA reader.

3.4.3 Calcium imaging

The intracellular calcium responses were induced by applying TG (Sigma Aldrich), OAG (Sigma Aldrich) and ATP (Sigma Aldrich), according to previously described methods [75]. Before the experiments, cells were incubated with 1 μM Fluo-4-AM (Molecular Probes) at 37°C for 20 min and then washed with a BSS buffer (5.4 mM KCl, 5.5 mM D-glucose, 1 mM MgSO4, 130 mM NaCl, 20 mM Hepes pH 7.4, and 2 mM CaCl2). Intracellular Ca^{2+} concentrations were calculated by using the ratio of fluorescence intensities emitted upon excitation with consecutive 3-s pulses of 488-nm light at a resolution of 1376 × 1038 pixels using an Olympus Cell^R IX81 fluorescence microscope (Olympus) equipped with an MT 20 illumination system (Olympus) and UPLanApo 10× objective lens.

3.4.4 Immunofluorescence assay

The ratio of the DNA damage marker 8-oxodG was determined with an immunofluorescence assay using an antibody against 8-oxodG (Merck Millipore). KC and HDF treated with or without Derinat were cultured on 24 mm coverslips in 35 mm 6-well plates. After 24 h, cells were irradiated with 50 mJ/cm^2 and 100 mJ/cm^2 by UVB respectively, then placed in normal medium for incubation for 24 h. After three washes with PBS, the cells were fixed by incubation with BD Cytofix for 10 min. The fixed cells were then briefly washed with PBS and incubated overnight at 4 ◦C in PBS containing 5% goat serum and 1% BSA with the appropriately diluted monoclonal

antibody, 8-oxodG. After three washes with PBS, the cells were incubated for 1 h at room temperature with Alexa 488-conjugated goat anti-mouse IgM (Invitrogen) for 8-oxodG. The coverslips were washed three times with PBS (5 min each) and counterstained with 500 ng/mL DAPI (Sigma Aldrich) for 3 min. The coverslips were slide-mounted with antifade mounting solution and imaged using an Olympus FV1000 laser-scanning microscope (Olympus, Japan).

3.4.5 Analysis of intracellular ROS production in skin tissue

The animal experiments had an affidavit of approval of animal use protocol from Kaohsiung Medical Univerity, IACUC approval number: 101119. Briefly, we cooperated with SOMAPEX BIOTECH. CO. (Kaohsiung, Taiwan) to develop a special hydrogel for Derinat (Derinat hydrogel). Male BALB/c-nu mice (6 weeks old) were purchased from the National Laboratory Animal Breeding and Research Center (Taipei, Taiwan). There were two mice in each group (three independent experiments) covered with Derinat hydrogel or pure hydrogel for 3 h and then irradiated with 360 mJ/cm^2 UVB. After seven days treatment, a small section of skin tissue was excised from the dorsal area in BALB/c-nu mice and stained with 5 μM DHE (dye for staining intracellular ROS) for 30 min. After staining, the skin tissue was embedded in 1.5 % low gelling agarose, sectioned into 100 μm slices with a DSK Microslicer (DTK-1000, TED PELLA, INC., USA) and mounted on coated slides. The intracellular ROS production in skin tissue was observed with an Olympus FV1000 laser-scanning microscope.

3.4.6 Immunohistochemistry of skin tissue

Briefly, the dorsal skin from BALB/c-nu mice was fixed and embedded in paraffin. The monoclonal antibody of 8-oxodG (Merck Millipore, 1:200) and polyclonal antibody of COX-2 (Abcam, 1:500) were used as previously described. The immunoreactivity was visualized by incubation with DAB substrate-chromogen solution (DAKO) according to the manufacturer's protocol.

3.4.7 Western blot analysis

Western blot analyses were performed utilizing whole-cell lysates. Briefly, cells were lysed by incubating for 30 min on ice in M-PER Mammalian Protein Extraction Reagent (Thermo), containing proteinase and phosphatase inhibitors. Cell debris was removed via centrifugation at 10,000g for 10 min at 4°C. The protein concentration of cell lysates was determined using the Bradford method (Bio-Rad). Proteins (100 μg) in cell lysates were resolved using sodium dodecyl sulfate-polyacrylamide gel electrophoresis in a 7% gel with or without 2-ME and then transferred to a Hybond-P

polyvinylidene fluoride membrane (Amersham Biosciences). The membrane was first incubated with primary antibodies against IP3R1 (Cell Signaling Technology), phospho-IP3R1 (Cell Signaling Technology), IP3R2 (Millipore), IP3R3 (BD Biosciences) and α-Tublin (Santa Cruz Biotech), and then with horseradish peroxidase-conjugated secondary antibodies. Immunoreactive proteins were visualized using enhanced chemiluminescence reagents (Amersham Biosciences).

3.4.8 ROS measurement using flow cytometry

DCFH-MA (Sigma-Aldrich) staining was used to quantify ROS generation from the cells. Briefly, cells were stained with 20 μM DCFH-DA at 37°C for 20 min and then washed with BSS buffer. The cells were collected after application of H_2O_2, reducing agent 2-ME, or H_2-gas-containing BSS (H2-BSS) at 37°C for 30 min. ROS production was determined using flow cytometry (LSR II, BD) with fluorescence emission at 488 nm.

3.4.9 H_2-gas-containing BSS and assessment of H2 content

Hydrogen-containing water (H_2 water) was produced using an Aurora H_2-water-making machine (Kyoyo Company, Japan). To generate H_2-containing BSS: first, H_2 water with one-tenth concentration of BSS was made from sterile water using the Aurora machine. Then, H_2 water (with 1/10 of 10 x of BSS stock solution) was mixed with 9/10 of 10 x BSS stock solution to make final H_2-containing BSS (pH=7.4). The H_2 content was measured using a hydrogen electrode (Kyoyo Company, Japan).

Chapter IV *O. tsutsugamushi* toxicant induced cytokine storm in human macrophage

The original work has been reported in PLOS ONE (2016), and the publisher, Public Library of Science, has allowed me to use this paper as part of my PhD thesis.

Previously the thesis discussed how skin cells responded to environment toxicants, arsenic, UVB and H_2O_2 ; it also discussed the importance of Ca^{2+} signaling in determination of death or survival in skin cells. Increased Ca^{2+} signaling causes a number of intracellular ROS productions, resulting in cell damage with DNA damage or inflammatory response. In the next part it will be explained how immune cells respond to pathogen infection by increasing Ca^{2+} which can lead to cell death or survival.

4.1 Inhibition of Ca^{2+} signaling by 2-APB restrained infectious pathogen-induced TNF-α production in macrophages

The immune system protects the human body from infectious pathogens in two major ways: innate and adaptive immunity. The innate immune system is the first line of the host defense system against invading organisms, with the convertible immune system functioning as the second line of defense [27]. The primary defense mechanisms of macrophages against pathogen infection are known as phagocytosis and cytokine production because pathogens and antigens are known as inducers of the inflammatory response [28]. Lipopolysaccharides, LPS, endotoxin antigens from gram-negative bacteria, bring on a major inflammatory response from macrophages [28], which are the primary target cells infected by the facultative gram-negative bacterium *O. tsutsugamushi* in human skin [83,84]. Sepsis is known to be induced by a cytokine storm, a strong inflammatory response that is difficult or impossible to control [85].

It has been established that only Ca^{2+} can regulate the production of a variety of cytokines as part of a severe inflammatory response due to complicated pathogen infections [86]. Since clinical studies have concentrated on the development of new therapeutic approaches against severe inflammation and sepsis, and a major focus so far has been on decreasing cytokine storms, especially TNF-α production [87,88]. Previously the blockade of TNF-α production seemed to be crucial for improving cell survival in the case of cecal ligation puncture sepsis and intra-abdominal sepsis [88,89], because TNF-α facilitates the induction of cell injury via the activation of caspase/p38 and JNK MAP kinase cascades [90]. However Ca^{2+} elevation, especially due to SOCE, is also involved in TNF-α release from microglial cells under chronic purinergic stimulation [91]. The mechanism of Ca^{2+} signaling in regulating TNF-α production under pathogen infection has not yet been clearly established.

4.2 **2-APB but not SKF96365 inhibited *O. tsutsugamushi*-induced intracellular Ca^{2+} elevation in macrophage**

The present study is based on the hypothesis that Ca^{2+} signaling is essential in regulating TNF-α production during *O. tsutsugamushi* infection. The proposed mechanism at present is that Ca^{2+} signaling disrupts intracellular Ca^{2+} elevation following a decrease of TNF-α production in macrophages. To elucidate whether SOCE plays a role in regulating TNF-α production during the infection process by *O. tsutsugamushi*, the experiments first compared the effect of SOCE inhibitors 2-APB and SKF96365 on Ca^{2+} influx when pathogens infected macrophages. Cell-Tracker-Red labeled *O. tsutsugamushi* at a dose of 100 pathogens per cell (high dose) [15] were employed to infect human THP-1 induced macrophages. The time course of the infection process was then traced by a fluorescent confocal microscope. Fluorescence images of macrophages infected with *O. tsutsugamushi* after 1 h of incubation are shown in Fig. 16A. Slightly increased intracellular Ca^{2+} via infection was inhibited well with 2-APB as indicated in Fig. 16B. After 24 h of incubation with *O. tsutsugamushi*, a transient Ca^{2+} elevation induced by TG , which is a standard method of examination for intracellular Ca signaling system, was found to be increased 1.7-fold, while applications of 50 and 100 μM 2-APB decreased the TG-induced Ca^{2+} response (Fig. 16C, 16D). 2-APB also blocked *O. tsutsugamushi* directly induced intracellular Ca^{2+} elevation at the indicated time point (Fig. 16B); this suppression was probably due to the mitigation of SOCE activated by *O. tsutsugamushi* (Fig. 16E). Similar results are also exhibited in Fig. 16F and 16G, where the induction of intracellular Ca^{2+} elevation by LPS treatment for 24 h was significantly suppressed by 2-APB application.

Unexpectedly, SKF96365, which has been reported to restrain LPS- and LPS-plus-IFN-γ-induced Ca^{2+} influx [29], enhanced *O. tsutsugamushi*-induced intracellular Ca^{2+} elevation (Fig. 16B, 16C and 16D). Based on a previous report, overexpression of Orai1 and STIM1 proteins have the potential to influence the function of SOCE [92], so there was further examination of whether 2-APB affected Orai1 and STIM1 expressions during *O. tsutsugamushi* infection. Fig. 16H demonstrated that pathogenic infection caused the induction of upregulated expression of Orail and STIM1, yet only Orai1 was attenuated to some extent by 2-APB. No change was found for other Ca^{2+} entry channels expression such as TRPV1, which is known to be activated by 2-APB stimulation [93]. Therefore, it is reasonable to conclude that 2-APB interrupted the pathogen-induced increase of intracellular Ca^{2+} concentration via the inhibition of SOCE activity in macrophages.

4.3 APB inhibited pathogen-induced TNF-α production

This study further decided the pathogen-induced production profiles of inflammatory cytokines, such as IL-1β, IL-6, IL-10, INF-γ, IL-12p70, and TNF-α, with *O. tsutsugamushi* infection for 24 h. The production of IL-1β, IL-6, IL-10, and TNF-α increased, especially that of TNF-α, which strikingly increased 2-fold relative to the control (Fig. 17A). Further experiments attempted to confirm whether pathogen activated TNF-α expression was repressed by SOCE inhibitors 2-APB and/or SKF96365. Akin to the results for TG induced-Ca^{2+} elevation shown in Fig. 17C, 17D, SKF96365 was unable to decrease *O. tsutsugamushi* induced TNF-α production and conversely promoted it, even though its concentration was sufficiently high (50 μM) (Fig. 17B, 17C). Previous studies reported that SOCE inhibitors SKF96365 and 2-APB downregulated TNF-α release under conditions of chronic stress [91], while the results in this experiment demonstrated that 2-APB decreased not only TNF-α release from macrophages, but also TNF-α expression (Fig 17B, 17C). As was previously reported, the TNF-α promoter has DNA binding elements with Ca^{2+} dependent transcription factors [94], such as NF-κB [95] or CREB [96]. Once intracellular Ca^{2+} elevation occurs, these transcription factors will translocate to the nucleus.

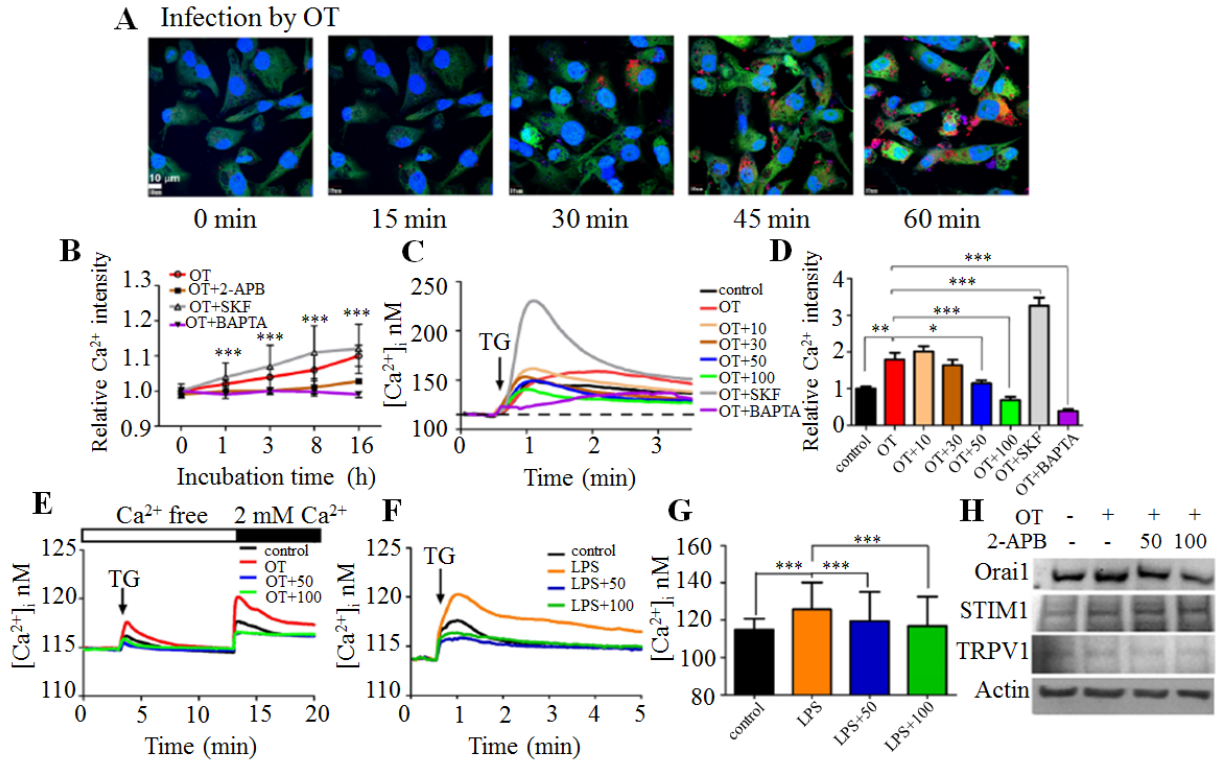

Figure 16. 2-APB reduced pathogen-activated Ca^{2+} signaling in macrophages. (A) Fluorescence images of OT-infected macrophages at indicated time points with staining by Celltrackers (cytoplasm, green; OT, red) and DAPI (uncles, blue). (B) *O. tsutsugamushi*-infected macrophages co-treatment with various Ca^{2+} inhibitors, 50 μM 2-APB (OT+2-APB), 50 μM SKF96365 (OT+SKF), or 25 μM BAPTA (OT+BAPTA) at indicated time points. (C) Effect of Ca^{2+} inhibitors, 2-APB (10 μM, 30 μM, 50 μM and 100 μM), SKF96365 (SKF) and BAPTA on intracellular Ca^{2+} concentration of *O. tsutsugamushi*-infected macrophages after 24 h of co-incubation. OT+10, OT+30, OT+50 and OT+100 indicate *O. tsutsugamushi* co-incubation with different concentrations of 2-APB. Ca^{2+} imaging analysis of TG-induced Ca^{2+}response after application of 1 μM TG (small black arrow) (n = 3). (D) Quantification of area (above dotted line) of intracellular Ca^{2+} responses shown in (C) (*, $p < 0.05$; **, $p < 0.01$; ***, $p < 0.001$). (E) $CaCl_2$ was extracellularly applied (large black bar) to enter Ca^{2+} via store-operated Ca^{2+} channels after application of TG (small black bars) in Ca^{2+} free BSS solution (open bar) (n = 3). Effect of 2-APB on (F) Ca^{2+}dynamics and (G) intracellular Ca^{2+} elevation in LPS-stimulated macrophages during 24 h of co-incubation (***, $p < 0.001$). LPS co-incubated with 50 μM 2-APB (LPS+50) and 100 μM 2-APB (LPS+100) respectively. (H) Orai1 expression was decreased by 2-APB, but not STIM1, TRPV1, or Actin in *O. tsutsugamushi*-infected macrophages, as determined by western blot analysis.

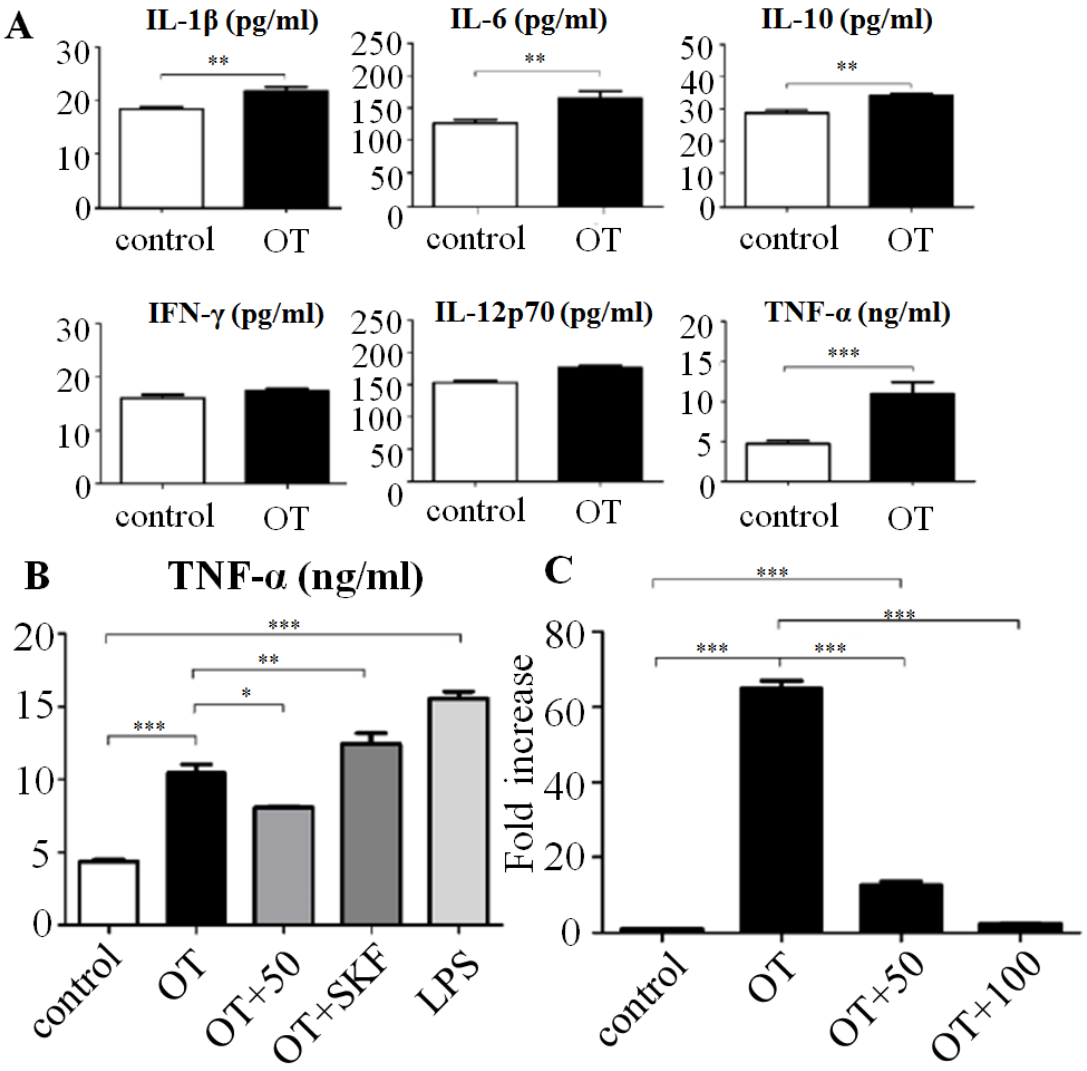

Figure 17. Effects of *O. tsutsugamushi* on cytokine production by macrophages. (A) Production of various cytokines was determined with ELISA system (eBioscience) at 24 h after infection (**, $p < 0.01$; ***, $p < 0.001$). 2-APB (50, 50 μM and 100, 100 μM). Reduction of *O. tsutsugamushi*-induced elevation of TNF-α expression was analyzed by (B) ELISA and (C) qRT-PCR in macrophages (*, $p < 0.05$; **, $p < 0.01$; ***, $p < 0.001$).

Therefore, it was not unexpected that 2-APB reduced TNF-α production and expression. As a follow up, the profiles of inflammatory cytokine production when macrophages weres stimulated with *O. tsutsugamushi* or LPS were studied. Interestingly, in the case of infection by *O. tsutsugamushi*, 2-APB significantly activated only IL-1β production (Fig. 18), which is known to be most important for the activation of adaptive immune cells, that is to say antigen-specific T cells [97]. 2-APB also slightly enhanced the amounts of IL-6 and IL-12p70, which are known to modulate Type 2 immune responses[94,95]. In contrast with the systemic innate immune response, the adaptive immune system specifically targets pathogens, and normalizes or eliminates pathogen activation [96]. The obligate intracellular bacterium *O. tsutsugamushi* targets and infects macrophages: IL-1β elevation by 2-APB provides an efficient policy to mitigate this infection. More noteworthy, 2-APB was found to downregulate the induction of TNF-α through stimulation by LPS or *O. tsutsugamushi* (Fig. 18).

4.4 2-APB induced upregulation of HSP70 under *O. tsutsugamushi* activated TNF-α expression

As was described above, 2-APB reduced the level of TNF-α production by reduced Ca^{2+} entry during pathogen infection in macrophages. Since induction of HSP70 has also been found to be involved in regulating TNF-α production [98], the reduced TNF-α production was expected to determine a latent link to bacterial LPS stimulation in monocytes or macrophages [99]. Since only HSP70 was upregulated by 2-APB, it was determined whether 2-APB affected expressions of HSP10, HSP40, HSP70, and HSP90 during *O. tsutsugamushi* infection (Fig. 19A). The obtained results suggested that several signal transduction pathways could be activated by 2-APB to promote HSP70 expression. Therefore, there was further investigation of the signaling pathway for 2-APB-induced upregulation of HSP70 expression. Initially, macrophages were exposed to *O. tsutsugamushi* or co-incubated with *O. tsutsugamushi* and then with 2-APB, followed by analysis of MAPK signaling pathways at the indicated time points. As shown in Fig. 19B, the expressions of both JNK and p38 were found to be attenuated by 2-APB except for ERK expression, which was unexpectedly increased. Simultaneously, interruption of the enhancements of ERK and HSP70 was revealed by using the MAPK/ ERK inhibitor PD98059 (Fig. 19C, 19E). Although it was unlikely when it was treated by LPS, PD98059 did not interrupt HSP70 and even promoted its expression with 100 μM 2-APB, despite disruption of HSP70 (Fig. 19D). Interestingly these increases in HSP70 expression were not available for the purpose of increasing cell viability under pathogenesis (Fig. 19F, 19G). Unexpectedly, 2-APB also promoted the ERK pathway in macrophages, and cell viability was extended afterwards by

PD98059 treatment (Fig. 19F, 19G). Thus, 2-APB-induced upregulation of HSP70 cannot enhance cell survival but it could be crucial to the activation of the ERK pathway in the regulation of HSP70 expression in *O. tsutsugamus* infected macrophages.

4.5 A role of HSP70 in macrophages

The majority of data reported so far indicates that HSP70 is a member of the protective system against endotoxin induced cell damage [100]. This defense mechanism is used together with the interruption of the NF-κB/TNF-α axis[98,99]. This signaling line was followed up on in order to demonstrate whether 2-APB-increased HSP70 participated in TNF-α expression. Since exogenous HSP70 also is known to have a therapeutic effect against endotoxin manifestations[101], initially HSP70 concentration was measured under various conditions of external media. As shown in Fig. 20A, however, there was no difference in HSP70 production under the various treatments. The data in this figure also demonstrates that both of activated pathogens and 2-APB induced HSP70 were not secreted to the exterior. To find out how HSP70 regulates TNF-α production, experiments attempted to knockdown HSP70 and identify the released and expressed TNF-α. Consistent with the results for *O. tsutsugamushi* infected macrophages as shown in Fig 18, obstructed HSP70 expression along with *O. tsutsugamushi* infection also stimulated TNF-α production, and this dramatically increased expression level was attenuated by 2-APB treatment (Fig. 20B, 20C). However, there was a difference between the release and expression of TNF-α for LPS stimulation; 2-APB eliminated TNF-α release, even if TNF-α expression levels were not reduced, and rather increased, after knockdown of HSP70 (Fig. 20B, 20C). Increased levels of HSP70 by 2-APB were also found in the knocked down HSP70 (Fig. 20D). A mechanism for why 2-APB dependent HSP70 increased TNF-α expression in endogenous HSP70 knockdown in LPS stimulated macrophages is not clear at present. Not all of the upregulated TNF-α was released to the outside due to 2-APB mitigating SOCE. Interestingly, together with pathogen stimulation, the activation of NF-κB in knocked down HSP70 was higher than that in the control, but restoration of HSP70 by 2-APB reduced the ratio of NF-κB translocation (Fig. 20E, 20F). It could be assumed that NF-κB drives a signaling pathway that is not major in LPS induced TNF-α expression. However, 2-APB may synergistically activate several signaling pathways to promote TNF-α expression with LPS. As a conclusion, 2-APB strategically mediates pathogen activated TNF-α production in a way that is decreasing the release by pitting SOCE and upregulating HSP70 to repress NF-κB activity against TNF-α expression in *O. tsutsugamushi* infected macrophages.

As was previously reported, HSP70 was induced via activation of the ERK pathway

[102] and 2-APB-stimulated ERK activity. [103] Activated SOCE is also linked with activation of ERK signaling and it is inhibited by CaMKII and Raf-1, though it is not in malignant melanoma[104]. In the present experiments it was shown that 2-APB treatment blocked SOCE but activated the EKR pathway to overexpress HSP70 in macrophages. Even so, another signal transduction pathway probably joins the regulation of HSP70, because PD98059 cannot repress HSP70 completely. The Stat3/HSP70 axis [105] and the HIF/HSP70 axis [106] are also candidate pathways involved in the 2-APB regulation of HSP70 upregulation. On the contrary, 2-APB is known to suppress reactive oxygen species production, which results from inflammation increased mitochondrial Ca^{2+} overloading[107]; accordingly, the HIF/HSP70 axis may not be involved in 2-APB-mediated HSP70 overexpression. Unusually, PD98059 inhibited 50 μM 2-APB-induced HSP70, but not 100 μM 2-APB induced HSP70. Even though 2-APB facilitates resistance to TNF-α production under LPS stimulation, 50 μM and 100 μM 2-APB may activate different pathways in LPS induced macrophages.

Conclusively, 2-APB strategically decreases TNF-α production by utilizing its unique mechanism in pathogen-infected macrophages. It does this by downregulating Ca^{2+} influx to interrupt the release and expression of TNF-α and upregulating HSP70 to suppress TNF-α expression via activation of ERK or other pathways (Fig. 21). Additionally, by increasing the number of adaptive-immunity-associated cytokines, IL-1β, IL-6, and IL-12p70, 2-APB efficiently attenuates a severe inflammatory response. Our findings show the potential for immune regulatory treatment in clinical studies using 2-APB.

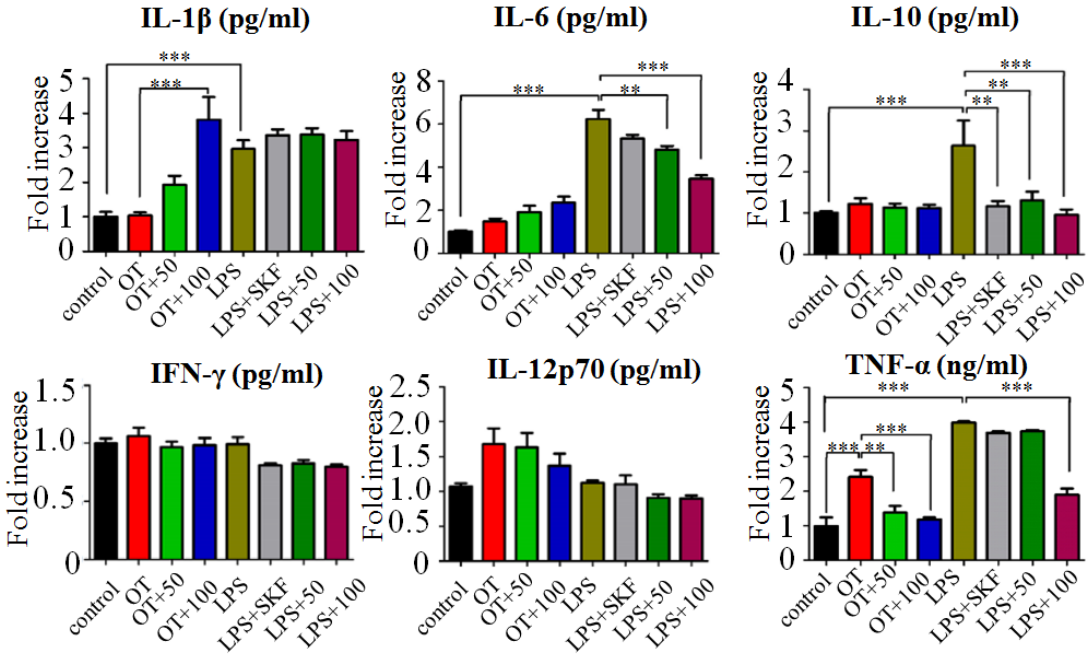

Figure 18. Effect of 2-APB on profiles of inflammatory cytokines in *O. tsutsugamushi*-infected and LPS-activated macrophages. Levels of cytokine production were measured with ELISA system (eBioscience) analysis during 24 h of co-treatment (*, $p < 0.05$; **, $p < 0.01$; ***, $p < 0.001$).

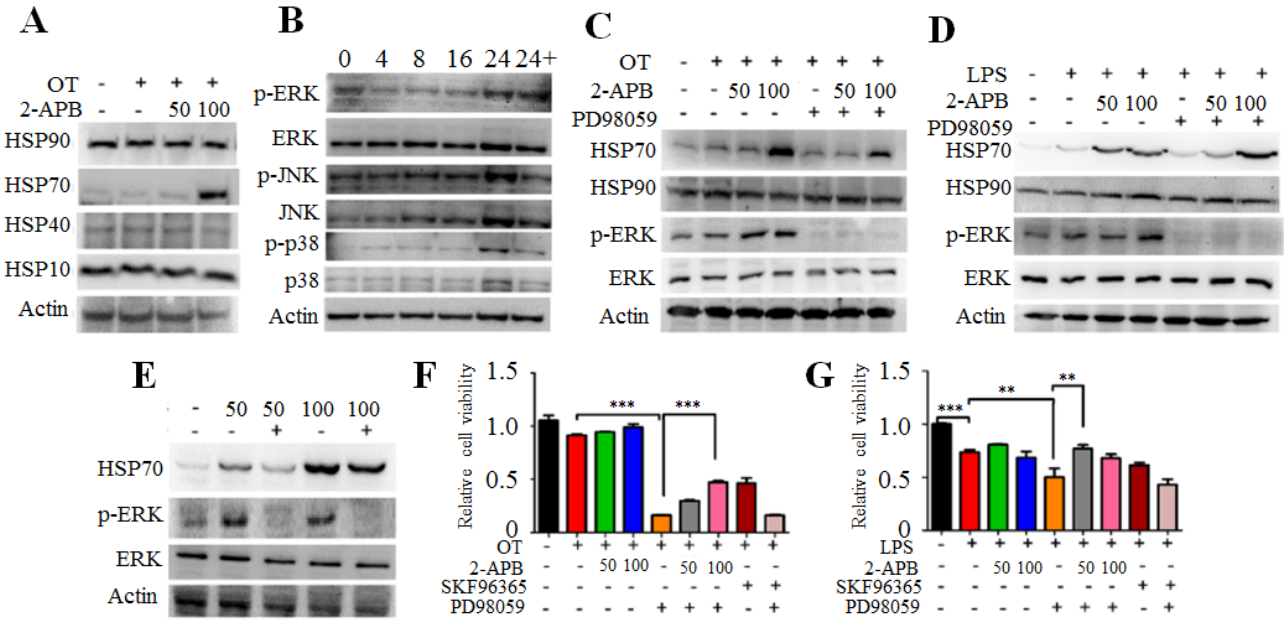

Figure 19. Increased level of HSP70 expression by treatment with 2-APB in *O. tsutsugamushi*-infected or LPS-stimulated macrophages. (A) Effect of 2-APB on expressions of HSP10, HSP40, HSP70, HSP90, and Actin in *O. tsutsugamushi* (OT)-infected macrophages. (B) Western blot analysis was utilized to measure MAPK signal pathways in *O. tsutsugamushi*-infected macrophages at indicated time points. Treatments included phosphorylated JNK (p-JNK), JNK, phosphorylated p38 (p-p38), and p38, which were interrupted by co-incubation with 50 μM of 2-APB for 24 h (24+). Further measurements were detected by expression of phosphorylated ERK (p-ERK), ERK, HSP70, and Actin, which were treated with MAP kinase (MEK) inhibitor, 50 μM PD98059, 2-APB (50, 50 μM and 100, 100 μM) or a combination for 24 h in (C) *O. tsutsugamushi*-infected and (D) LPS-stimulated macrophages. (E) Western blot analysis of expression of the ERK pathway, HSP70, and Actin without pathogen infection in macrophages. Survival probability is displayed for each condition in the panel with (F) *O. tsutsugamushi*-stimulated macrophages and (G) LPS-stimulated macrophages for 24 h (**, $p < 0.01$; ***, $p < 0.001$).

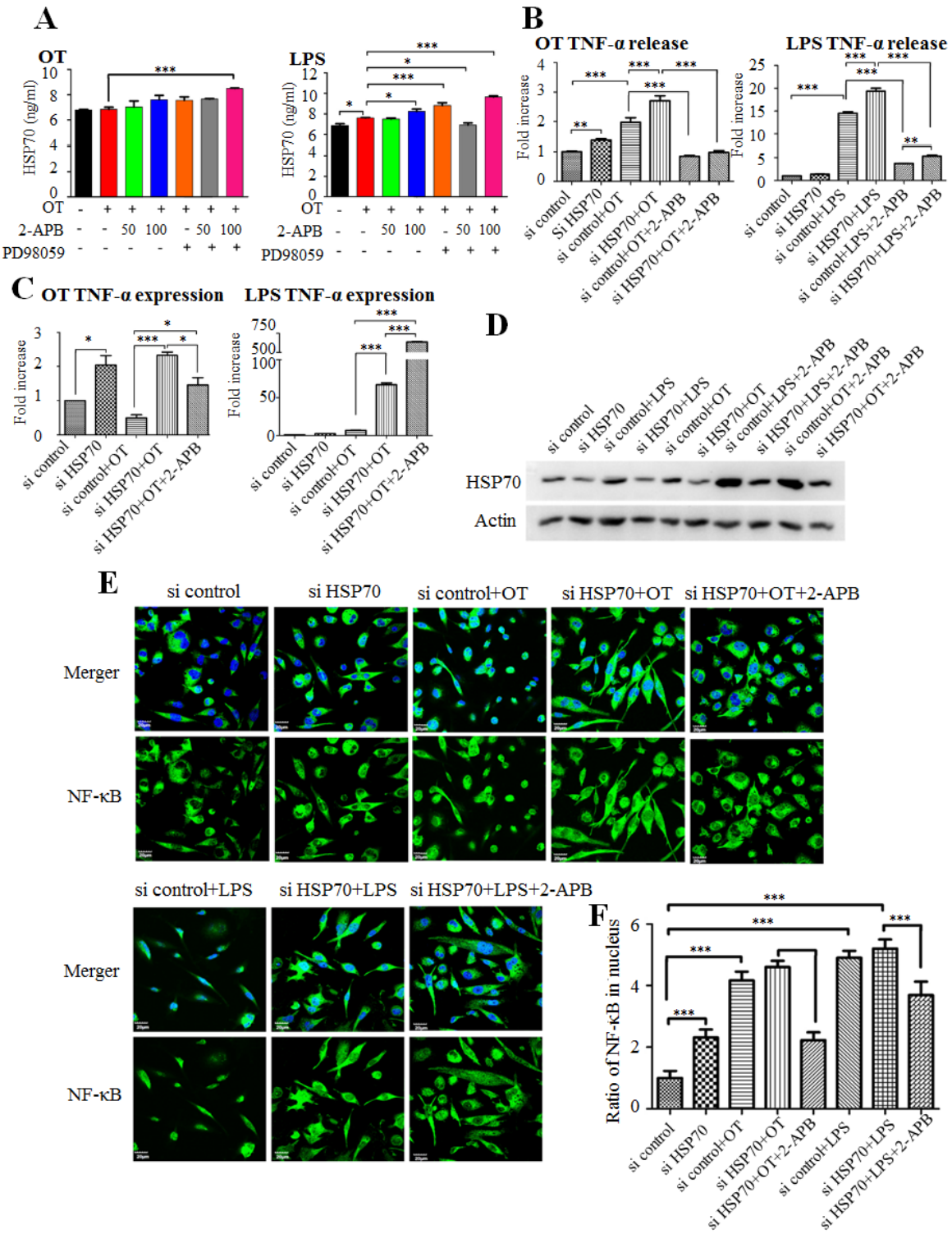
A
OT
LPS
HSP70 (ng/ml)
OT
2-APB
PD98059
B
OT TNF-α release
LPS TNF-α release
Fold increase
si control
Si HSP70
si control+OT
si HSP70+OT
si HSP70+OT+2-APB
si control+LPS
si HSP70+LPS
si control+LPS+2-APB
si HSP70+LPS+2-APB
C
OT TNF-α expression
LPS TNF-α expression
D
HSP70
Actin
si control+OT+2-APB
si HSP70+OT+2-APB
E
si control
si HSP70
si control+OT
si HSP70+OT
si HSP70+OT+2-APB
si control+LPS
si HSP70+LPS
si HSP70+LPS+2-APB
Merger
NF-κB
F
Ratio of NF-κB in nucleus

Figure 20. *O. tsutsugamushi* activated TNF-α production was restrained by elevated levels of HSP70 in macrophages. (A) Cells were co-incubated with pathogens and 2-APB or PD98059 for 24 h. There was no effect on HSP70 production after treating with 2-APB or PD98059 in *O. tsutsugamushi*-infected and LPS-activated macrophages, as determined utilizing ELISA system (Enzo Life Sciences) (*, $p < 0.05$; ***, $p < 0.001$). HSP70 was knocked down by HSP70 siRNA, and then co-treated with pathogens and 2-APB for 24 h. (B) TNF-α release and (C) TNF-α expression were calculated utilizing ELISA system and qRT-PCR analysis, respectively (*, $p < 0.05$; **, $p < 0.01$; ***, $p < 0.001$). (D) Western blot analysis of expression of HSP70 shown in (B) and (C). (E) Knocked down HSP70 promotes translocation of NF-κB (green) to nucleus (blue) with pathogenic stimulation by immunofluorescence analysis. (F) Activation of NF-κB quantified by measurement of fluorescent intensity of NF-κB in nucleus area utilizing an Olympus fluorescence microscope with an average fluorescence intensity of more than 1000 cells (*, $p < 0.05$; ***, $p < 0.001$).

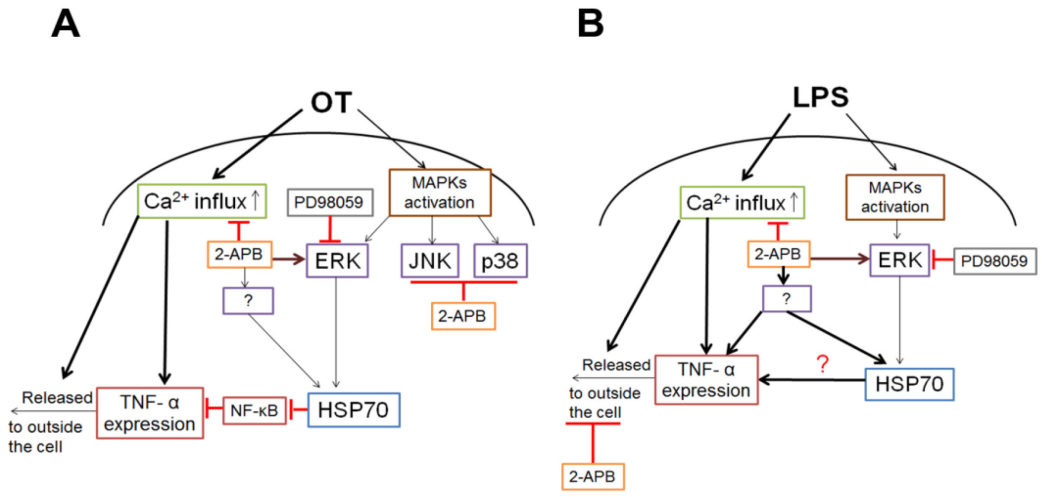

Figure 21. Schematic diagram of 2-APB activity in strategically regulating *O. tsutsugamushi*-induced and LPS-stimulated TNF-α production in macrophages. (A) Pathogenic infection induced increased levels of TNF-α, which was attenuated by 2-APB interrupting Ca^{2+} signaling activity; suppressed Ca^{2+} mobilization also suppressed release and expression of TNF-α. MAPK pathway is involved in regulating TNF-α production during *O. tsutsugamushi* infection; however, 2-APB restrains the signal pathway of JNK and p38 but activates the ERK pathway to promote upregulation of HSP70, which facilitates downregulation of TNF-α expression by blocking NF-κB translocation to nucleus. (B) Although 2-APB attenuates LPS-stimulated TNF-α production, a different mechanism regulates TNF-α expression. The importance of 2-APB in LPS stimulated macrophages is to block TNF-α release rather than inducing ERK pathway to activate upregulation of HSP70.

4.6 Materials and Methods

4.6.1 Infection of macrophages by *O. tsutsugamushi*

Human monocytic THP-1 cells were purchased from the Taiwan Bioresource Collection and Research Center (BRCR, Taiwan). RPMI 1640 medium, which contained 10% (vol/vol) FBS, 2 mM L-glutamine, 10 mM HEPES, 25 mM glucose, 1% (vol/vol) penicillin-streptomycin, and 1 mM sodium pyruvate, was prepared to maintain the THP-1 monocytes in humidified 5% CO_2 and a 37 °C incubator. 100 ng/mL PMA (Sigma Aldrich) was utilized to induce THP-1 monocyte differentiation into macrophages. 2×10^5 cells were seeded into a 6-well plate with 100 ng/mL PMA. After 48 h, the cells were washed three times with PBS and cultured overnight in fresh RPMI 1640 medium containing 2% FBS. The PMA-induced macrophages were infected with *O. tsutsugamushi*, TW-1 strain, which belongs to Karp strains, the most common (33.6%) and a highly virulent strain in Taiwan[108]. This strain was received from the Taiwan Centers for Disease Control. The methods used for TW-1 culture, isolation, and quantification can be found in our previous study[109]. THP-1-induced macrophages were infected with a high infection dose (one macrophage infected by 100 pathogens) [109].

4.6.2 Tracing of *O. tsutsugamushi*

The effective invasion of *O. tsutsugamushi* into macrophages was determined by labelling macrophages with CellTracker® Green Fluorescent Probe (Lonza) and labeling *O. tsutsugamushi* with CellTracker™ Red CMTPX (Invitrogen) in living status, respectively, before infection. The infected cells were fixed with 4% paraformaldehyde at 0, 15, 30, 45, and 60 min and nuclei were stained with DAPI (Sigma-Aldrich). The dynamics of intracellular infection were detected using an Olympus FV1000 confocal microscope equipped with an UPLanApo 100× objective lens [109].

4.6.3 Calcium imaging

Ca^{2+} mobility was estimated by application of thapsigargin (TG; Sigma-Aldrich), according to methods previously described [75]. Before the experiments, cells were stained with 1 μM Fluo-4-AM (Molecular Probes) at 37 °C for 20 min and then washed with BSS buffer (5.4 mM KCSl, 5.5 mM D-glucose, 1 mM $MgSO_4$, 130 mM NaCl, 20 mM Hepes pH 7.4, and 2 mM $CaCl_2$). Intracellular Ca^{2+} concentrations were determined based on the ratio of fluorescence intensities. The intracellular Ca^{2+} concentration was calculated using calibration curves as previously described[75].

4.6.4 Quantitative reverse transcription polymerase chain reaction (qRT-PCR)

Total RNA was extracted from pathogen-stimulated macrophages with Trizol reagent (Invitrogen). Reverse transcriptase reactions required 1 μg of RNA to synthesize complementary cDNA using an RT kit (Invitrogen). Incubation conditions were 10 min at 25 °C, 120 min at 37 °C, and 5 min at 85 °C. The resulting cDNAs were used to identify the TNF-α expression level with quantitative polymerase chain reaction (PCR) utilizing the SybrGreen PCR Master Mix Kit (Applied Biosystems, Carlsbad, CA, USA) and specific primers: TNF-α forward: CCC AGG GAC CTC TCT CTA ATC A and reverse: GCT ACA GGC TTG TCA CTC GG; GAPDH (GenBank accession number, NM_ 002046), forward: TGC ACC ACC AAC TGC TTA GC and reverse: GGC ATG GAC TGT GGT CAT GAG. Thermal cycling was conducted in an Applied Biosystems 7900HT fast real-time PCR system using the following cycling conditions: 95 °C for 10 min, and 40 cycles at 95 °C for 5 s, and 60 °C for 30 s. Each complete amplification stage was followed by a dissociation stage at 95 °C for 15 s and 60 °C for 30 s [10].

4.6.5 Cell viability assay

THP-1-induced macrophages were incubated with pathogens (*O. tsutsugamushi* or 1 μg/mL LPS) or co-incubated with 2-APB, PD98059, or SKF96365 for 24 h. Cell viability was determined by MTT assay (Sigma-Aldrich) at a final concentration of 500 μg/mL in PBS (Gibco), and incubation in the dark at 37 °C for 3 h. After the resulting formazan crystals were dissolved by incubation with dimethyl sulfoxide at 37 °C for 5 min, the solution was transferred to a 96-well ELISA plate and read at 570 nm in an ELISA reader.

4.6.6 Western blot analysis

Total cell lysates (100 μg) were analyzed using SDS-PAGE on a 12% gel. After electro-blotting to a nitrocellulose membrane, membranes were blocked with 1% BSA for 1 h at room temperature. Membranes were washed with 0.1% TBST three times and then incubated with primary antibodies overnight at 4 °C. Antibodies against Orai1(Merck Millipore), STIM1(OriGene), TRPV1 (Novus Biologicals), phospho-ERK (Cell Signaling Technology), ERK (Cell Signaling Technology), phosphor-JNK (BD Transduction Laboratories™), JNK (BD Transduction Laboratories™), phosphor-p38 (BD Transduction Laboratories™), p38 (BD Transduction Laboratories™), HSP10 (Enzo Life Sciences), HSP40 (Enzo Life Sciences), HSP70 (Enzo Life Sciences), HSP90 (Calbiochem, Merck Millipore), and β-actin (Santa Cruz) were utilized as the primary antibodies. The membranes were then treated with horseradish peroxidase-conjugated secondary antibodies (Amersham

Biosciences). Immunoreactive proteins were visualized using enhanced chemiluminescence reagents (Amersham Biosciences).

4.6.7 HSP70 knockdown

THP-1-induced macrophages were treated with 40 μM HSP70 siRNA (Santa Cruz) and GenMuteTM siRNA transfection reagent (SignaGen Laboratories) in accordance with the manufacturer's protocol for 24 h, then incubated with pathogens (*O. tsutsugamushi* or LPS) or co-incubated with 2-APB for 24 h. Knockdown of HSP70 in pathogen-stimulated macrophage assays was performed to further identify TNF-α production.

4.6.8 Immunofluorescence assay

The ratio of the NF-κB translocation was determined with an immunofluorescence assay using an antibody against NF-κB (Santa Cruz). Pathogen-stimulated THP-1 was cultured on 24-mm coverslips in 35-mm 6-well plates. After three washes with PBS, the cells were fixed by incubation with 4% paraformaldehyde for 10 min. The fixed cells were then briefly washed with PBS and incubated overnight at 4 °C in PBS containing 5% goat serum and 1% BSA with the appropriately diluted monoclonal antibody, NF-κB. After three washes with PBS, the cells were incubated for 1 h at room temperature with Alexa-488-conjugated goat anti-mouse IgG (Invitrogen) for NF-κB. The coverslips were washed three times with PBS (5 min each) and counterstained with 500 ng/mL 4,6-diamidino-2-phenylindole (DAPI, Sigma Aldrich) for 3 min. The coverslips were slide-mounted with an antifade mounting solution and imaged using an Olympus FV1000 laser scanning microscope [10].

4.6.9 Statistical analysis

GraphPad Prism (La Jolla, CA) was used to generate bar charts, where error bars indicate standard deviations. One-way, two-tailed analysis of variance (ANOVA) was utilized to compare the means of each group. A *p*-value of less than 0.05 for differences between groups was considered statistically significant.

Chapter V Discussion

As is described above, almost all data were already published in international scientific journals and evaluated fairly. The most important findings in these experiments are that all types of environmental toxicants can induce the activation of Ca^{2+}→ROS →HSPs line in the human defense system. Detailed explanation will be given in the following 5 sections.

5.1 The oxidation and reduction of functional proteins in the living cell

According to the aging theory, accumulation of dysfunctional proteins is based on oxidation by ROS emitted from mitochondria produced with ATP [61]. A living cell has its own strategy to reduce dysfunctional proteins maintaining cell homeostasis, such as HSPs or GSH[68]; to quench the oxidative stress, the SOD system facilitates attenuation of ROS thus preventing proteins from oxidation. However, when the cell can't quench ROS and recover the dysfunctional proteins, the survival and death balance is disturbed. As shown in this study and previous reports, Ca^{2+} signaling is downregulated in the aging process; many studies indicate that the inflammatory response inducing an increased level of Ca^{2+} is a crucial process to tend cell to aging[10,110]. According to this study, it seems the inflammation-induced Ca^{2+} elevation enhances a large number of ROS productions, resulting in dysfunctional proteins with disulfide bond formation by oxidative stress. Tthe role Ca^{2+} signaling plays in the aging process is still unclear.

5.2 Significance of transient but not sustained Ca^{2+} elevation for cell survival

As was discussed previously, Ca^{2+} levels increase in the inflammatory response and further induces oxidative stress to cause dysfunctional proteins, finally restraining Ca^{2+} signaling due to damaged IP3Rs in the aged cell. To maintain cell physiological homeostasis, significant transient Ca^{2+} signaling is presented in each cell type. Sustained Ca^{2+} elevation as shown in inflammatory response induces cell death[91]. The switch between transient Ca^{2+} elevation and sustained Ca^{2+} elevation are established independently. Based on the present study, however, the aging process is affected through environmental toxicants, due to the induction of intracellular Ca^{2+} elevation and ROS production. The accumulation of dysfunctional proteins elicits HSPs or GSH to assist recovery from the misfolded proteins. Interestingly, the transient Ca^{2+} signaling from ER, especially IP3Rs or RyRs, regulates cell physiological effects, such as neuronal transmission or muscle contraction [111]; the sustained Ca^{2+} signaling is from TRP channels, such as TRPCs in inflammation[112]. Despite induction of HSPs by the activation of Ca^{2+} signaling, it is so far unknown how the activation of TRP channels and HSPs line up.

5.3 Role of TRP channels in the induction of HSPs for cell survival

HSPs are expressed in response to any kind of stress signal that compromises cell survival. In mammals, HSPs appear when body temperature is above 39°C to 41°C [113,114]. Irradiation by IR or NIR enhances the expression level of HSPs [115]. Nevertheless, according to one study, not only rising body temperature but also heavy metals (As, Cd), ethanol, oxygen radicals, and peroxides are all agents that can induce heat-shock responses. HSPs expression are modulated by the change in cell signaling molecules, such as intracellular pH, cAMP, Ca^{2+}, IP3, PKC, and protein phosphatases. According to the results, elevated intra-cellular Ca^{2+} greatly attenuates the translocation of HSF from cytosol to nucleus, HSP gene expression, and protein synthesis. Also IP3 is crucial in the regulation of HSPs expression, because treatment with pertussis toxin, cholera toxin, and forskolin increased IP3 production, which results in the upregulated gene level of HSPs in human epidural cells. However, an inhibitor of IP3 production diminishes the heat-induced expression of HSPs[116,117]. This fact is supported by the finding that the binding of IP3 to its receptor of ER alters RNA splicing and regulates the expression of multiple gene products[118]. The involvement of PKC and phosphoprotein phosphatase is also confirmed. Conclusively, the previous results indicate that calcium signaling is also important to understand the molecular mechanism by which heat produces HSPs. It is not so easy to combine hyperthermia and IP3-induced Ca^{2+} signaling, but it will be possible if it is assumed that the involvement of TRP channels during hyperthermia induces HSPs production. The roles of several types of skin TRP channels in the regulation of HSPs production via increased intracellular Ca^{2+} induced ROS generation after IR and NIR exposure should be investigated. Thus, the coexistence of TRPV1 and TRPA1 potentially supports a model to explain how hyperthermia can produce HSPs in the cell. This coexistence fulfills the necessary and sufficient conditions to produce HSPs; for HSPs production in the nucleus, an IP3 signal is needed.

5.4 Significance of Ca^{2+} signaling in initiating skin aging or aging associated diseases, especially cancer

As was discussed previously, once HSPs can't recover from ROS-induced cell damage, cells tend to age or develop aging associated diseases; cancer may be a good example representing the aging process. Based on the results of chapter III, blockage of TRPCs by Derinat facilitates inhibition of UVB-induced skin damage of several different kinds; such as intracellular ROS production, DNA damage and COX-2 expression. It seems that an initial increase of Ca^{2+} signaling may induce cell aging and malignance. According to the results obtained here, Ca^{2+} entry from outside that is associated with stimulation of environmental toxicants in turn influences intracellular

Ca^{2+} homeostasis, resulting in the large amount of intracellular ROS production via overloading Ca^{2+} in mitochondria. Many articles have reported how ROS destroys the cell, and causes genomic instability--activation of oncogenes and suppression (mutation) of tumor suppressor genes; malignancy formation is often established with genomic instability[119]. In contrast, a second different model is that the chemical toxicants directly activate oncogenes and decrease of tumor suppressor genes, influencing genomic instability [5]; suppression of Ca^{2+} release from IP3R1 maintains cell survival to resist genomic instability. Chemical contamination is a special case to discuss; the overloading of intracellular Ca^{2+} from outside indeed contributes to cell damage via further DDR and SIR, which are the natural dividends of aging and aging associated process. An increasing of Ca^{2+} signaling is more initiative than inflammatory response in the aging process. The study Chapter IV in *O. tsutsugamushi* toxicant infection also supports this theory. The cytokine storm is produced from *O. tsutsugamushi* toxicant infection, contributing to sever inflammatory response and cell death due to the large ROS accumulation. Similar results as shown in Shinichiro Yamamoto et al. study was published in Nature Medicine 2008; TRPM2 Ca^{2+} influx regulates the ROS-induced signaling cascade responsible for chemokine production, which aggravates inflammation[120] and functional interruption of TRPM2 channel by 2-APB as a novel therapeutic approach for treating inflammatory diseases[121]. Therefore it may be suggested that the disruption of intracellular Ca^{2+} elevation with environmental toxicants stimulation could be more efficient against aging and aging associated diseases, especially cancer.

5.5 Novel model of survival and death balance including TRP-HSPs line activation

With respect to the environmental toxicants-induced cell damage and aging or even aging associated diseases, I have suggested to use Ca^{2+}permeating TRP channel inhibitor, such as Derinat or aspirin [122] in order to decrease intracellular Ca^{2+} concentration and ROS production. Besides, according to this study, H_2 containing water decreases the disulfide bonds formation while protects HSP60 from ROS damage, it also enhances survival signal in opposition to death signal. Therefore, in order to accelerate survival signal to eliminate aging or aging associated diseases, the new model of TRP-HSPs line is established in this study. As was discussed previously, Ca^{2+} signaling influences cell's determination—swinging of survival and death program; the balance between survival and death is interrupt when cell is exposure in environmental toxicants with elevation of intracellular Ca^{2+}. Even though blocking TRP channels, increase of HSPs is also efficient to restrain death signaling. As shown in chapter IV, 2-APB upregulates HSP70 expression to attenuate pathogens-induced

TNF-α production (death signal); heat or irradiation of IR or NIR promotes the expression level of HSPs [8]. Enhancement of survival signal against death signal from aging or aging associated diseases efficiently promotes human healthy and lifespan.

5.6 Conclusion

As shown in Fig. 22, each environmental toxicant has its own potential to affect the cell death and survival balance; however, the most important factors in determining cell death or survival are dependent on Ca^{2+} signaling in the initial stages. Arsenic initially decreases Ca^{2+} release from ER through phosphorylating IP3R1 associated with activation of AKT cascades, further inducing genomic instability of oncogenes upregulation and tumor suppressor genes downregulation or mutation. However, UVB irradiation or pathogen stimulation activates Ca^{2+} influx, leading to production of ROS, which induces oxidation of proteins and DNA and further induces genomic instability. Regulation of Ca^{2+} signaling in the initial stages of exposure to environmental toxicants efficiently promotes survival signals over death signals. Thus, the proposed model of TRP-HSPs was supported by this study: inhibition of TRP channels by Derinat or SKF96365 or increase of HSPs by 2-APB, or by heat or IR (NIR) irradiation. Maintaining survival signals by initial stimulation of Ca^{2+} entry by environmental toxicants attenuates aging and aging associated diseases, because of interruption of DDR and SIR. The present study shows how the human defense system responds to environmental toxicants and defines the role of Ca^{2+} signaling as crucial in the initial stages and to influence the survival or death of the cell, even in the earliest stages prior to intracellular ROS production and inflammation. Therefore, blockage of intracellular Ca^{2+} elevation and/or enhancement of HSPs induction promote survival even in the face of aging and aging associated diseases, which are exacerbated by environmental toxicants-induced damage.

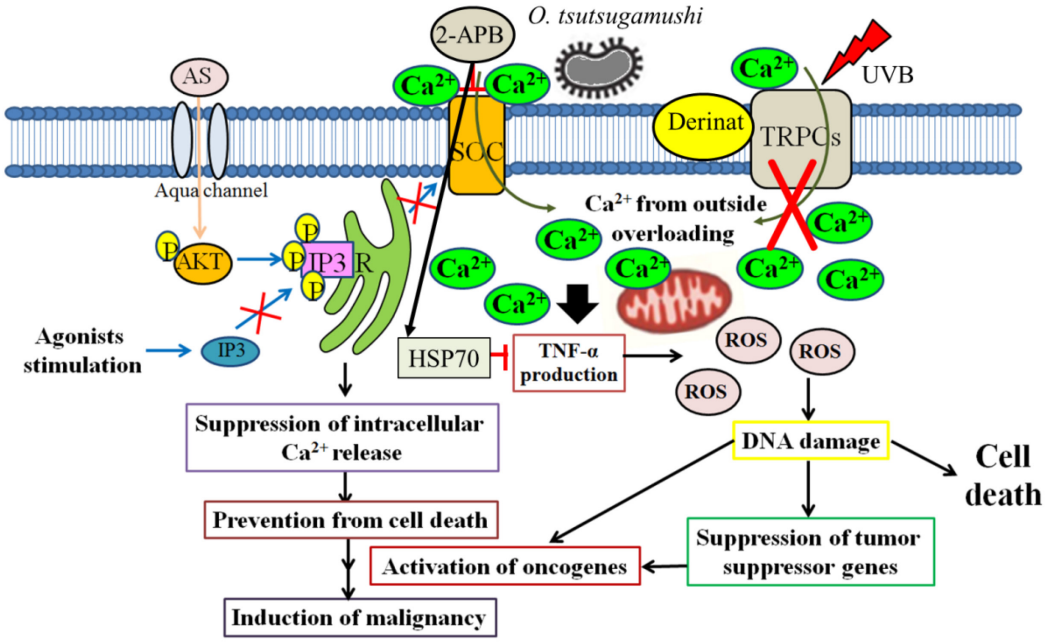

Figure 22. Schematic representation of the role of intracellular Ca^{2+} to make death and survival balance. The environmental toxicant arsenic phosphorylates IP3R via activating the AKT pathway, suppressing Ca^{2+} release and preventing cell death. Malignancy is then induced by the activation of oncogenes and inhibition of tumor suppressor genes in primary KC. UVB induces skin damage and malignance by increasing TRPCs-activated Ca^{2+} entry, intracellular ROS production and DNA damage; Derinat protects skin cells from UVB-induced damage and malignance with interruption TRPC channels. *O. tsutsugamushi* infection induced increased levels of TNF-α, which was attenuated by 2-APB interrupting store-operated channel (SOC) Ca^{2+}entry; suppressed Ca^{2+} mobilization also suppressed release and expression of TNF-α by 2-APB-induced HSP70.

References

1 **Curtis Klaassen (Author), J. B. W. I.** ***Casarett & Doull's Essentials of Toxicology, Third Edition*****. Third edition edn, (McGraw-Hill Education / Medical, 2015).**

2 **Scandalios, J. G. Oxidative stress: molecular perception and transduction of signals triggering antioxidant gene defenses.** ***Brazilian journal of medical and biological research = Revista brasileira de pesquisas medicas e biologicas / Sociedade Brasileira de Biofisica ... [et al.]*** **38, 995-1014, doi:/S0100-879X2005000700003 (2005).**

3 **Tseng, C. H. Blackfoot disease and arsenic: a never-ending story.** ***Journal of environmental science and health. Part C, Environmental carcinogenesis & ecotoxicology reviews*** **23, 55-74, doi:10.1081/GNC-200051860 (2005).**

4 **Guo, H. R., Yu, H. S., Hu, H. & Monson, R. R. Arsenic in drinking water and skin cancers: cell-type specificity (Taiwan, ROC).** ***Cancer causes & control : CCC*** **12, 909-916 (2001).**

5 **Liao, W. T., Lan, C. C., Lee, C. H. & Yu, H. S. Concentration-dependent cellular responses of arsenic in keratinocytes.** ***The Kaohsiung journal of medical sciences*** **27, 390-395, doi:10.1016/j.kjms.2011.05.006 (2011).**

6 **Bhattacharjee, P., Banerjee, M. & Giri, A. K. Role of genomic instability in arsenic-induced carcinogenicity. A review.** ***Environment international*** **53, 29-40, doi:10.1016/j.envint.2012.12.004 (2013).**

7 **Martinez-Reyes, I. & Cuezva, J. M. The H(+)-ATP synthase: a gate to ROS-mediated cell death or cell survival.** ***Biochimica et biophysica acta*** **1837, 1099-1112, doi:10.1016/j.bbabio.2014.03.010 (2014).**

8 **Yoshioka, W.-L. H. a. T. Role of TRP channels in the induction of heat shock proteins (Hsps) by heating skin.** ***BIOPHYSICS*** **11, 25-32, doi:doi: 10.2142/biophysics.11.25 (2015).**

9 **He, Y. D.** ***et al.*** **Polydatin suppresses ultraviolet B-induced cyclooxygenase-2 expression in vitro and in vivo via reduced production of reactive oxygen species.** ***The British journal of dermatology*** **167, 941-944, doi:10.1111/j.1365-2133.2012.10951.x (2012).**

10 **Hsu, W. L.** ***et al.*** **Derinat Protects Skin against Ultraviolet-B (UVB)-Induced Cellular Damage.** ***Molecules*** **20, 20297-20311, doi:10.3390/molecules201119693 (2015).**

11 **Korac, R. R. & Khambholja, K. M. Potential of herbs in skin protection from ultraviolet radiation.** ***Pharmacognosy reviews*** **5, 164-173, doi:10.4103/0973-7847.91114 (2011).**

12 **Tsay, R. W. & Chang, F. Y. Serious complications in scrub typhus.** ***Journal***

of microbiology, immunology, and infection = Wei mian yu gan ran za zhi **31, 240-244 (1998).**

13 Wang, C. C. *et al.* Acute respiratory distress syndrome in scrub typhus. *The American journal of tropical medicine and hygiene* 76, 1148-1152 (2007).

14 Lee, B. J. *et al.* Otalgia and eschar in the external auditory canal in scrub typhus complicated by acute respiratory distress syndrome and multiple organ failure. *BMC infectious diseases* 11, 79, doi:10.1186/1471-2334-11-79 (2011).

15 Tsai, M. H. *et al.* Cross-Regulation of Proinflammatory Cytokines by Interleukin-10 and miR-155 in Orientia tsutsugamushi-Infected Human Macrophages Prevents Cytokine Storm. *The Journal of investigative dermatology* 136, 1398-1407, doi:10.1016/j.jid.2015.11.034 (2016).

16 Janardhanan, J. *et al.* Single-nucleotide polymorphisms in Toll-like receptor (TLR)-2, TLR4 and heat shock protein 70 genes and susceptibility to scrub typhus. *Journal of human genetics* 58, 707-710, doi:10.1038/jhg.2013.89 (2013).

17 West, A. P. *et al.* TLR signalling augments macrophage bactericidal activity through mitochondrial ROS. *Nature* 472, 476-480, doi:10.1038/nature09973 (2011).

18 Vione, D., Maurino, V., Minero, C. & Pelizzetti, E. The atmospheric chemistry of hydrogen peroxide: a review. *Annali di chimica* 93, 477-488 (2003).

19 Winans, B., Humble, M. C. & Lawrence, B. P. Environmental toxicants and the developing immune system: a missing link in the global battle against infectious disease? *Reproductive toxicology* 31, 327-336, doi:10.1016/j.reprotox.2010.09.004 (2011).

20 Salmon, J. K., Armstrong, C. A. & Ansel, J. C. The skin as an immune organ. *The Western journal of medicine* 160, 146-152 (1994).

21 Yeh, S., How, S. W. & Lin, C. S. Arsenical cancer of skin. Histologic study with special reference to Bowen's disease. *Cancer* 21, 312-339 (1968).

22 Yanofsky, V. R., Mercer, S. E. & Phelps, R. G. Histopathological variants of cutaneous squamous cell carcinoma: a review. *Journal of skin cancer* 2011, 210813, doi:10.1155/2011/210813 (2011).

23 Yu, H. S., Liao, W. T. & Chai, C. Y. Arsenic carcinogenesis in the skin. *Journal of biomedical science* 13, 657-666, doi:10.1007/s11373-006-9092-8 (2006).

24 Kitchin, K. T. Recent advances in arsenic carcinogenesis: modes of action,

animal model systems, and methylated arsenic metabolites. ***Toxicology and applied pharmacology*** **172, 249-261, doi:10.1006/taap.2001.9157 (2001).**

25 Masaki, H., Izutsu, Y., Yahagi, S. & Okano, Y. Reactive oxygen species in HaCaT keratinocytes after UVB irradiation are triggered by intracellular Ca(2+) levels. ***The journal of investigative dermatology. Symposium proceedings / the Society for Investigative Dermatology, Inc. [and] European Society for Dermatological Research*** **14, 50-52, doi:10.1038/jidsymp.2009.12 (2009).**

26 Mittal, M., Siddiqui, M. R., Tran, K., Reddy, S. P. & Malik, A. B. Reactive oxygen species in inflammation and tissue injury. ***Antioxidants & redox signaling*** **20, 1126-1167, doi:10.1089/ars.2012.5149 (2014).**

27 Brodsky, I. E. & Medzhitov, R. Targeting of immune signalling networks by bacterial pathogens. ***Nature cell biology*** **11, 521-526, doi:10.1038/ncb0509-521 (2009).**

28 Artis, D. & Spits, H. The biology of innate lymphoid cells. ***Nature*** **517, 293-301, doi:10.1038/nature14189 (2015).**

29 Ye, Y. ***et al.*** **Calcium influx blocked by SK&F 96365 modulates the LPS plus IFN-gamma-induced inflammatory response in murine peritoneal macrophages.** ***International immunopharmacology*** **12, 384-393, doi:10.1016/j.intimp.2011.12.011 (2012).**

30 Brookes, P. S., Yoon, Y., Robotham, J. L., Anders, M. W. & Sheu, S. S. Calcium, ATP, and ROS: a mitochondrial love-hate triangle. ***American journal of physiology. Cell physiology*** **287, C817-833, doi:10.1152/ajpcell.00139.2004 (2004).**

31 Paiva, C. N. & Bozza, M. T. Are reactive oxygen species always detrimental to pathogens? ***Antioxidants & redox signaling*** **20, 1000-1037, doi:10.1089/ars.2013.5447 (2014).**

32 Ruei-Cheng Yang, W.-L. H. a. T. Y. ***A Novel Concept on the Repetitive Calcium Elevation*****. (NOVA science publishers, 2014).**

33 Decuypere, J. P. ***et al.*** **IP(3) Receptors, Mitochondria, and Ca Signaling: Implications for Aging.** ***J Aging Res*** **2011, 920178, doi:10.4061/2011/920178 (2011).**

34 Venkatachalam, K. & Montell, C. TRP channels. ***Annual review of biochemistry*** **76, 387-417, doi:10.1146/annurev.biochem.75.103004.142819 (2007).**

35 Toth, B. I., Olah, A., Szollosi, A. G. & Biro, T. TRP channels in the skin. ***British journal of pharmacology*** **171, 2568-2581, doi:10.1111/bph.12569 (2014).**

36 **Clapham, D. E. SnapShot: mammalian TRP channels. *Cell* 129, 220, doi:10.1016/j.cell.2007.03.034 (2007).**

37 **Tano, J. Y., Lee, R. H. & Vazquez, G. Macrophage function in atherosclerosis: potential roles of TRP channels. *Channels* 6, 141-148, doi:10.4161/chan.20292 (2012).**

38 **Riera, C. E. *et al.* TRPV1 pain receptors regulate longevity and metabolism by neuropeptide signaling. *Cell* 157, 1023-1036, doi:10.1016/j.cell.2014.03.051 (2014).**

39 **Ivanova, H. *et al.* Inositol 1,4,5-trisphosphate receptor-isoform diversity in cell death and survival. *Biochimica et biophysica acta* 1843, 2164-2183, doi:10.1016/j.bbamcr.2014.03.007 (2014).**

40 **Stutzmann, G. E. & Mattson, M. P. Endoplasmic reticulum Ca(2+) handling in excitable cells in health and disease. *Pharmacological reviews* 63, 700-727, doi:10.1124/pr.110.003814 (2011).**

41 **Trachootham, D., Lu, W., Ogasawara, M. A., Nilsa, R. D. & Huang, P. Redox regulation of cell survival. *Antioxidants & redox signaling* 10, 1343-1374, doi:10.1089/ars.2007.1957 (2008).**

42 **Beere, H. M. Death versus survival: functional interaction between the apoptotic and stress-inducible heat shock protein pathways. *The Journal of clinical investigation* 115, 2633-2639, doi:10.1172/JCI26471 (2005).**

43 **Pellegrino, M. W., Nargund, A. M. & Haynes, C. M. Signaling the mitochondrial unfolded protein response. *Biochimica et biophysica acta* 1833, 410-416, doi:10.1016/j.bbamcr.2012.02.019 (2013).**

44 **Szado, T. *et al.* Phosphorylation of inositol 1,4,5-trisphosphate receptors by protein kinase B/Akt inhibits Ca2+ release and apoptosis. *Proceedings of the National Academy of Sciences of the United States of America* 105, 2427-2432, doi:10.1073/pnas.0711324105 (2008).**

45 **Soghoian, D., Jayaraman, V., Silane, M., Berenstein, A. & Jayaraman, T. Inositol 1,4,5-trisphosphate receptor phosphorylation in breast cancer. *Tumour biology : the journal of the International Society for Oncodevelopmental Biology and Medicine* 26, 207-212, doi:10.1159/000086954 (2005).**

46 **Berridge, M. J. Inositol trisphosphate and calcium signalling mechanisms. *Biochimica et biophysica acta* 1793, 933-940, doi:10.1016/j.bbamcr.2008.10.005 (2009).**

47 **Cruz, C. M. *et al.* ATP activates a reactive oxygen species-dependent oxidative stress response and secretion of proinflammatory cytokines in macrophages. *The Journal of biological chemistry* 282, 2871-2879,**

doi:10.1074/jbc.M608083200 (2007).

48 Kadenbach, B., Arnold, S., Lee, I. & Huttemann, M. The possible role of cytochrome c oxidase in stress-induced apoptosis and degenerative diseases. *Biochimica et biophysica acta* 1655, 400-408, doi:10.1016/j.bbabio.2003.06.005 (2004).

49 Inesi, G. *et al.* Studies of Ca2+ ATPase (SERCA) inhibition. *Journal of bioenergetics and biomembranes* 37, 365-368, doi:10.1007/s10863-005-9472-1 (2005).

50 Liu, L. Z. *et al.* Role and mechanism of arsenic in regulating angiogenesis. *PloS one* 6, e20858, doi:10.1371/journal.pone.0020858 (2011).

51 Ji, C. *et al.* Perifosine sensitizes UVB-induced apoptosis in skin cells: new implication of skin cancer prevention? *Cellular signalling* 24, 1781-1789, doi:10.1016/j.cellsig.2012.05.003 (2012).

52 Punnonen, K. & Yuspa, S. H. Ultraviolet light irradiation increases cellular diacylglycerol and induces translocation of diacylglycerol kinase in murine keratinocytes. *The Journal of investigative dermatology* 99, 221-226 (1992).

53 Rae, M. G., Hilton, J. & Sharkey, J. Putative TRP channel antagonists, SKF 96365, flufenamic acid and 2-APB, are non-competitive antagonists at recombinant human alpha1beta2gamma2 GABA(A) receptors. *Neurochemistry international* 60, 543-554, doi:10.1016/j.neuint.2012.02.014 (2012).

54 Morley, N., Curnow, A., Salter, L., Campbell, S. & Gould, D. N-acetyl-L-cysteine prevents DNA damage induced by UVA, UVB and visible radiation in human fibroblasts. *Journal of photochemistry and photobiology. B, Biology* 72, 55-60 (2003).

55 Rosen, J. E., Prahalad, A. K. & Williams, G. M. 8-Oxodeoxyguanosine formation in the DNA of cultured cells after exposure to H2O2 alone or with UVB or UVA irradiation. *Photochemistry and photobiology* 64, 117-122 (1996).

56 Wang, S. C., Chen, B. H., Wang, L. F. & Chen, J. S. Characterization of chondroitin sulfate and its interpenetrating polymer network hydrogels for sustained-drug release. *International journal of pharmaceutics* 329, 103-109, doi:10.1016/j.ijpharm.2006.08.041 (2007).

57 Mi, F. L. *et al.* pH-sensitive behavior of two-component hydrogels composed of N,O-carboxymethyl chitosan and alginate. *Journal of biomaterials science. Polymer edition* 16, 1333-1345 (2005).

58 Hsu, W. L. *et al.* A soft coral natural product, 11-episinulariolide acetate, inhibits gene expression of cyclooxygenase-2 and interleukin-8 through

attenuation of calcium signaling. *Molecules* 18, 7023-7034, doi:10.3390/molecules18067023 (2013).

59 Athar, M. *et al.* Ultraviolet B(UVB)-induced cox-2 expression in murine skin: an immunohistochemical study. *Biochemical and biophysical research communications* 280, 1042-1047, doi:10.1006/bbrc.2000.4201 (2001).

60 Muller, F. L., Lustgarten, M. S., Jang, Y., Richardson, A. & Van Remmen, H. Trends in oxidative aging theories. *Free Radic. Biol. Med.* 43, 477-503, doi:10.1016/j.freeradbiomed.2007.03.034 (2007).

61 Cross, C. E. *et al.* Oxygen radicals and human disease. *Annals of internal medicine* 107, 526-545 (1987).

62 Polis, B. D., Grandizio, M. & Polis, E. Some in vitro and in vivo effects of a new prostaglandin derivative. *Adv. Exp. Med. Biol.* 33, 213-220 (1972).

63 Brookes, P. S., Yoon, Y., Robotham, J. L., Anders, M. W. & Sheu, S. S. Calcium, ATP, and ROS: a mitochondrial love-hate triangle. *Am. J. Physiol. Cell Physiol.* 287, C817-833, doi:10.1152/ajpcell.00139.2004 (2004).

64 Kucherenko, Y. V., Huber, S. M., Nielsen, S. & Lang, F. Decreased redox-sensitive erythrocyte cation channel activity in aquaporin 9-deficient mice. *J. Membr. Biol.* 245, 797-805, doi:10.1007/s00232-012-9482-y (2012).

65 Noda, M., Fujita, K., Lee, C. H. & Yoshioka, T. The principle and the potential approach to ROS-dependent cytotoxicity by non-pharmaceutical therapies: optimal use of medical gases with antioxidant properties. *Curr. Pharm. Des.* 17, 2253-2263 (2011).

66 Sohal, R. S. & Sohal, B. H. Hydrogen peroxide release by mitochondria increases during aging. *Mech. Ageing Dev.* 57, 187-202 (1991).

67 Thomas, J. A. & Mallis, R. J. Aging and oxidation of reactive protein sulfhydryls. *Exp. Gerontol.* 36, 1519-1526 (2001).

68 Cumming, R. C. *et al.* Protein disulfide bond formation in the cytoplasm during oxidative stress. *The Journal of biological chemistry* 279, 21749-21758, doi:10.1074/jbc.M312267200 (2004).

69 Berridge, M. J. Inositol trisphosphate and calcium signalling mechanisms. *Biochim. Biophys. Acta* 1793, 933-940, doi:10.1016/j.bbamcr.2008.10.005 (2009).

70 Karlstad, J., Sun, Y. & Singh, B. B. Ca(2+) signaling: an outlook on the characterization of Ca(2+) channels and their importance in cellular functions. *Adv. Exp. Med. Biol.* 740, 143-157, doi:10.1007/978-94-007-2888-2_6 (2012).

71 Lory, P., Bidaud, I. & Chemin, J. T-type calcium channels in differentiation and proliferation. *Cell calcium* 40, 135-146,

doi:10.1016/j.ceca.2006.04.017 (2006).

72 Decuypere, J. P. *et al.* IP(3) Receptors, Mitochondria, and Ca Signaling: Implications for Aging. *J. Aging Res.* 2011, 920178, doi:10.4061/2011/920178 (2011).

73 Mattson, M. P. ER calcium and Alzheimer's disease: in a state of flux. *Sci. Signal.* 3, pe10, doi:10.1126/scisignal.3114pe10 (2010).

74 Ermak, G. & Davies, K. J. Calcium and oxidative stress: from cell signaling to cell death. *Mol. Immunol.* 38, 713-721 (2002).

75 Hsu, W. L. *et al.* Differential effects of arsenic on calcium signaling in primary keratinocytes and malignant (HSC-1) cells. *Cell calcium* 52, 161-169, doi:10.1016/j.ceca.2012.05.007 (2012).

76 Sato, Y. *et al.* Hydrogen-rich pure water prevents superoxide formation in brain slices of vitamin C-depleted SMP30/GNL knockout mice. *Biochem. Biophys. Res. Commun.* 375, 346-350, doi:10.1016/j.bbrc.2008.08.020 (2008).

77 Cumming, R. C. *et al.* Fanconi anemia group C protein prevents apoptosis in hematopoietic cells through redox regulation of GSTP1. *Nat. Med.* 7, 814-820, doi:10.1038/89937 (2001).

78 Delaunay, A., Pflieger, D., Barrault, M. B., Vinh, J. & Toledano, M. B. A thiol peroxidase is an H2O2 receptor and redox-transducer in gene activation. *Cell* 111, 471-481 (2002).

79 Manalo, D. J., Lin, Z. & Liu, A. Y. Redox-dependent regulation of the conformation and function of human heat shock factor 1. *Biochemistry* 41, 2580-2588 (2002).

80 Turrens, J. F. Mitochondrial formation of reactive oxygen species. *J. Physiol.* 552, 335-344, doi:10.1113/jphysiol.2003.049478 (2003).

81 Ohsawa, I. *et al.* Hydrogen acts as a therapeutic antioxidant by selectively reducing cytotoxic oxygen radicals. *Nat. Med.* 13, 688-694, doi:10.1038/nm1577 (2007).

82 Keten, S., Chou, C. C., van Duin, A. C. & Buehler, M. J. Tunable nanomechanics of protein disulfide bonds in redox microenvironments. *J. Mech. Behav. Biomed. Mater.* 5, 32-40, doi:10.1016/j.jmbbm.2011.08.017 (2012).

83 Moron, C. G., Popov, V. L., Feng, H. M., Wear, D. & Walker, D. H. Identification of the target cells of Orientia tsutsugamushi in human cases of scrub typhus. *Modern pathology : an official journal of the United States and Canadian Academy of Pathology, Inc* 14, 752-759, doi:10.1038/modpathol.3880385 (2001).

84 **Seong, S. Y., Choi, M. S. & Kim, I. S. Orientia tsutsugamushi infection: overview and immune responses. *Microbes and infection / Institut Pasteur* 3, 11-21 (2001).**

85 **Wang, H. & Ma, S. The cytokine storm and factors determining the sequence and severity of organ dysfunction in multiple organ dysfunction syndrome. *The American journal of emergency medicine* 26, 711-715, doi:10.1016/j.ajem.2007.10.031 (2008).**

86 **Hotchkiss, R. S. & Karl, I. E. Calcium: a regulator of the inflammatory response in endotoxemia and sepsis. *New horizons* 4, 58-71 (1996).**

87 **Murdaca, G., Colombo, B. M. & Puppo, F. Anti-TNF-alpha inhibitors: a new therapeutic approach for inflammatory immune-mediated diseases: an update upon efficacy and adverse events. *International journal of immunopathology and pharmacology* 22, 557-565 (2009).**

88 **Newham, P. *et al.* Determination of the safety and efficacy of therapeutic neutralization of tumor necrosis factor-alpha (TNF-alpha) using AZD9773, an anti-TNF-alpha immune Fab, in murine CLP sepsis. *Inflammation research : official journal of the European Histamine Research Society ... [et al.]* 63, 149-160, doi:10.1007/s00011-013-0683-3 (2014).**

89 **Goode, S., Tierney, G. & Deighton, C. Life threatening intra-abdominal sepsis in patients on anti-TNF-alpha therapy. *Gut* 55, 590-591, doi:10.1136/gut.2005.085449 (2006).**

90 **Zhao, X. *et al.* TNF-alpha stimulates caspase-3 activation and apoptotic cell death in primary septo-hippocampal cultures. *Journal of neuroscience research* 64, 121-131, doi:10.1002/jnr.1059 (2001).**

91 **Ikeda, M. *et al.* Ca(2+) spiking activity caused by the activation of store-operated Ca(2+) channels mediates TNF-alpha release from microglial cells under chronic purinergic stimulation. *Biochimica et biophysica acta* 1833, 2573-2585, doi:10.1016/j.bbamcr.2013.06.022 (2013).**

92 **Collins, H. E., Zhu-Mauldin, X., Marchase, R. B. & Chatham, J. C. STIM1/Orai1-mediated SOCE: current perspectives and potential roles in cardiac function and pathology. *American journal of physiology. Heart and circulatory physiology* 305, H446-458, doi:10.1152/ajpheart.00104.2013 (2013).**

93 **Colton, C. K. & Zhu, M. X. 2-Aminoethoxydiphenyl borate as a common activator of TRPV1, TRPV2, and TRPV3 channels. *Handbook of experimental pharmacology*, 173-187, doi:10.1007/978-3-540-34891-7_10 (2007).**

94 **Dienz, O. & Rincon, M. The effects of IL-6 on CD4 T cell responses.**

Clinical immunology **130, 27-33, doi:10.1016/j.clim.2008.08.018 (2009).**

95 Kalinski, P. *et al.* IL-4 is a mediator of IL-12p70 induction by human Th2 cells: reversal of polarized Th2 phenotype by dendritic cells. *Journal of immunology* 165, 1877-1881 (2000).

96 Iwasaki, A. & Medzhitov, R. Control of adaptive immunity by the innate immune system. *Nature immunology* 16, 343-353, doi:10.1038/ni.3123 (2015).

97 Nambu, A., Nakae, S. & Iwakura, Y. IL-1beta, but not IL-1alpha, is required for antigen-specific T cell activation and the induction of local inflammation in the delayed-type hypersensitivity responses. *International immunology* 18, 701-712, doi:10.1093/intimm/dxl007 (2006).

98 Mitsuhashi, M., Yamaguchi, M., Kojima, T., Nakajima, R. & Kasai, K. Effects of HSP70 on the compression force-induced TNF-alpha and RANKL expression in human periodontal ligament cells. *Inflammation research : official journal of the European Histamine Research Society ... [et al.]* 60, 187-194, doi:10.1007/s00011-010-0253-x (2011).

99 Meng, X. & Harken, A. H. The interaction between Hsp70 and TNF-alpha expression: a novel mechanism for protection of the myocardium against post-injury depression. *Shock* 17, 345-353 (2002).

100 Kim, H. P., Morse, D. & Choi, A. M. Heat-shock proteins: new keys to the development of cytoprotective therapies. *Expert opinion on therapeutic targets* 10, 759-769, doi:10.1517/14728222.10.5.759 (2006).

101 Rozhkova, E. *et al.* Exogenous mammalian extracellular HSP70 reduces endotoxin manifestations at the cellular and organism levels. *Annals of the New York Academy of Sciences* 1197, 94-107, doi:10.1111/j.1749-6632.2009.05375.x (2010).

102 Keller, J. M., Escara-Wilke, J. F. & Keller, E. T. Heat stress-induced heat shock protein 70 expression is dependent on ERK activation in zebrafish (Danio rerio) cells. *Comparative biochemistry and physiology. Part A, Molecular & integrative physiology* 150, 307-314, doi:10.1016/j.cbpa.2008.03.021 (2008).

103 Inoue, K. & Xiong, Z. G. Silencing TRPM7 promotes growth/proliferation and nitric oxide production of vascular endothelial cells via the ERK pathway. *Cardiovascular research* 83, 547-557, doi:10.1093/cvr/cvp153 (2009).

104 Umemura, M. *et al.* Store-operated Ca2+ entry (SOCE) regulates melanoma proliferation and cell migration. *PloS one* 9, e89292, doi:10.1371/journal.pone.0089292 (2014).

105 **Zorzi, E. & Bonvini, P. Inducible hsp70 in the regulation of cancer cell survival: analysis of chaperone induction, expression and activity. *Cancers* 3, 3921-3956, doi:10.3390/cancers3043921 (2011).**

106 **Xia, L. M. *et al.* [Hypoxia induces heat shock protein HSP70-2 expression in a HIF-1 dependent manner]. *Zhonghua gan zang bing za zhi = Zhonghua ganzangbing zazhi = Chinese journal of hepatology* 17, 207-212 (2009).**

107 **Conejeros, I. *et al.* 2-Aminoethoxydiphenyl borate (2-APB) reduces respiratory burst, MMP-9 release and CD11b expression, and increases l-selectin shedding in bovine neutrophils. *Research in veterinary science* 92, 103-110, doi:10.1016/j.rvsc.2010.10.005 (2012).**

108 **Lu, H. Y. *et al.* Phylogenetic analysis of 56-kDa type-specific antigen gene of Orientia tsutsugamushi isolates in Taiwan. *The American journal of tropical medicine and hygiene* 83, 658-663, doi:10.4269/ajtmh.2010.09-0608 (2010).**

109 **Tsai, M. H. *et al.* Cross-regulation of Pro-inflammatory Cytokines by Interleukin-10 and MiR-155 in Orientia tsutsugamushi-infected Human Macrophages Prevents Cytokine Storm. *The Journal of investigative dermatology*, doi:10.1016/j.jid.2015.11.034 (2016).**

110 **Gabuzda, D. & Yankner, B. A. Physiology: Inflammation links ageing to the brain. *Nature* 497, 197-198, doi:10.1038/nature12100 (2013).**

111 **Bahar, E., Kim, H. & Yoon, H. ER Stress-Mediated Signaling: Action Potential and Ca(2+) as Key Players. *International journal of molecular sciences* 17, doi:10.3390/ijms17091558 (2016).**

112 **Ding, J. *et al.* Effects of a non-selective TRPC channel blocker, SKF-96365, on melittin-induced spontaneous persistent nociception and inflammatory pain hypersensitivity. *Neuroscience bulletin* 28, 173-181, doi:10.1007/s12264-012-1213-y (2012).**

113 **Kim, M. S., Kim, Y. K., Cho, K. H. & Chung, J. H. Infrared exposure induces an angiogenic switch in human skin that is partially mediated by heat. *The British journal of dermatology* 155, 1131-1138, doi:10.1111/j.1365-2133.2006.07510.x (2006).**

114 **Calapre, L. *et al.* Heat-mediated reduction of apoptosis in UVB-damaged keratinocytes in vitro and in human skin ex vivo. *BMC dermatology* 16, 6, doi:10.1186/s12895-016-0043-4 (2016).**

115 **Tang, H. *et al.* CW/pulsed NIR irradiation of gold nanorods: effect on transdermal protein delivery mediated by photothermal ablation. *Journal of controlled release : official journal of the Controlled Release Society* 171, 178-183, doi:10.1016/j.jconrel.2013.07.003 (2013).**

116 **Liu, H. T. *et al.* Primary evidence for involvement of IP3 in heat-shock signal transduction in Arabidopsis. *Cell research* 16, 394-400, doi:10.1038/sj.cr.7310051 (2006).**

117 **Kiang, J. G. & Tsokos, G. C. Heat shock protein 70 kDa: molecular biology, biochemistry, and physiology. *Pharmacology & therapeutics* 80, 183-201 (1998).**

118 **Katusic, Z. S. & Stelter, A. M. Type I inositol-triphosphate receptor gene is alternatively spliced in human cerebral arteries. *Biochemical and biophysical research communications* 214, 803-809, doi:10.1006/bbrc.1995.2358 (1995).**

119 **Abbas, T., Keaton, M. A. & Dutta, A. Genomic instability in cancer. *Cold Spring Harbor perspectives in biology* 5, a012914, doi:10.1101/cshperspect.a012914 (2013).**

120 **Yamamoto, S. *et al.* TRPM2-mediated Ca2+influx induces chemokine production in monocytes that aggravates inflammatory neutrophil infiltration. *Nature medicine* 14, 738-747, doi:10.1038/nm1758 (2008).**

121 **Togashi, K., Inada, H. & Tominaga, M. Inhibition of the transient receptor potential cation channel TRPM2 by 2-aminoethoxydiphenyl borate (2-APB). *British journal of pharmacology* 153, 1324-1330, doi:10.1038/sj.bjp.0707675 (2008).**

122 **Kokoska, E. R., Smith, G. S. & Miller, T. A. Store-operated calcium influx in human gastric cells: role of endogenous prostaglandins. *Surgery* 124, 429-437 (1998).**

Acknowledgements

"Life is like a box of chocolates, you never know what you're going to get." Fifteen years ago, I had no idea that I would devote myself to research, study for a master's degree, and even acquire my PhD at Waseda University in Japan. I am very lucky to find my favorite work (doing research) as my career, although the process of my research work has been full of frustration and stress. Actually, I tried to give up my favorite work; almost six years ago, I couldn't even look for a suitable job in research work, just because I didn't graduate from one of the top universities in Taiwan, and even though I studied very hard and possessed many research techniques. At that time, I met Prof. Tohru Yoshioka (吉岡亨 教授), who was a visiting professor in Kaohsiung Medical University. I really, really appreciate that Prof. Yoshioka gave me a job opportunity and also appreciate he that he taught me a lot of things, not only in research but also in life. If there was no Prof. Yoshioka, I could not have sustained my research work, my favorite work. Also thanks to Prof. Chu-Huang (Mendel) Chen (陳珠璜 教授); he always encouraged and provided support for me, when I faced pressure and failure in my experiments. I have enormous appreciation for the tremendous help of Prof. Etsuro Ito(伊藤悦朗 教授). Because of the close cooperation between Kaohsiung Medical University and Waseda University, I have learned advanced neuroscience information from him and thanks to his effort to help me recruit a PhD committee in Waseda University, and because of his teaching, I was able to finish my PhD thesis. Thanks to Prof. Hsin-Su Yu (余幸司 教授), Prof. Ching-Kuan Liu (劉景寬 教授) and Prof. Hsiu-Hung Wang (王秀紅 教授), those professors who have supported our lab with the resources and funding to finish our research work. Thanks to Dr. Maurice, Dr. Karen, Dr. Lin and Dr. Liang, I am was lucky enough to be able to discuss my work with you so that I can always get very good ideas for my research work. Thanks to our sweet research assistant Ian (顏顏) and undergraduate students; because of your kind support, I can completely finish my experiments. Finally, I would like to say "thank you" and express my love to my sweet family, my parents and husband Allen. Thanks to your huge help and support, I can pursue my dream and do my favorite work without any interruption.

Bibliography

早稲田大学　博士（理学）　学位申請　研究業績書

氏名　　許　　文俐　　印

（2017 年　1 月　現在）

種類別	題名、　発表・発行掲載誌名、　発表・発行年月、　連名者（申請者含む）
論文 （査読有） ○	A novel strategy for TNF-alpha production by 2-APB induced downregulated SOCE and upregulated HSP70 in *O. tsutsugamushi*-Infected human macrophages. PLOS ONE, 11: e0159299 (2016). Ching-Ying Wu*, **Wen-Li Hsu***, Chun-Hsiung Wang, Jui-Lin Liang, Ming-Hsien Tsai, Chia-Jung Yen, Hsiu-Wen Li, Siou-Jin Chiu, Chung-Hsing Chang, Yaw-Bin Huang, Ming-Wei Lin and Tohru Yoshioka. (*co-first author. Note that Dr. Ching-Ying Wu does not need to use this paper for her thesis.) Cross-regulation of proinflammatory cytokines by interleukin-10 and miR-155 in *Orientia tsutsugamushi*-infected human macrophages prevents cytokine storm. Journal of Investigating Dermatology, 136: 1398-407 (2016). Ming-Hsien Tsai, Chung-Hsing Chang, Rong-Kung Tsai, Yi-Ren Hong, Tsung-Hsien Chuang, Kan-Tang Fan, Chi-Wen Peng, Ching-Ying Wu, **Wen-Li Hsu**, Lih-Shinn Wang, Li-Kuang Chen and Hsin-Su Yu.
○	The role of Derinat in the protection against cellular damage induced by ultraviolet-B (UVB) in skin. Molecules, 20: 20297-20311 (2015). **Wen-Li Hsu**, Jian-He Lu, Mami Noda, Ching-Ying Wu, Jiadai Liu, Manabu Sakakibara, Ming-Hsien Tsai, Hsin-Su Yu, Ming-Wei Lin, Shian-Jang Yan and Tohru Yoshioka. Salvia miltiorrhiza induces tonic contraction of the lower esophageal sphincter in rats via activation of extracellular Ca^{2+} influx. Molecules, 20: 14504-14521 (2015). Ching-Chung Tsai, Li-Ching Chang, Shih-Che Huang, Shu-Leei Tey, **Wen-Li Hsu**, Yu-Tsun Su, Ching-Wen Liu and Tong-Rong Tsai. A role of TRP channel to induce heat shock proteins (Hsps) by heating skin. BIOPHYSICS. 11: 25-32. (2015). **Wen-Li Hsu** and Tohru Yoshioka. A potential connection between activation of transient receptor potential channels by electromagnetic wave radiation and induction of heat shock proteins in living cells. Journal of Biochemistry and Molecular Biology Research. 1: 3 (2015). Etsuro Ito, **Wen-Li Hsu**, Tomoko Warita, Tohru Yoshioka. Study of the association between ITPKC genetic polymorphisms and calcium nephrolithiasis. BioMed Research International, 2014, Article ID 397826 (2014). Wei-Chih Kan, Yii Her Chou, Siou-Jin Chiu, Yu-Wen Hsu, Hsing-fang Lu, **Wen-Li Hsu** and Wei Chiao Chang.

Ｎｏ.2

早稲田大学　博士（理学）　学位申請　研究業績書

種 類 別	題名、　発表・発行掲載誌名、　発表・発行年月、　連名者（申請者含む）
論文 （査読有） ○	A role for proton signaling in the induction of somatic cells to pluripotent embryonic stem cells. Journal of Physical Chemistry and Biophysics, 4: Article ID 1000138 (2014). Etsuro Ito, **Wen-Li Hsu** and Tohru Yoshioka. Involvement of STIM1/Orai1 calcium signaling, ERK and Akt pathways in EGF-mediated cell growth in retinal pigment epithelial cells. Journal of Biomedical Science, 20: 41 (2013). I-Hui Yang, Yao-Ting Tsai, Siou-Jin Chiu, Li-Teh Liu, Yih-Chi Hu, Hsuan-Hung Lee, Ming-Feng Hou, **Wen-Li Hsu**, Wei-Chiao Chen, and Wei-Chiao Chang. A soft coral natural product, 11-episinulariolide acetate, inhibited gene expression of cyclooxygenase-2 and interleukin-8 through attenuation of calcium signaling. Molecules, 18: 7023-7034 (2013). **Wen-Li Hsu**, Siou-Jin Chiu, Che-Mai Chang, Jaw-Yan Wang, Eric Terry Wang, Ming-Feng Hou, Chiung-Yao Huang, Jyh-Horng Sheu and Wei-Chiao Chang. Indomethacin inhibits cancer cell migration via attenuation of cellular calcium mobilization. Molecules, 18: 6584-6596 (2013). Yuh-Cherng Guo, Che-Mai Chang, **Wen-Li Hsu**, Siou-Jin Chiu, Yao-Ting Tsai, Yii-Her Chou, Ming-Feng Hou, Jaw-Yan Wang, Ke-Li Tsai and Wei-Chiao Chang. A role for epstein-barr viral BALF1 in facilitating tumor formation and metastasis potential. Virus Research, 163: 617-627 (2012). **Wen-Li Hsu**, Pei-Jung Chung, Ming-Hsien Tsai, Cicero Lee-Tian Chang and Chih-Lung Liang. Differential effects of arsenic on calcium signaling in primary keratinocytes and malignant (HSC-1) cells. Cell Calcium, 52: 161-169 (2012). **Wen-Li Hsu**, Ming-Hsien Tsai, Ming-Wei Lin, Y.C. Chiu, Jian-He Lu, Chung-Hsing Chang, Hsin-Su Yu and Tohru Yoshioka.
著書 （章の執筆）	A novel concept on the repetitive calcium elevation. New Development in Calcium Signaling Reserch. NOVA publisher. Chapter IV, Page67-87 (2013). Ruei-Cheng Yang, **Wen-Li Hsu** and Tohru Yoshioka.